

AD-A174 947

(12)

TGAL-85-4

## MULTICHANNEL DECONVOLUTION OF P WAVES AT SEISMIC ARRAYS

Z.A. Der, R.H. Shumway, A.C. Lees, and E. Smart  
Teledyne Geotech Alexandria Laboratories  
314 Montgomery Street  
Alexandria, Virginia 22314-1581

OCTOBER 1986 (Revised)

FINAL TECHNICAL REPORT: TASK 2  
ARPA ORDER NO: 5143  
PROJECT TITLE: Finite Difference Cratering Support  
CONTRACT: MDA903-84-C-0289

Approved for Public Release; Distribution Unlimited.

DTIC FILE COPY

Prepared for:  
DEPARTMENT OF THE ARMY  
Defense Supply Service  
Room 1D 245, The Pentagon  
Washington, D.C. 20310

Monitored By:  
DARPA/DSO/GSD  
1400 Wilson Boulevard  
Arlington, Virginia 22209

DTIC  
ELECTED  
DEC 12 1986  
S A D

The views and conclusions contained in this report are those of the authors and should not be interpreted as representing the official policies, either expressed or implied, of the Defense Advanced Research Projects Agency or the U.S. Government.

86 12 12 096

UNCLASSIFIED

~~SECURITY CLASSIFICATION OF THIS PAGE~~

Form Approved  
OMB No 0704-0188  
Exp Date Jun 30 1986

REPORT DOCUMENTATION PAGE					Form Approved OMB No 0704-0188 Exp Date Jun 30, 1986
1a REPORT SECURITY CLASSIFICATION Unclassified			1b RESTRICTIVE MARKINGS		
2a SECURITY CLASSIFICATION AUTHORITY			3 DISTRIBUTION/AVAILABILITY OF REPORT Approved for public release. Distribution Unlimited.		
2b DECLASSIFICATION/DOWNGRADING SCHEDULE					
4 PERFORMING ORGANIZATION REPORT NUMBER(S) TGAL-85-4			5. MONITORING ORGANIZATION REPORT NUMBER(S)		
6a NAME OF PERFORMING ORGANIZATION Teledyne Geotech Alexandria Laboratories		6b OFFICE SYMBOL (if applicable)	7a NAME OF MONITORING ORGANIZATION Department of the Army DSSW		
6c ADDRESS (City, State, and ZIP Code) 314 Montgomery Street Alexandria, VA 22314-1581			7b ADDRESS (City, State, and ZIP Code) Room 1D 245, The Pentagon Washington, D.C. 20310		
8a. NAME OF FUNDING/SPONSORING ORGANIZATION DARPA		8b OFFICE SYMBOL (if applicable) GSD	9. PROCUREMENT INSTRUMENT IDENTIFICATION NUMBER MDA903-84-C-0289 /		
8c. ADDRESS (City, State, and ZIP Code) 1400 Wilson Blvd. Arlington, VA 22209			10. SOURCE OF FUNDING NUMBERS		
			PROGRAM ELEMENT NO	PROJECT NO.	TASK NO 2
					WORK UNIT ACCESSION NO
11. TITLE (Include Security Classification) Multichannel Deconvolution of P Waves at Seismic Arrays					
12. PERSONAL AUTHOR(S) Z.A. Der, R.H. Shumway, A.C. Lees, and E. Smart					
13a TYPE OF REPORT Final Technical		13b TIME COVERED FROM 6/84 TO 6/85		14. DATE OF REPORT (Year, Month, Day) 1986 October 20	15 PAGE COUNT 177
16. SUPPLEMENTARY NOTATION					
17. COSATI CODES			18. SUBJECT TERMS (Continue on reverse if necessary and identify by block number)		
FIELD	GROUP	SUB-GROUP			
19 ABSTRACT (Continue on reverse if necessary and identify by block number)  The results of a new multichannel deconvolution method applied to array recordings of teleseismic P waves are presented and interpreted in terms of possible surface reflections and other arrivals from Nevada Test Site, Eastern Kazakh Test Site, and Astrakhan nuclear explosions. The deconvolution method utilizes the well known fact that P wave spectra can be decomposed into source and receiver spectral factors. The results are discussed in terms of the outcomes of other, less complex deconvolution methods including spectral ratio techniques for estimating pP delay times and stacked deconvolution methods for enhancing the pP phase on seismic records. For most events, the deconvolved source time functions appear to contain a pP arrival but they also show later, unexplained arrivals. The site functions are also complex in many cases. About half of the late coda in P appears to be due to each of the source and the					
20. DISTRIBUTION/AVAILABILITY OF ABSTRACT <input type="checkbox"/> UNCLASSIFIED/UNLIMITED <input checked="" type="checkbox"/> SAME AS RPT <input type="checkbox"/> DTIC USERS			21 ABSTRACT SECURITY CLASSIFICATION Unclassified		
22a NAME OF RESPONSIBLE INDIVIDUAL Dr. Robert R. Blandford			22b. TELEPHONE (Include Area Code) (202) 697-6506		22c OFFICE SYMBOL GSD

UNCLASSIFIED

SECURITY CLASSIFICATION OF THIS PAGE

19. (Continued)

receiver. The recordings for an Eastern Kazakh cratering event show a distinctly different source function when compared to deeper, buried explosions at the same test site. From the deconvolved source-time functions, the cratering to non-cratering  $m_b$  bias is estimated to be between 0.09 and 0.22 magnitude units.

## ABSTRACT

The results of a new multichannel deconvolution method applied to array recordings of teleseismic P waves are presented and interpreted in terms of possible surface reflections and other arrivals from Nevada Test Site, Eastern Kazakh Test Site, and Astrakhan nuclear explosions. The deconvolution method utilizes the well-known fact that P wave spectra can be decomposed into source and receiver spectral factors. The results are discussed in terms of the outcomes of other, less complex deconvolution methods including spectral ratio techniques for estimating pP delay times and stacked deconvolution methods for enhancing the pP phase on seismic records. For most events, the deconvolved source time functions appear to contain a pP arrival but they also show later, unexplained arrivals. The site functions are also complex in many cases. About half of the late coda in P appears to be due to each of the source and the receiver. The recordings for an Eastern Kazakh cratering event show a distinctly different source function when compared to deeper, buried explosions at the same test site. From the deconvolved source-time functions, the cratering to non-cratering  $m_b$  bias is estimated to be between 0.09 and 0.22 magnitude units.

Keywords:

Primary waves (Seismic waves),

Seismic data, Maximum

Likelihood estimation; Nuclear  
explosion detection.



Accession For	
NTIS GRA&I	<input checked="" type="checkbox"/>
DTIC TAB	<input type="checkbox"/>
Unannounced	<input type="checkbox"/>
Justification	
By _____	
Distribution/	
Availability Codes	
Dist	Avail and/or Special
A1	

**(THIS PAGE INTENTIONALLY LEFT BLANK)**

**TABLE OF CONTENTS**

	Page
ABSTRACT	iii
LIST OF FIGURES	vi
LIST OF TABLES	x
INTRODUCTION	1
BACKGROUND	3
SPECTRAL RATIOS	10
STACKED DECONVOLUTIONS	13
MAXIMUM LIKELIHOOD MULTICHANNEL DECONVOLU- TIONS	20
Description of the Deconvolution Method	20
Results of the Data Analyses	24
CONCLUSIONS	44
SUGGESTED FUTURE WORK	45
REFERENCES	48
APPENDIX A - Spectral ratios of pairs of NTS events at NORSAR stations and pairs of NORSAR stations for NTS events.	51
APPENDIX B - Deconvolved site time functions and resolution kernels from deconvolutions.	61
APPENDIX C - Original traces of explosion data.	75
APPENDIX D - Reconstructed traces of explosion data.	121

## LIST OF FIGURES

Figure No.	Title	Page
1	Three spike sequences with identical power spectra, but different phases. The second spike sequence might be interpreted as "P" plus "low frequency pP".	4
2	Three spike sequences with identical power spectra, but different phase.	5
3	Synthetic inputs (on left) and their "intercorrelations" (on right) with the resulting correlation coefficients.	7
4	Synthetic inputs (on left) and their "intercorrelations" (on right) with the resulting correlation coefficients.	8
5	(a) West-to-east model for geologic structure across Yucca Valley used infinite difference simulations. The model is shown with 5-to-1 vertical exaggeration, and each region is labeled with its P-wave velocity. P-wave velocities of 1.34, 2.14, 3.00, and 4.57 km/sec are indicated for the geologic units of alluvium, unsaturated tuff, saturated tuff, and Paleozoic carbonates, respectively. The source locations are indicated by numbered dots across the middle of the figure. (b) Synthetics for source locations 4,5, and 6 at take-off angle of 15 degrees (solid lines) compared to synthetics for a plane-layered model (dashed lines). (c) spectra of the synthetics for source location 5 of the Yucca Valley model (left) and for the plane-layered model (right) showing the much more distinct spectral nulls in the spectra of the synthetics from the flat-layered model (after McLaughlin et al 1986).	12
6	Deconvolutions of theoretical source time functions. The original source time functions on the left were made using the von Seggern and Blandford (1972) model (vSB) while those on the right were made using the Mueller and Murphy (1971) model; all four source time functions were deconvolved with the vSB model using Wiener filter. The upper two source functions were not prewhitened; the lower two were prewhitened by increasing the zero lag autocorrelation value by 50%. The only difference in the deconvolutions due to the different source functions is a slight asymmetry.	15
7	Stacked deconvolutions of five NTS events recorded at NORSAR. Estimates of the pP delay time inferred from the deconvolutions are shown to the right of the traces.	17



- 16 Magnitude difference estimates between the presumed cratering event at eastern KTS and four buried eastern KTS explosions for yields of 60, 125, and 300 kt. The magnitude differences were calculated from equations (6) and (7) in the text.  $A_a$  and  $A_c$  are the "a" phase and "c" phase amplitudes, respectively, and cr and n-cr refer to cratering and non-cratering event, respectively. 36
- 17 Examples of filtered site terms for the set of NTS data recorded at NORSAR. In each pair, the top trace is the deconvolved site term, which has been filtered in the bottom trace with a von Seggern and Blandford wavelet assuming a yield of 500 kt,  $t^* = 0.45$  sec, and a NORSAR instrument response. 37
- 18 Examples of filtered site terms for the set of KTS data recorded at EKA. In each pair, the top trace is the deconvolved site term, which has been filtered in the bottom trace with a von Seggern and Blandford wavelet assuming a yield of 130 kt,  $t^* = 0.15$  sec and an EKA instrument response. 38
- 19 Examples of filtered site terms for the set of Astrakhan data recorded at the RSTN. In each pair, the top trace is the deconvolved site term, which has been filtered in the bottom trace with a von Seggern and Blandford wavelet assuming a yield of 22 kt,  $t^* = 0.15$  sec, and an RSTN instrument response. The predicted location of the PcP arrival is also marked. 39
- 20 Deconvolved site terms for NORSAR receivers used in studies of data from both NTS and KTS. Both the NTS and KTS data sets were deconvolved separately in the 0.4 to 3.5 Hz frequency band. There appear to be some azimuthal dependencies in these site terms. 41
- 21 Five traces from the NTS explosion Mast as recorded at NORSAR (top of each pair of traces), along with their reconstructions (bottom of each pair of traces). The receiver names are given to the left of each pair of traces, as is the correlation coefficient between each original trace and its reconstruction. 42
- 22 Five traces from the eastern KTS cratering shot of 15 January 1965 as recorded at EKA (top of each pair of traces), along with their reconstructions (bottom of each pair of traces). The receiver names are given to the left of each pair of traces, as is the correlation coefficient between each original trace and its reconstruction. 43

A1	Spectral ratios between NTS events Inlet and Kasseri at NORSAR stations.	53
A2	Spectral ratios between NTS events Inlet and Mast at NORSAR stations.	54
A3	Spectral ratios between NTS events Mast and Kasseri at NORSAR stations.	55
A4	Spectral ratios between NTS events Stilton and Inlet at NORSAR stations.	56
A5	Spectral ratios between NORSAR receivers NB4 and NB2 at NTS events.	57
A6	Spectral ratios between NORSAR receivers NB5 and NB1 at NTS events.	58
A7	Spectral ratios between NORSAR receivers NB5 and NB2 at NTS events.	59
A8	Spectral ratios between NORSAR receivers NB5 and NB4 at NTS events.	60
B1	Deconvolved site terms for NTS events recorded at NORSAR.	62
B2	Deconvolved site terms for KTS events recorded at NORSAR.	63&64
B3	Deconvolved site terms for KTS events recorded at EKA.	65-67
B4	Deconvolved site terms for Astrakhan events recorded at the RSTN.	68
B5	Resolution kernels for NTS events recorded at NORSAR.	69
B6	Resolution kernels for KTS events recorded at NORSAR.	70&71
B7	Resolution kernels for KTS events recorded at EKA.	72
B8	Resolution kernels for Astrakhan events recorded at the RSTN.	73

## LIST OF TABLES

Table No.	Title	Page
1	Source Parameters for NTS Events Recorded at NORSAR	26
2	Source Parameters for Eastern Kazakh Events Recorded at NORSAR	26
3	Source Parameters for Eastern Kazakh Events Recorded at EKA	27
4	Source Parameters for Astrakhan Events Recorded at the RSTN	27
5	Parameters used in Deconvolutions	28
A1	Parameters used in Forming Synthetic Spectral Ratios	52

## Introduction

The determination of the effect of surface reflection and other secondary arrivals on the estimated yields of nuclear explosions has been a major problem in nuclear monitoring work. The major philosophical issues in such work are the following:

- a) Are the source functions simple superpositions of P and pP pulses or are more complex source time histories appropriate?
- b) Can we predict the effect of the secondary arrivals on the yields estimated from time domain measurements on the first cycle of the P wave signal?
- c) What is the effect of these secondary arrivals on frequency domain measures of yield?
- d) What are the limitations on the resolution of secondary arrivals imposed by Q and the noise?
- e) And, in general, what processes, e.g. Q, scattering, near source and receiver wave conversions, spall, Rayleigh-to-P conversions, etc., determine the waveforms and spectra of teleseismic P waves?

These problems are not trivial. In the case of a simple pP reflection we understand how it biases the various time domain measurements and we are thus able to make corrections for it if the amplitude, arrival time and spectral characteristics of the pP are known. If, on the other extreme, the P wave consists of various multipathed and focused arrivals in conjunction with complex source functions consisting of many pulses of unknown origin, then there is no physical model on which we could base any methods to "correct" our readings, since it becomes doubtful, not understanding the nature of arrivals, that even the first arrival amplitude is uncontaminated and well understood. The pP yield correction is based on the belief that there are only two pulses present, the amplitude of the first of which is a measure of direct radiation

from an explosive source. If there are other pulses present then we still have to assume that the first, upward motion is due to an uncontaminated direct arrival from the source.

Another important issue is the basic resolution attainable in determining the time delay of pP, provided it is present. For band-limited signals and small pP delays we may not be able to resolve this time accurately enough to get a meaningful correction, even if the simple P+pP model is valid. For such signals it may be possible to obtain spectacular waveform fits, but these do not prove that the model is valid. Most of these questions, the validity of the models, the resolution of the data, and the nature of multiple pulses, have to be decided on the basis of analyses of data rather than by intuitive reasoning or fitting the data to unverified theoretical models.

In this report, we discuss work done to help resolve the questions discussed above about the nature of the first several seconds of the direct P waveform from explosion sources. First, we discuss previous work on this problem and pitfalls associated with attempting to identify the pP phase on short period records of explosions. Subsequently we shall briefly present results from spectral ratio techniques for estimating the pP-P delay times and amplitudes and from stacked deconvolutions which enhance the pP phase on seismic records. The rest of this report is a description of the results of using a maximum likelihood multichannel deconvolution technique for estimating time domain spike series for both the source and site terms. Four appendixes at the back of the report contain further examples of the data and results of the work. Finally, we present suggestions for future work.

We find that explosion source time functions, while they generally appear to contain a phase that is readily ascribable to pP, also contain a number of other arrivals. Both source and site terms contribute to the presence of P coda. The deconvolution of a presumed cratering event shows a more complex initial P waveform than that obtained from buried explosions,

without a clearly discernible pP. From these deconvolutions, we estimate the cratering-noncratering  $m_b$  bias to be 0.09 to 0.22 magnitude units.

### Background

A variety of methods have been proposed for estimating pP times and amplitudes. Spectral methods (Cohen 1970, 1975; Shumway and Blandford 1978) attempt to make use of the spectral modulation due to pP and are successful only if no other secondary arrivals are present. In the presence of numerous secondary arrivals the spectra are modulated according to combinations of all of the time differentials of the various arrivals, thus resulting in a complex modulation pattern that cannot be inverted easily. In the case of complex site related modulation of P wave spectra, the spectral minima due to any, even solitary, pP arrival besides the direct P, may be completely disguised, thus making the interpretation of spectral minima difficult. Moreover, even in the absence of site related modulations it is impossible to reconstruct the source related spike sequences from power spectra, since these methods discard the phase information. The same power spectrum can correspond to an infinite set of spike sequences and these spike sequences can be derived from each other by applying arbitrary "dispersive" filters to them (Robinson and Treitel 1980). In Figures 1 and 2 we illustrate sets of time functions that have *exactly* the same power spectra. Several of these could be interpreted as complex "pP" and "spall" arrivals following a P. As soon as we allow even a distorted pP we have nonuniqueness since a combination of a "P" and a "low frequency pP" can have spectra not different from that of a single delta function (Figure 1).

Time domain methods include various deconvolution schemes (Marshall 1972; Bakun and Johnson 1973; Kemerait and Sutton 1982; Israelson 1983) which generally preserve the phase information. Least squares ( $L_2$  norm) deconvolution models work well, but those that use the  $L_1$

Spike Sequences with  
the same Power Spectrum

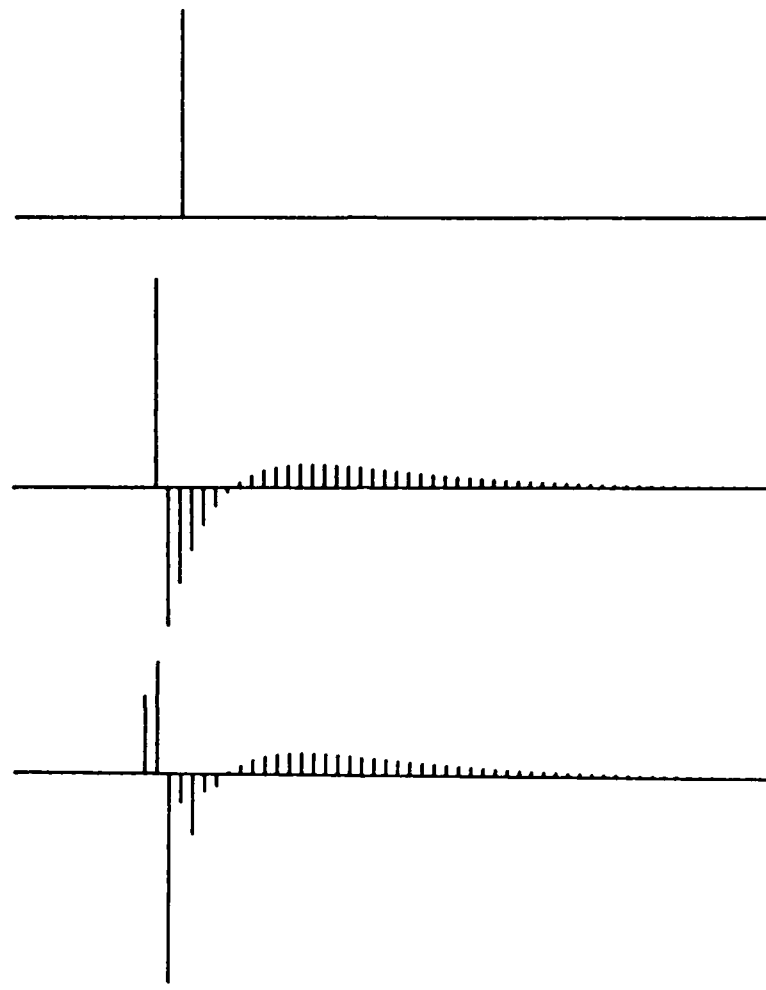


Figure 1. Three spike sequences with identical power spectra, but different phase. The second spike sequence might be interpreted as "P" plus "low frequency pP".

Spike Sequences with  
the same Power Spectrum

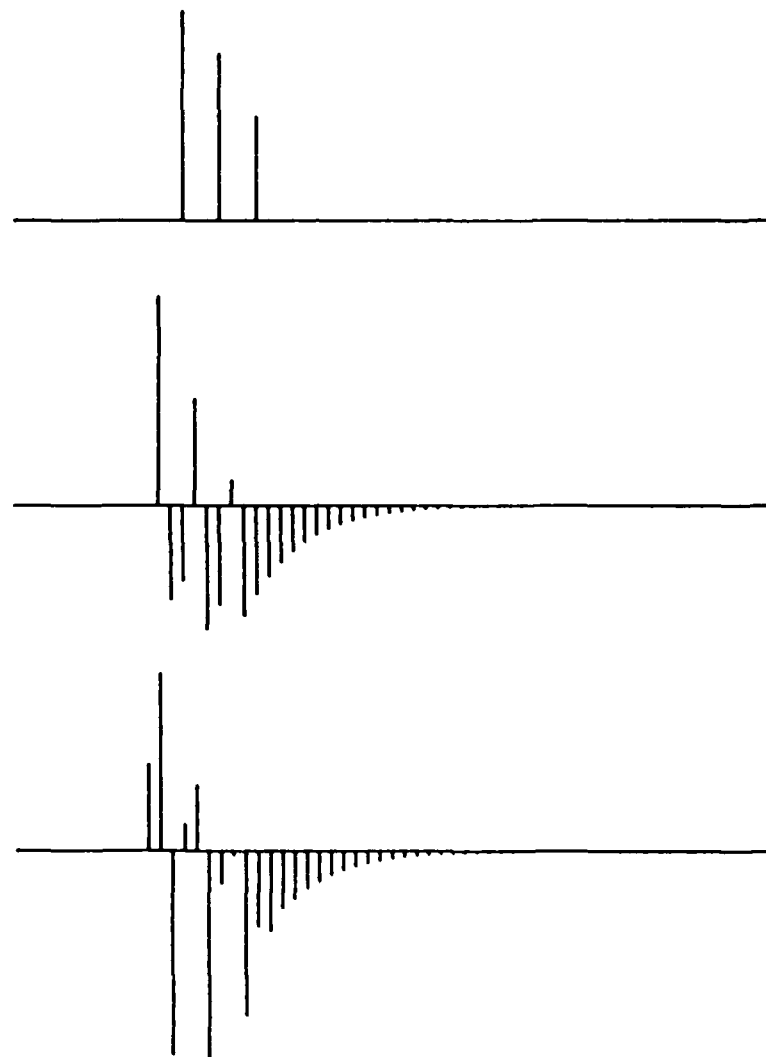
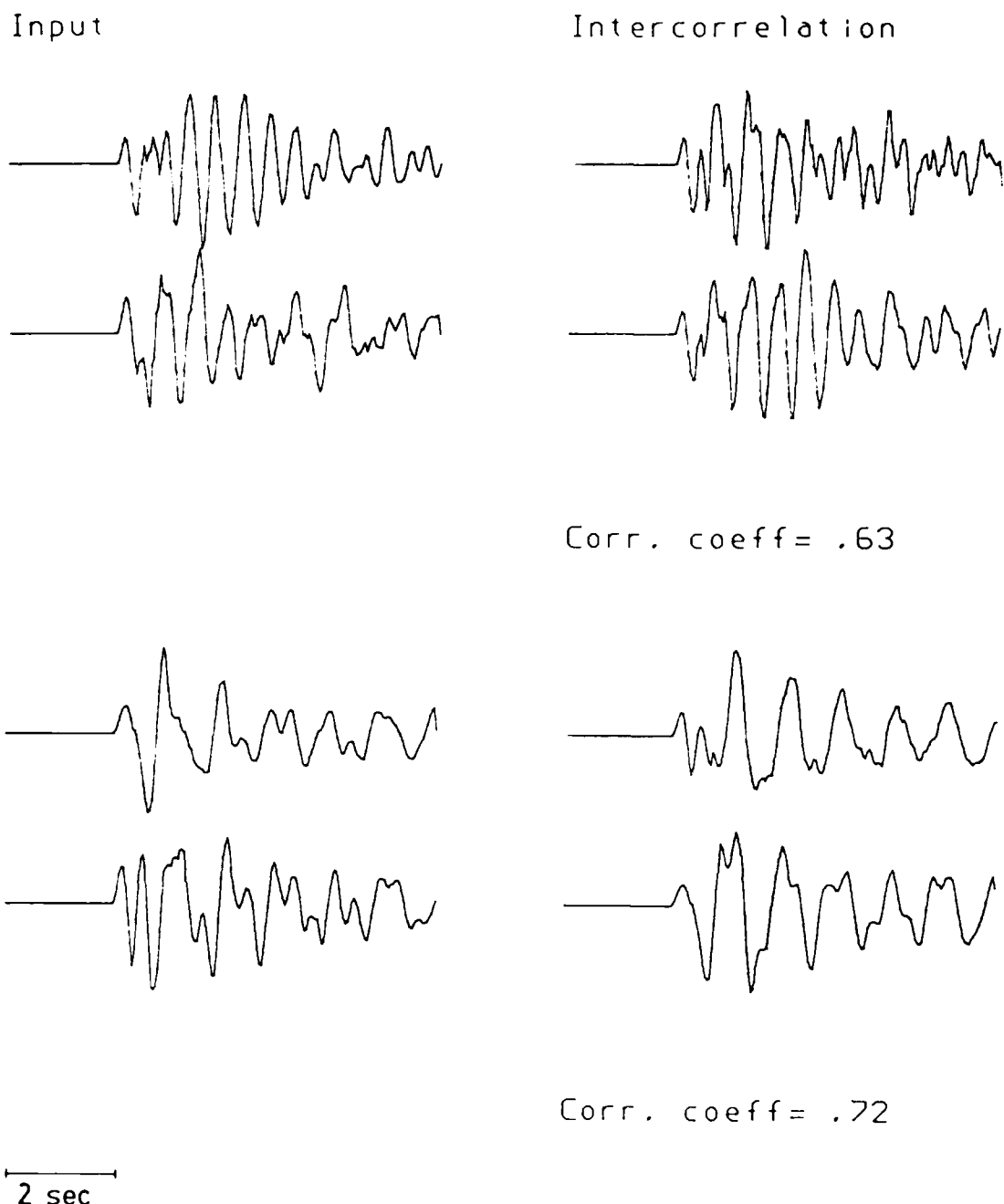
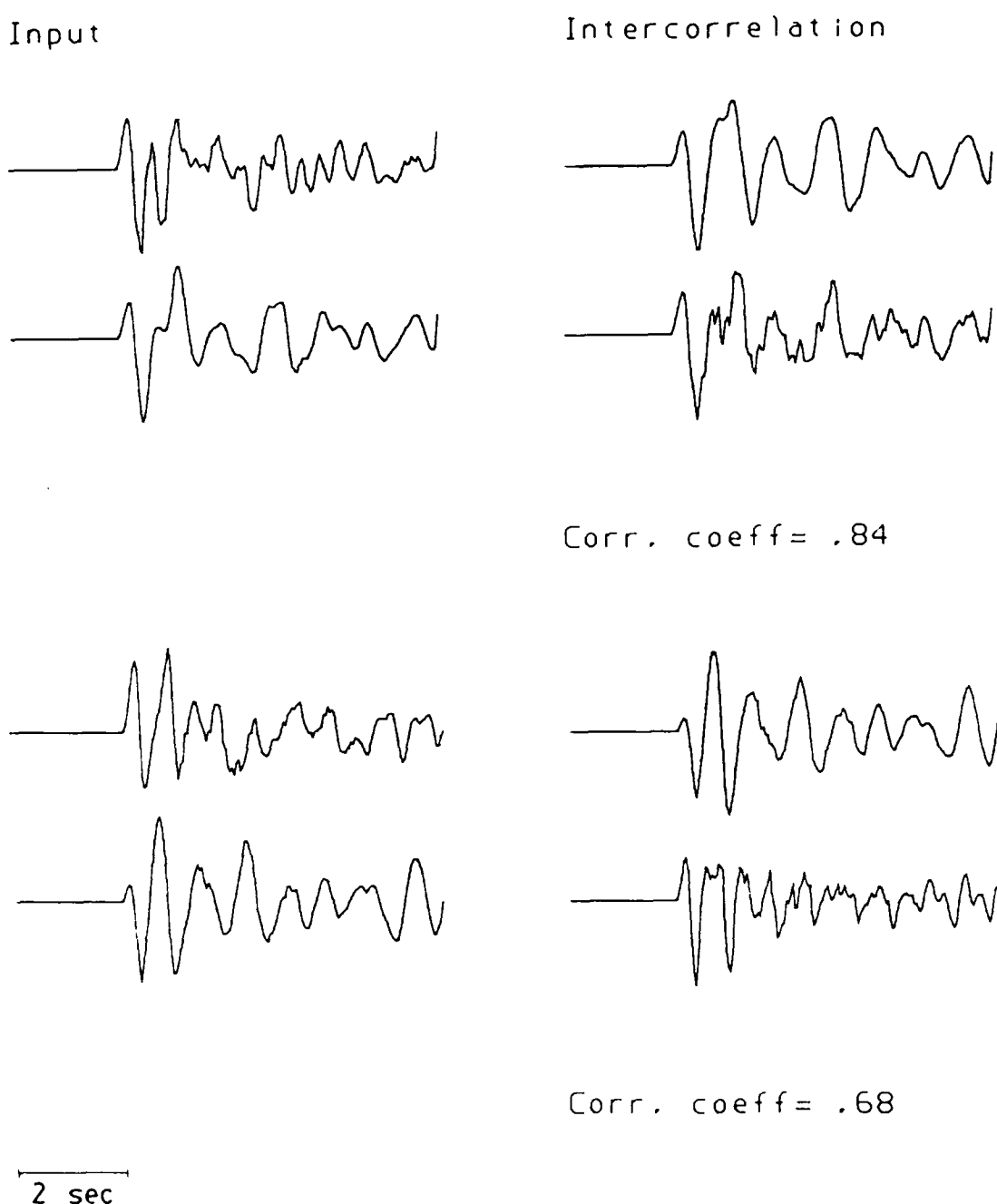


Figure 2. Three spike sequences with identical power spectra, but different phase.

norm (Levy and Fullagar 1981; Mellman et al 1984) were shown by Jurkevics and Wiggins (1984) to result in erroneous deconvolutions as judged by synthetic simulations. Another method that has been tried for the determination of pP times is the direct modeling of P waveforms. It has been shown (Cormier 1982) that such waveform fits are highly nonunique because  $t^*$ , pP times and amplitudes, and the various explosion source parameters trade off against each other. A different approach that has been proposed involves cross-equalization (or as the authors call it, "intercorrelation") of waveforms (Mellman and Kaufman 1981; Lay et al 1984a). This method produces "pseudo-pP" delay times and amplitudes, i.e. the best fits to simple P+pP models. Since the results are not deconvolutions in the true sense they do not prove the existence or correctness of such models. The problem with such time domain methods is that there is no established quantitative relationship between the quality of fit, where the fit is commonly based on the use of some kind of a norm (Lay et al 1984a; Mellman et al 1984), and the level of confidence attached to a hypothesis that the P+pP model is valid. This can be illustrated by synthetically simulating the case in which many secondary arrivals are present. We have constructed "receiver functions" by appending an impulse with a gradually decaying Gaussian noise sequence. For the source pulse we have used a narrow band pulse of the type commonly generated by seismic sources at teleseismic distances as seen through WWSSN type instruments and then generated a "source spike series" by following a unit impulse with a burst of Gaussian random noise of unit maximum amplitude with a duration of 1.25 seconds. These are certainly more complex than a P+pP sequence. Despite this, applying the "intercorrelation" method we were able to achieve correlation coefficients of the same order as those seen in the study of Lay et al (1984a). Figures 3 and 4 show four examples of the input traces, the traces after intercorrelation, and the resultant correlation coefficient. Thus the "intercorrelations" with real data prove that the P+pP models are too simplistic, since otherwise, instead of values near 0.6 to 0.9, we should be able to obtain, routinely, correlation



**Figure 3.** Synthetic inputs (on left) and their "intercorrelations" (on right) with the resulting correlation coefficients.



**Figure 4.** Synthetic inputs (on left) and their "intercorrelations" (on right) with the resulting correlation coefficients.

coefficients near 0.95. It appears that with narrow band data it is possible to convert practically anything into anything as long as the spike sequences of the various sources have short time durations (which seems to be the case). Thus, the intercorrelation method may sometimes yield valid results, but only if the obtained correlation coefficients are very high, say above 0.95. Most of the time, however the low values of the correlation coefficients obtained after "intercorrelation" indicate that the underlying model is wrong.

As the last item on our list of deconvolution methods, we mention the approach suggested by Mellman et al (1984) that consists of a set of trial deconvolutions varying the P-pP time lag. It is claimed that the changes in the waveform characteristics and amplitudes in the deconvolution results indicate the "best" pP delay. Unfortunately, this is not the case. Since the inverse of the P+pP pair is an exponentially decreasing comb filter it will always produce the simplest waveform with the minimum amplitude near half the dominant period of the original wave and will give a ringing, large amplitude waveform for lag times close to the period of the wave. The nature of the output is thus determined by the dominant period and has nothing to do with pP characteristics.

Basically, the same kinds of problems affect all methods proposed for the estimation of the pP times of nuclear explosions. Generally speaking, it may be stated that all proposed techniques seem to work quite well with synthetic data that incorporate the assumptions about the makeup of the P wavetrain that were used in the design of the deconvolution method itself. Most of the new methods for determining pP parameters have been carefully checked to verify that the method works for the signal model it was based on. The same care was not applied, generally, to verify from the data that the underlying models are valid. This explains why the results obtained from real data are so ambiguous. The advantage of the maximum likelihood estimation method discussed later in this study is that it assumes little about the nature of the

source and site factors, and it is based mostly on the factorable nature of P wave spectra which is verified by the successful reconstruction of the original data. We must caution the reader also that the successful reconstructions (resulting in high values of measures of coherence between synthetic and real data) or cross-equalizations (Lay et al 1984a) of narrow-band body wave data do not by themselves prove the correctness or uniqueness of the pP, spall, and other parameters derived by such methods. Generally, waveform matches are nonunique and are not valid substitutes for true deconvolutions in which the multiple arrivals, if any, are separated and become identifiable by the enhancement of the high frequency content. Only deconvolved records overcome the weakness in human perception that makes us unable to distinguish multiple arrivals convolved with filters that severely limit the bandwidth. In addition, statistical techniques are needed to gauge the resolution available with the given data.

We conclude, therefore, that our preconceptions about the structure of teleseismic body waves are more likely to be at fault than any techniques that were proposed. In other words, if the teleseismic P waves were simply convolutions of a P-pP pair of pulses with some random time function appropriate to a seismic path the problem of finding unique pP estimates would have been solved long ago. The continuing "lack of success" in this field must thus be due to the fact that even "simple" events such as nuclear explosions radiate quite complex wavetrains and the underlying physical processes are not well understood.

### Spectral Ratios

In this section, we briefly discuss the results of using a simple spectral ratio method to put constraints on the pP amplitude and arrival time. Spectral ratios between two explosions from the same source region were taken at various stations of NORSAR. Thus, since the events were from the same source region, near-source site effects should nearly cancel out, as

should receiver effects since both events in each pair arrive on nearly the same azimuth. The sequence of peaks and nulls that make up the spectra should then simply be due to the interference of the different pP amplitudes and delay times of the two events.

Representative spectral ratios between the same pair of events at different NORSAR receivers are shown in Figures A1 to A4 of Appendix A. Synthetic spectral ratios are also shown on each figure. These were made assuming a von Seggern and Blandford (1972) source time function for each event, and using yield, pP amplitude, and pP time estimates from Lay et al (1984a) as shown in Table A1 in Appendix A. For each pair of events, the spectral ratios at the different receivers have many similarities in even small details of these spectral ratios at the various receivers. It is clear that the synthetic spectral ratios derived from the simple P+pP model are generally not consistent with the observed ratios. This cannot be attributed merely to incorrect estimates of pP delay times and amplitudes, but a more likely reason is the presence of additional arrivals in the initial part of the P wave record besides possible P and pP. The existence of complex multiple arrivals originating from the source is also confirmed by our deconvolution results presented below.

The presence of additional complications in the source time function is also suggested by the spectra themselves. Few spectra from nuclear explosions, with some notable exceptions such as the very deep Amchitka shots and the Bukara shot (Marshall 1972), show clear spectral nulls at the times predicted from the interference of P and pP. Also, spectra of synthetic wavelets generated for propagation through random media by the finite difference method show only hints of spectral nulls, while spectra of synthetics generated by propagation through simple, plane layered media show distinct spectral nulls (McLaughlin et al 1986). An example of such results is shown in Figure 5, which compares the expected teleseismic P waveforms from explosion sources in a two-dimensional model of Yucca Flats with those computed for a simi-

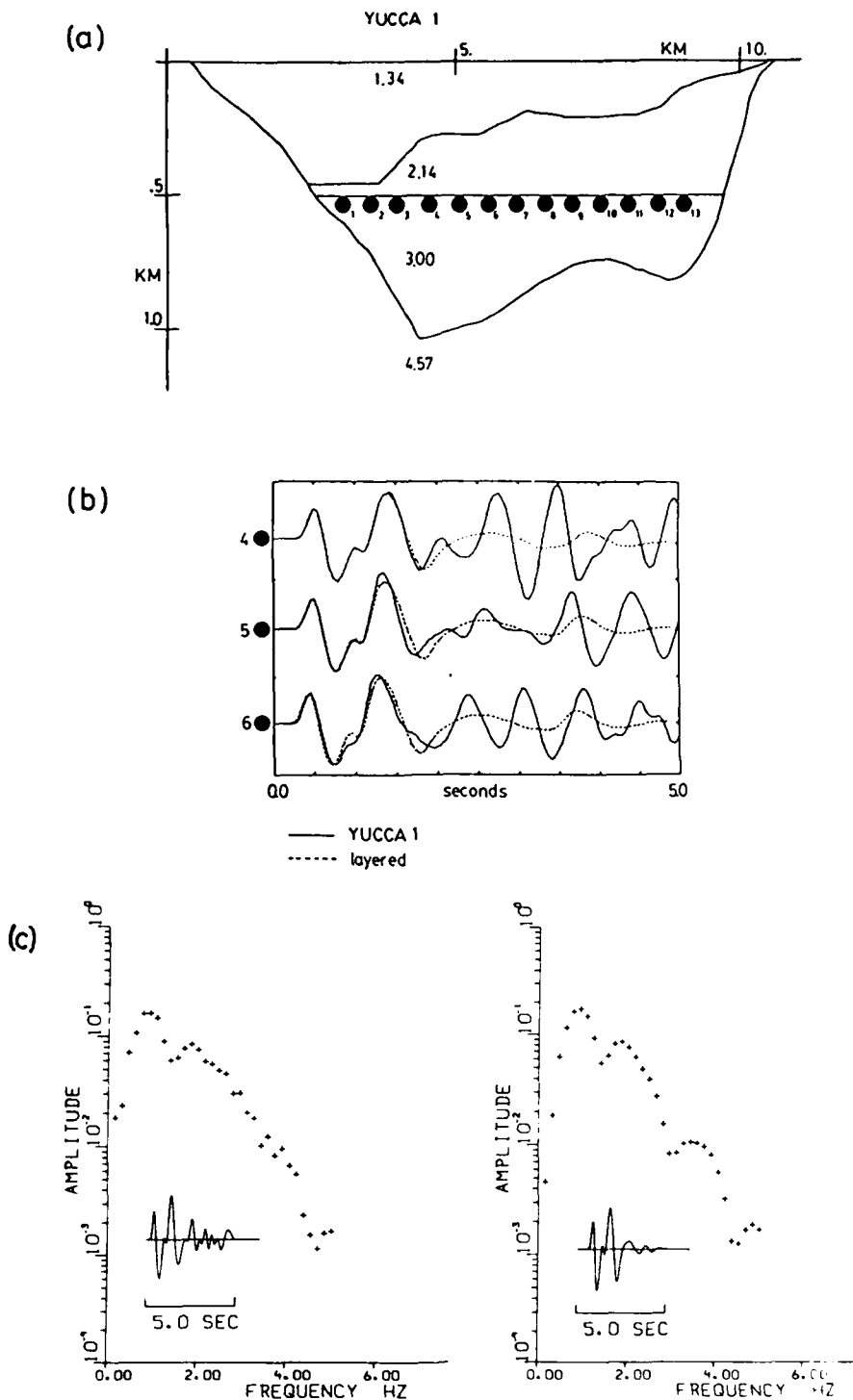


**Figure 5.** (a) West-to-east model for geologic structure across Yucca Valley used in finite difference simulations. The model is shown with 5-to-1 vertical exaggeration, and each region is labeled with its P-wave velocity. P-wave velocities of 1.34, 2.14, 3.00, and 4.57 km/sec are indicated for the geologic units of alluvium, unsaturated tuff, saturated tuff, and Paleozoic carbonates, respectively. The source locations are indicated by numbered dots across the middle of the figure. (b) Synthetics for source locations 4, 5, and 6 at take-off angle of 15 degrees (solid lines) compared to synthetics for a plane-layered model (dashed lines). (c) Spectra of the synthetics for source location 5 of the Yucca Valley model (left) and for the plane-layered model (right) showing the much more distinct spectral nulls in the spectra of the synthetics from the flat-layered model (after McLaughlin *et al* 1986).

lar but flat layered structure. After the initial 1.5 seconds, the waveforms from the two models are very different. This example illustrates that complex multiple arrivals, not simple combinations of P and pP, should be generally observed from many laterally varying geological structures containing sources. The physical nature of the complex later arrivals in this case is probably conversion of Rayleigh waves to P at the sides of the valley.

Complications are also observed in the receiver terms. Figures A5 to A8 in Appendix A show intersensor spectral ratios at NORSAR for Nevada Test Site (NTS) nuclear explosions; use of ratios cancels out the source spectra. While the shapes of spectral ratios below 4 Hz are similar for the same pairs of sensors, the strong variations in these ratios with frequency indicates that details in the spectral shapes at any given site are unstable for arrivals from a limited source region. This result is not surprising, since waves propagated through media with random velocity variations commonly reveal variations in details of their spectra while the gross shapes are relatively constant after propagating roughly the same distance (Frankel and Clayton 1984). Moreover, even if one assumes a flat layered medium for a crustal structure, it would change the details in the spectral shapes, while leaving the overall slope relatively constant. Thus, there are too many variations in the source and receiver information derived from the spectral ratio methods used here to provide significant estimates of the amplitude and delay time of pP or to provide information on other phases which are part of the initial P wavetrain.

### Stacked Deconvolutions

Another simple method for the estimation of pP parameters is by deconvolving the records assuming that the source pulse is known. We assume that the source pulse is made up of the explosion far-field pulse, a constant Q operator, and the instrument impulse response. Although several models were proposed for the explosion far field pulse and its scaling with

respect to yield and depth (Mueller and Murphy 1971; von Seggern and Blandford 1972, Lay et al 1984b), the differences between them do not influence the practical results much. To illustrate this, in Figure 6 we show some deconvolutions of wavelets, where the wavelets were derived from convolving a short period instrument response and an attenuation operator with source pulses of the von Seggern-Blandford and Mueller-Murphy types. The deconvolutions used two-sided Wiener filters designed from the autocorrelation functions of the wavelets to which a 50% delta function was added to simulate white noise. The effect of this adjustment is to make the deconvolution less precise, thus avoiding swamping the results with amplified high frequency noise. This has the same effect as the  $\theta$  parameter in the maximum likelihood deconvolutions shown below. Each wavelet was deconvolved separately with both source pulses. The only effect of using the wrong type of source pulse in the deconvolutions is some asymmetry in the deconvolved wavelets which would hardly cause problems in any practical work in separating pulses. Therefore, the most important contributions to the shape of the "wavelet" are the instrument response and the Q operator. While the explosion source model includes a spectral scaling feature, which helps us to deal with explosions of vastly different sizes, we could have used an impulse instead and the results would not have been much different. Thus it appears that the past lack of success in deconvolutions (or rather in finding a simple pP) of real data could hardly be due to uncertainties in the explosion source models. Even if we had used the model by Lay et al (1984b), a model that in our opinion is invalid because it gives the wrong high frequency spectral falloff rate (Murphy and Day 1984), it would not have affected the results much.

The time domain representation of the attenuation operator also depends somewhat on whether Q is frequency dependent or not in the short period band, but refinements such as those to our models must wait until more is known about the frequency dependence of Q. The apparent  $t^*$  along most seismic paths should be estimable from the gross shapes of spectra with

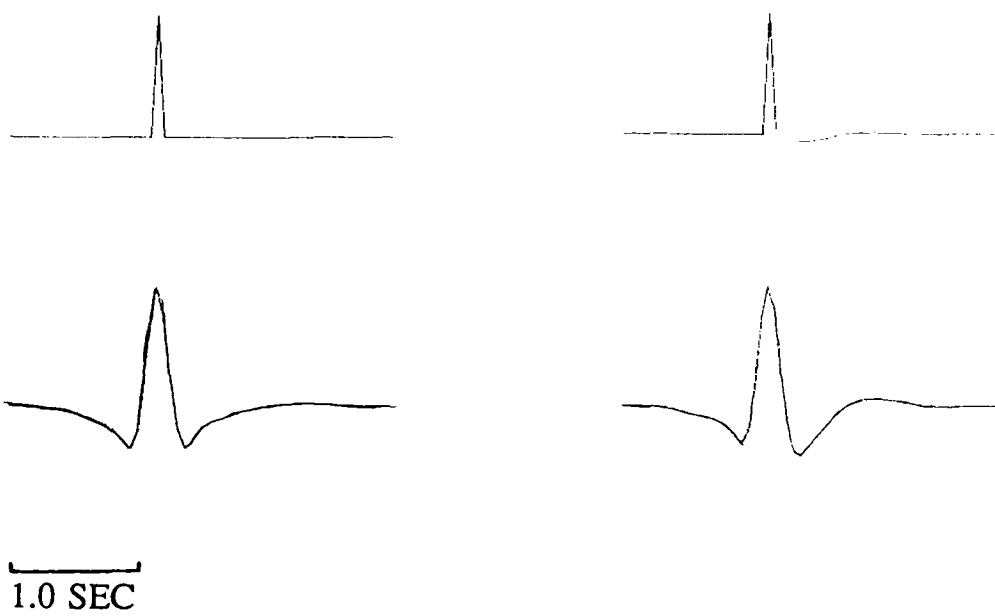


**Figure 6.** Deconvolutions of theoretical source time functions. The original source time functions on the left were made using the von Seggern and Blandford (1972) model (vSB) while those on the right were made using the Mueller and Murphy (1971) model; all four source time functions were deconvolved with the vSB model using a Wiener filter. The upper two source functions were not prewhitened; the lower two were prewhitened by increasing the zero lag autocorrelation value by 50%. The only difference in the deconvolutions due to the different source functions is a slight asymmetry.

an accuracy of about 0.1 sec (Der et al 1985).

In order to reduce the effects of site related distortion of the pulses we follow Marshall (1972) in stacking the deconvolutions over widely distributed sensors of large arrays. This way we obtain, hopefully, deconvolved source spike sequences in which the site effects are averaged out, or at least, reduced. These results are equivalent to the outputs of the first iteration in the multichannel deconvolution method described later in this report. As we shall see later the results are quite similar, but because of the more refined nature of the latter we place more trust in the results of the iterative method. Nevertheless, the results of this simpler approach serve as good preliminary checks of the multichannel iterative method.

Results of the stacked deconvolutions for 5 NTS events at NORSAR are shown in Figure 7. Most of these events show a late negative pulse near 1 second after the first arrival, but are more complex than a simple P+pP pair. Stilton shows an early arrival of negative polarity, and Inlet shows a very early arrival of negative polarity.

The stacked deconvolutions of four Eastern Kazakh explosions at EKA in Figure 8 show an early (0.4 sec) inverted pulse following the first positive pulse. The top trace appears to be different from the rest in the deconvolved waveform; this is an assumed cratering event that will be discussed again in more detail below.

The stacked deconvolutions in Figure 9 of the same Kazakh explosion recorded at three AWRE arrays are interesting in that they are very similar. It appears that this event was fairly symmetric azimuthally and was probably not associated with significant strain release or other asymmetries in radiation, at least in the short period band.

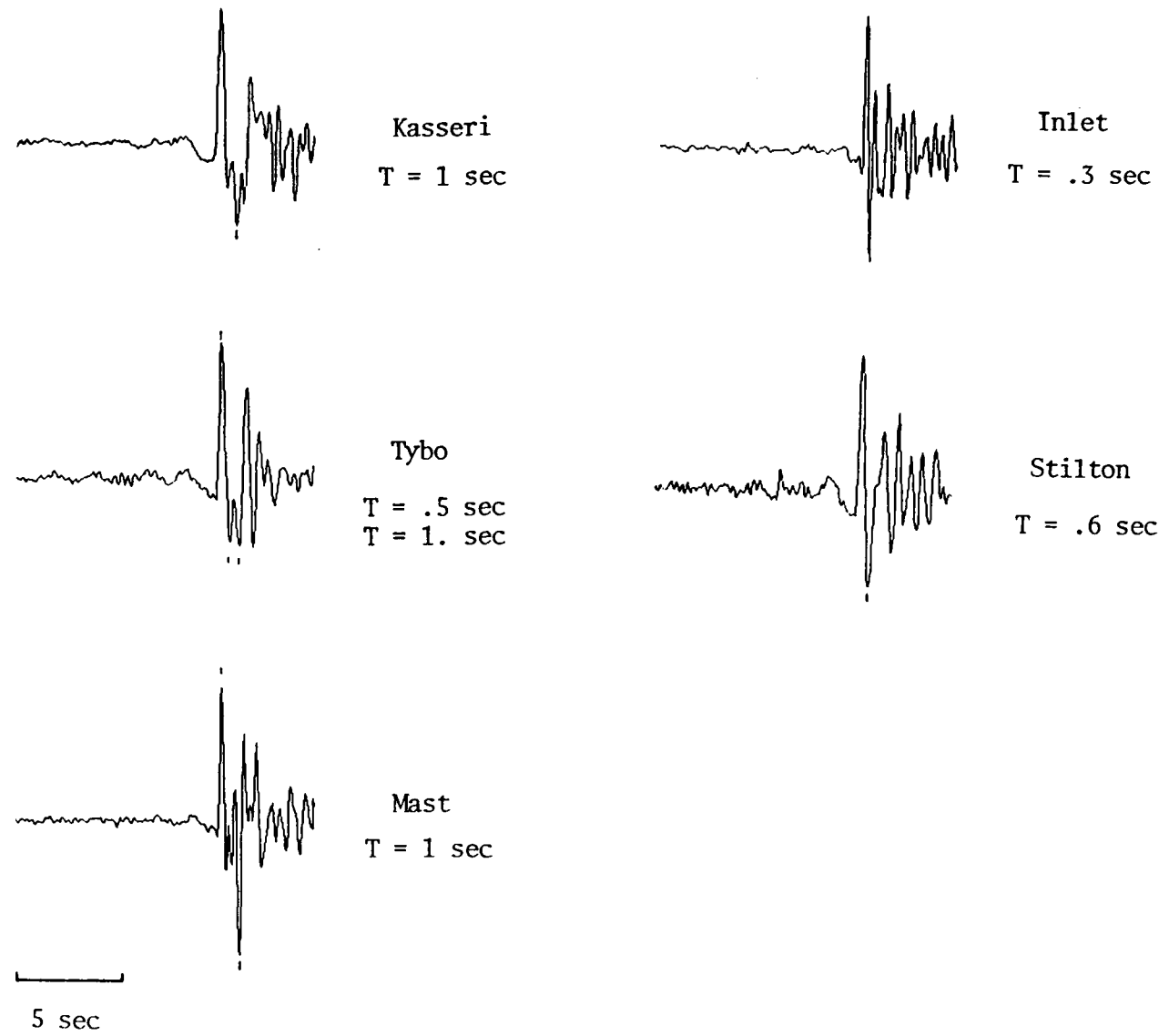
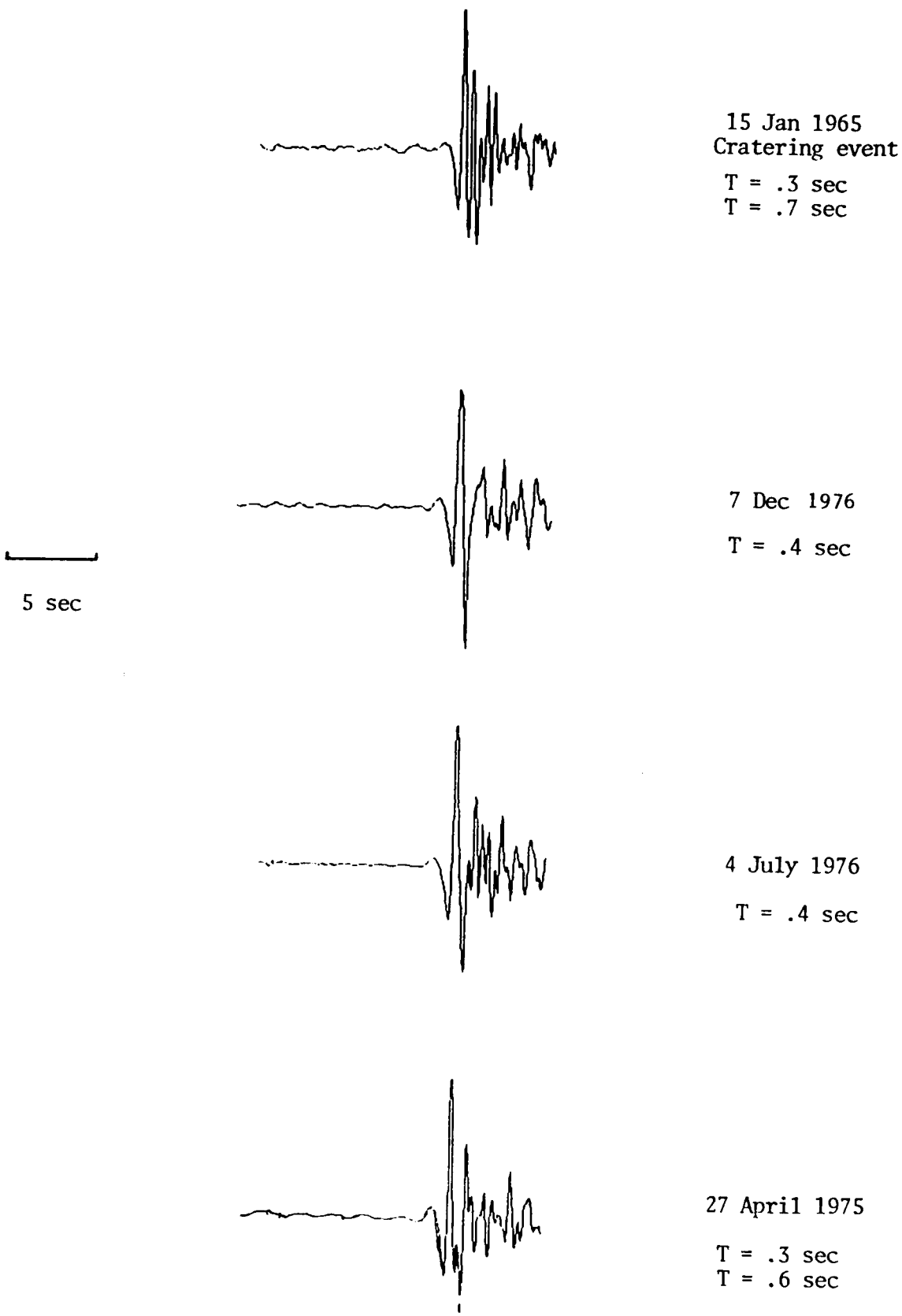
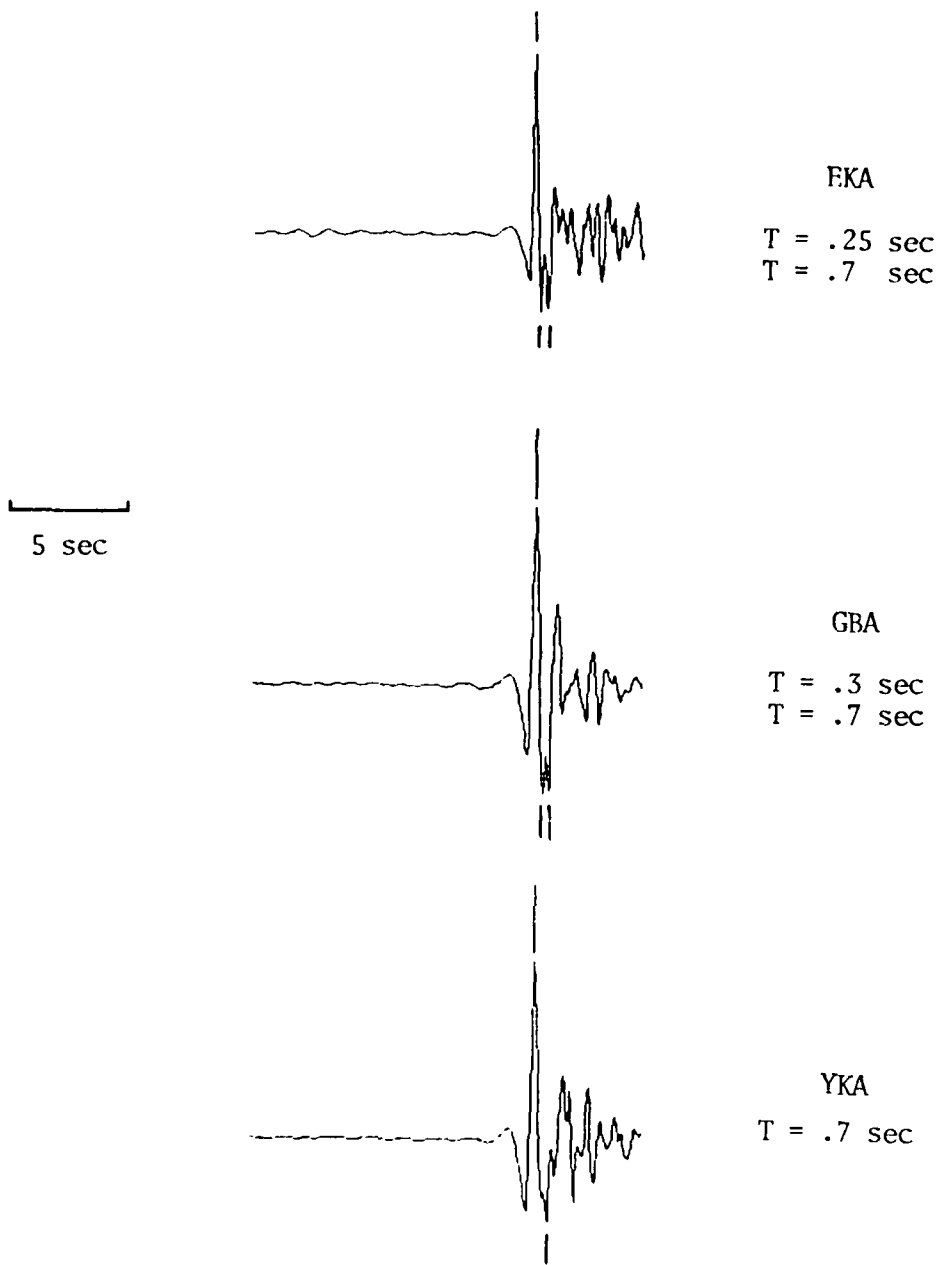


Figure 7. Stacked deconvolutions of five NTS events recorded at NORSAR. Estimates of the pP delay time inferred from the deconvolutions are shown to the right of the traces.



**Figure 8.** Stacked deconvolutions of five Eastern Kazakh explosions recorded at EKA. The top event is a presumed cratering explosion and has a noticeably more complex deconvolved waveform. Estimates of the pP delay time inferred from the deconvolutions are shown to the right of the traces.



**Figure 9.** Stacked deconvolutions of an Eastern Kazakh explosion (20 February 1975) recorded at the AWRE arrays EKA, GBA, and YKA. The similarity of the results for the same event recorded at different azimuths suggests that the source was fairly symmetric. Estimates of the pP delay time inferred from the deconvolutions are shown to the right of the traces.

### Maximum Likelihood Multichannel Deconvolutions

#### Description of the Deconvolution Method

A major advance in the understanding of the structure of teleseismic P waves was the finding by Filson and Frasier (1972) that P wave spectra from a set of events observed at a narrow range of azimuths at multiple array sites may be factored as

$$Y_{ij}(\omega) = R_i(\omega) S_j(\omega), \quad (1)$$

where  $Y_{ij}(\omega)$  are the P wave spectra,  $S_j(\omega)$  are source factors, and  $R_i(\omega)$  are factors appropriate to the receiver sites. The validity of this equation has been verified for a number of seismic arrays as well as more widely separated receivers (Lundquist et al 1980) and the idea was also exploited for deriving "relative receiver functions", which are time domain representations of intersite transfer functions (Lundquist et al 1980) including Q effects.

In this report we shall talk of "receiver factors" and "source factors" in order to make the distinction from the related concept of "relative receiver functions", which also incorporate some additional assumptions (Hart et al 1979), such as the maximum "spikiness" condition (Wiggins 1978), which are not required by the physics of the problem. We separate the Q operator, the instrument, and a von Seggern and Blandford (1972) source wavelet from the "source factor" and combine these in an assumed known source wavelet,  $A_j$ . Thus,  $S_j(\omega) = A_j(\omega)X_j(\omega)$  where  $A_j(\omega)$  is the spectrum of the combined source wavelet, instrument, and t\*. This way the "source factor",  $X_j(\omega)$ , is a Fourier transform of a spike sequence associated with the radiation from a source and the "receiver factor",  $R_i(\omega)$ , is the Fourier transform of the site transfer function. Since the receiver factors strongly depend on the azimuths and distances of the sources, they may be assumed to be constant for a given sensor only for limited source regions.

If we have  $N$  receivers and  $M$  sources, we may describe ( $N \times M$ ) P wave spectra (or time series) in terms of  $N + M$  factors; there is thus a considerable degree of redundancy in the problems with  $N$  and  $M$  sufficiently large. This helps us to separate the  $R_i(\omega)$  from the  $X_j(\omega)$ . This cannot be achieved uniquely, however, unless something is known *a priori* about the properties of each. Otherwise, common spectral factors can be assigned to either the source or receiver factors, or canceling, reciprocal factors may be assigned to both the receiver and source factors as indicated below:

$$Y_{ij}(\omega) = [R_i(\omega) F(\omega)] [F^{-1}(\omega) X_j(\omega)] \quad (2)$$

Since all P wave signals are embedded in the noise backgrounds, it is desirable that the deconvolution-factoring process is optimized in some way with respect to the noise i.e., we are trying to find some compromise between the resolution and the S/N ratio. Although the original derivation of Shumway (1984) includes weighting with respect to noise spectra, in this work we are not striving for maximizing the S/N ratio, but seek some compromise between the time resolution of the deconvolution and the output noise level.

The detailed derivation of the multichannel deconvolution method is given in Der et al (1983) and Shumway and Der (1985). Only the key formulas are repeated here:

$$\hat{X}_j = \frac{\sum_i \bar{A}_j \bar{R}_i Y_{ij}}{\sum_i |A_j|^2 |R_i|^2 + \theta_j} \quad \text{where } \theta_j = \frac{P_v}{P_{x_j}}, \quad (3)$$

$$\sigma_j^2 = P_v \left[ \sum_i |A_j|^2 |R_i|^2 + \theta_j \right]^{-1}, \quad \text{and} \quad (4)$$

$$\hat{R}_i = \frac{\sum_j \bar{A}_j \bar{X}_j Y_{ij}}{\sum_j |A_j|^2 \left( |\hat{X}_j|^2 + \sigma_j^2 \right)}, \quad (5)$$

where

$Y_{ij}$  data

$A_j$  source wavelet spectrum

$R_i$  receiver spike response

$X_j$  source spike sequence

$\theta$  adjustable S/N ratio

$P_v$  noise power spectrum

$P_z$  initial signal power

$\sigma_j^2$  effective noise power in second step

and an overbar denotes the complex conjugate. The  $i$ 's correspond to the individual receiver sites and the  $j$ 's to the individual sources. Equations 3 through 5 are very similar to those presented by Oldenburg (1981) and Oldenburg et al (1981), and are essentially multichannel versions of the same.

The deconvolution is done in the frequency domain. The first step is to factor out the "known" spectra consisting of  $t^*$ , the source function, and the instrument response. Since we are working with source and receiver arrays, we assume that the attenuation parameter  $t^*P$  is the same for all sensors and that all instruments have the same response. At the start of the iteration process the source and site functions are each initialized to an impulse in the time domain. The flow diagram of the iterations is depicted in Figure 10. After several iterations, each source term will contain the terms common to that source at all receivers including the source pulse, pP and spall arrivals, and any scattering contributions that may be associated with

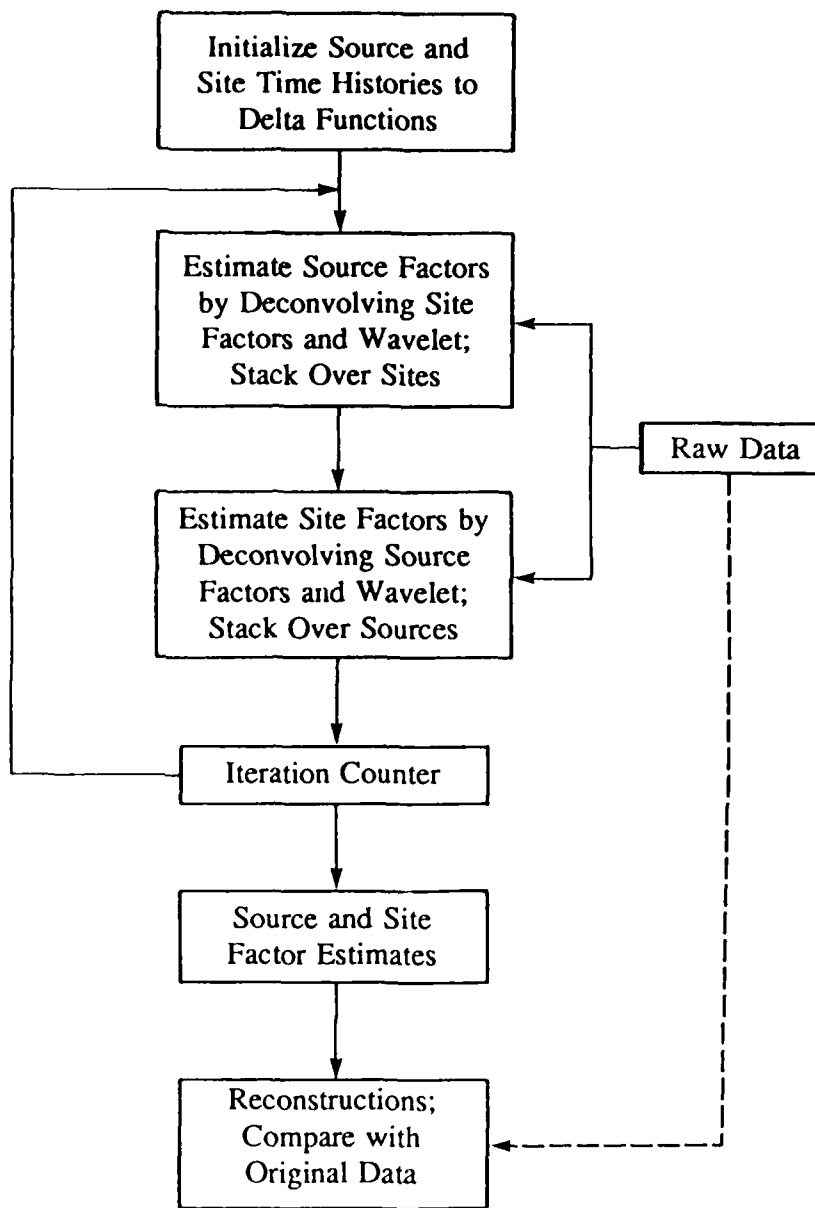


**Figure 10.** Flow diagram of the iterative maximum likelihood multichannel deconvolution algorithm. In the center, the second and third boxes from the top correspond to equations (3) and (5) in the text, respectively.

a particular source. Each site term will contain the terms common to that site for all sources, mostly the random scattering effects attributable to the structure near the receiver. The results are checked by reconstructing each input trace from the convolution of the appropriate source and site terms with the wavelet consisting of the von Seggern and Blandford source pulse,  $t^*$ , and instrument response. The differences between the original and reconstructed seismograms can be inferred as a measure of the scattering unique to each individual path i.e., energy unaccounted for by either site or source factors, and thus missing in the reconstructions.

This multichannel deconvolution approach for estimating source and site region characteristics has several advantages. First, the method utilizes both amplitude and phase information in the frequency domain calculations. Furthermore, no *a priori* assumptions need to be made about the complexity of either the source or the site spike series, e.g. the presence of pP does not need to be presupposed by providing an initial guess of the pP delay time and amplitude.

These iterative formulas yield progressively improved estimates of the source and receiver factors and their equivalent time functions. It is apparent from equation (3) that the procedure is similar to the iterative beaming method (Blandford et al 1973) in which the previous estimates of the site and receiver factors are deconvolved in each step. The resolution kernels characterizing the attainable resolution with the given bandwidth are also plotted at the conclusion of the iterative process.

### Results of the Data Analyses

Four data sets have been analyzed in this study: five nuclear explosions from the Nevada Test Site (NTS) recorded at five stations of NORSAR, eight explosions from the East Kazakh Test Site (KTS) recorded at five stations of NORSAR, four Astrakhan explosions recorded at four RSTN stations, and 5 KTS explosions, including a presumed cratering explosion, recorded

at twelve stations of the AWRE array EKA. The events in each data set are described in Tables 1 to 4 and the parameters used in the deconvolutions are in Table 5.

The following approach was used to prepare the data. All traces were lined up in time on the first arrival. Since we are not interested in the absolute amplitudes in the context of estimating relative pP times and amplitudes, and because we want to give roughly equal weight to all the traces to ensure effective factoring, we multiplied each trace with two factors, one appropriate to the event, the other one to the site, which were designed to approximately equalize all peak amplitudes. This method is in agreement with the multiplicative structure of the spectra, and the exact values of the equalizing factors do not matter. The equalizing of traces conflicts some with the optimization of the S/N ratios in the output, but as mentioned above this is not our main goal. After processing, the initial normalization factors can be divided out to estimate the proper relative amplitudes of the deconvolved traces.

The iteration procedure is started with the initialization of the time domain representations of the source and site factors to delta functions. The source factors are estimated first by summing the deconvolved results over the sites. This way the first estimates of source functions are similar to those obtained by Marshall (1972), but during the subsequent iterations both the source and site factors have been further refined by factoring.

In order to ensure the desired deconvolution effect we removed the division by the noise spectra, which would have resulted, especially for NTS events which have the maxima in S/N ratio below 1 Hz, in no visible deconvolution at all. Instead, we have assigned a unit weight to all frequencies which had S/N ratios above 1 and excluded the frequency ranges with poor S/N ratios from the iterations. Again, this degrades the S/N in the output, but we accept this as the price of increased resolution.

**Table 1**

Source Parameters for NTS Events Recorded at NORSAR			
Date	Name	Location	$m_b$ (ISC)
14 May 1975	Tybo	Pahute Mesa	5.9
03 Jun 1975	Stilton	Pahute Mesa	5.8
19 Jun 1975	Mast	Pahute Mesa	5.9
28 Oct 1975	Kasseri	Pahute Mesa	6.2
20 Nov 1975	Inlet	Pahute Mesa	5.9

**Table 2**

Source Parameters for Eastern Kazakh Events Recorded at NORSAR		
Date	Location	$m_b$ (ISC)
22 Mar 1971	Central KTS	5.8
30 Jun 1971	Eastern KTS	5.4
29 Nov 1971	Central KTS	5.5
16 Feb 1973	Central KTS	5.6
27 Dec 1974	Eastern KTS	5.6
11 Mar 1975	Central KTS	5.4
30 Jun 1975	Eastern KTS	4.8
7 Aug 1975	Central KTS	5.2

KTS=Eastern Kazakh Test Site

Central and Eastern KTS correspond to testing sites within the KTS as identified by Dahlman and Israelson (1977, pp 182-183).

**Table 3**

Source Parameters for Eastern Kazakh Events Recorded at EKA		
Date	Location	$m_b$ (ISC)
15 Jan 1965	Eastern KTS	6.3
27 Apr 1975	Eastern KTS	5.6
4 Jul 1976	Eastern KTS	5.8
7 Dec 1976	Eastern KTS	5.9
11 Jun 1978	Eastern KTS	5.9

KTS=Eastern Kazakh Test Site

Eastern KTS corresponds to a testing sites within the KTS as identified by Dahlman and Israelson (1977, pp 182-183).

**Table 4**

Source Parameters for Astrakhan Events Recorded at the RSTN		
Date	Origin Time	$m_b$ (ISC)
6 Oct 1982	05:59:57.4	5.2
6 Oct 1982	06:04:57.4	5.2
6 Oct 1982	06:09:57.4	5.2
6 Oct 1982	06:14:57.4	5.4

**Table 5**

Parameters used in Multichannel Deconvolutions						
Source Region	Receiver Array	Number of Sources	Number of Receivers	Frequency Bandwidth (Hz)	t* (sec)	Sample Rate (sec <sup>-1</sup> )
NTS	NORSAR	5	5	0.4-3.5	0.45	20
KTS	NORSAR	8	7	0.4-5.0	0.15	20
KTS	EKA	5	12	0.4-5.0	0.15	20
Astrakhan	RSTN	4	4	0.6-5.0	0.15	40

Figures 11 to 14 show the deconvolved source-time functions for the four data sets. Most of the buried explosions show phases which could readily be interpreted as pP, though all the waveforms show a good deal more complexity than can be described simply by P + pP. A good deal of energy arrives for a couple of seconds after the "P + pP" in nearly all the events. Average estimates of pP delay times are 0.7 sec for NTS events recorded at NORSAR (Figure 11), 0.55 sec for KTS events recorded at NORSAR (Figure 12), 0.4 sec for KTS events recorded at EKA (Figure 13), and 1.0 sec for Astrakhan events recorded at RSTN stations (Figure 14). In general, the KTS events (Figures 12 and 13) have simpler source time functions than the NTS events (Figure 11). From figures 12 and 13, there is no obvious difference in the pP delay times between shots at the eastern and central test sites of the KTS (see pages 182 and 183 of Dahlman and Israelson [1977] for a description of the division of the KTS into eastern, central, and western testing sites). The presumed cratering event of 15 January 1965 (bottom of Figure 13) is a notable exception to the other events. The source waveform is visibly more complex than those associated with buried explosions at the eastern KTS and the definition of pP is much more ambiguous. The Astrakhan events (Figure 14) also have fairly complex waveforms (perhaps due to the sharply contrasting velocity structure in a salt dome environment) and long inferred pP times, consistent with suggestions of deep burial.

There is remarkable agreement between the deconvolved source terms from these deconvolutions and from the stacked deconvolutions presented in the previous section. In particular, compare Figure 7 with Figure 11 and Figure 8 with Figure 13.

The deconvolved source terms for the KTS explosions at EKA (Figure 13) were used to estimate the magnitude bias between the four buried explosions and the cratering shot. In an effort to compensate for the differences in yields between the five events, the deconvolved source terms were normalized so that the first zero to peak swing of the P wave has an ampli-

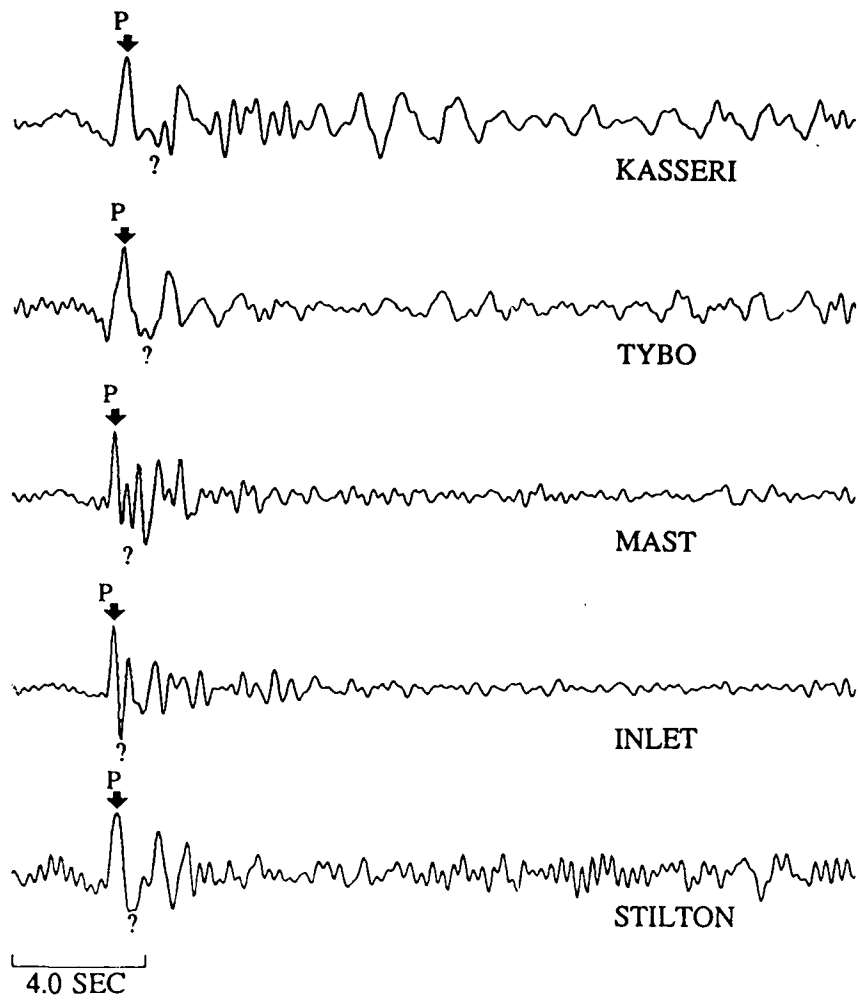


**Figure 11.** Deconvolved source terms for NTS events recorded at NORSAR. Each trace is labeled with the event name and the locations of the P and pP (if observed) phases. Event parameters for these events are given in Table 1.

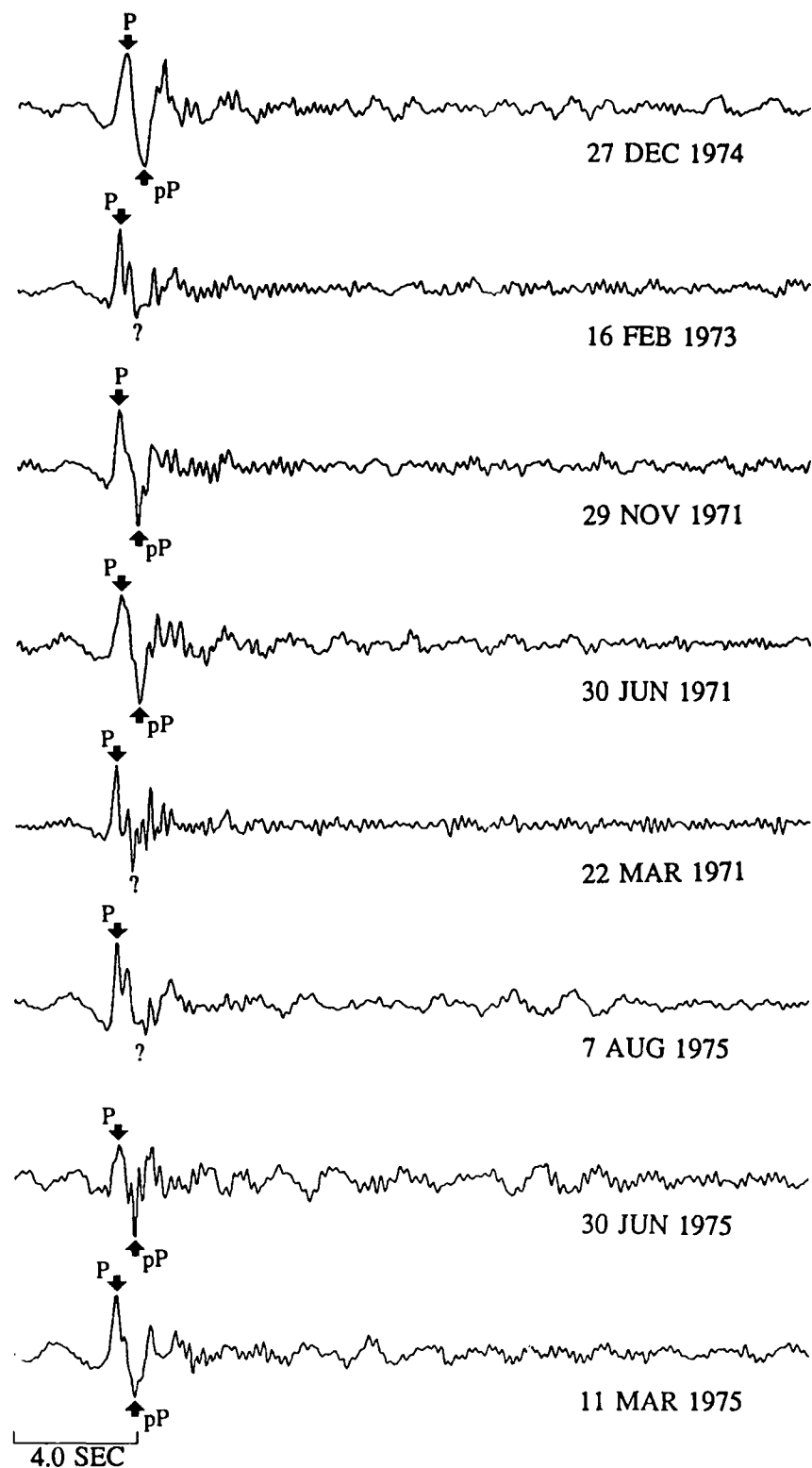


**Figure 12.** Deconvolved source terms for Eastern Kazakh Test Site (KTS) events recorded at NORSAR. Each trace is labeled with the event name and the locations of the P and pP (if observed) phases. Event parameters for these events are given in Table 2.

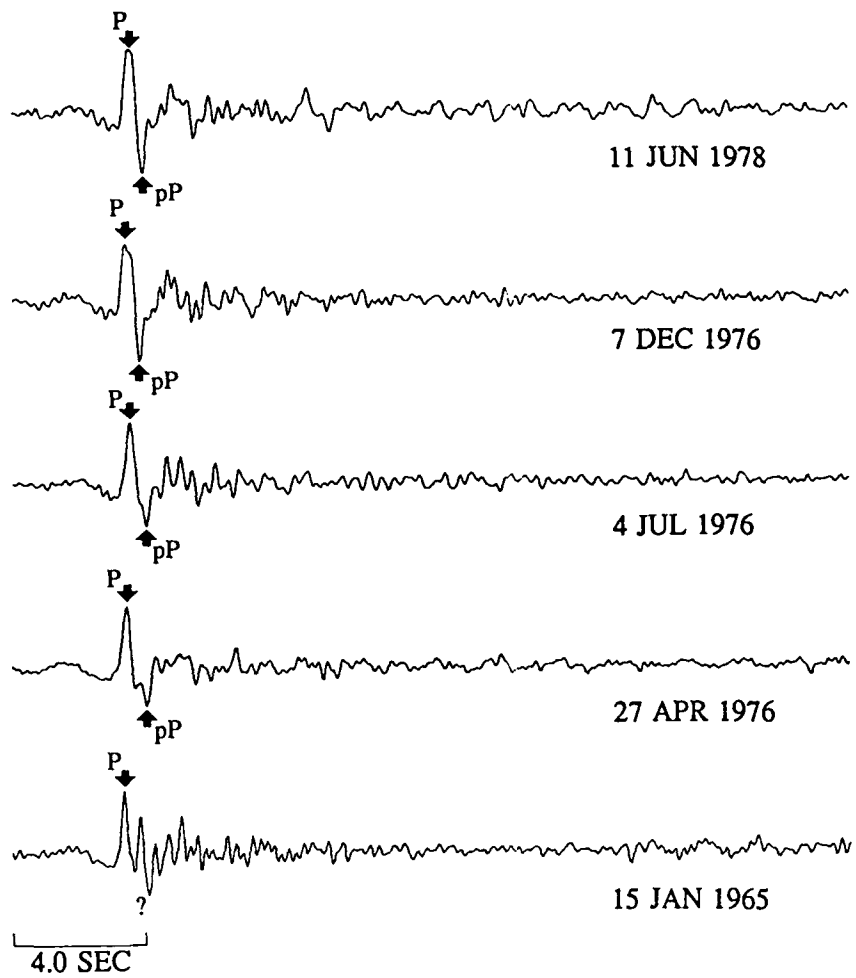


**Figure 13.** Deconvolved source terms for KTS events recorded at EKA. Each trace is labeled with the event name and the locations of the P and pP (if observed) phases. Event parameters for these events are given in Table 3. The bottom trace is a presumed cratering event.

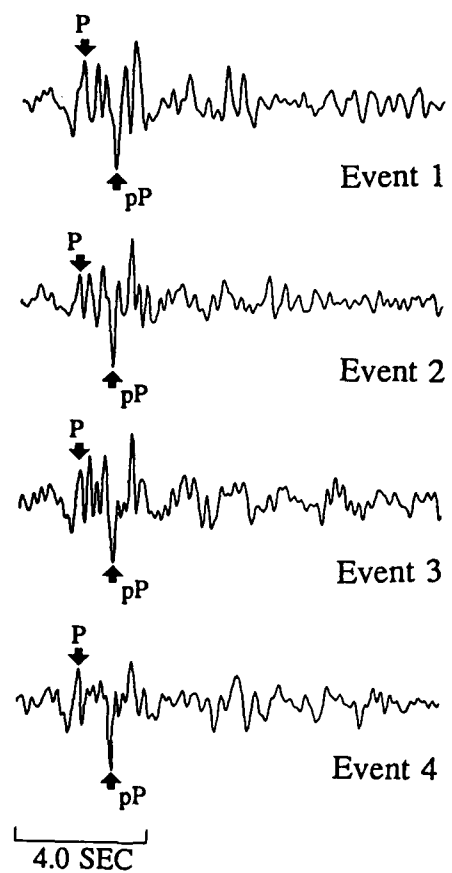


**Figure 14.** Deconvolved source terms for Astrakhan events recorded at the RSTN. Each trace is labeled with the event name and the locations of the P and pP (if observed) phases. Event parameters for these events are given in Table 4.

tude of 1. Then each trace was convolved with a wavelet derived from a von Seggern and Blandford source function,  $t^* = 0.15$  sec, and an EKA instrument response. An example of such filtered source terms is shown in Figure 15 for a yield of 125 kt. Thus, the magnitude bias is estimated from the differences in waveforms due to the differences in the deconvolved source time functions between the cratering and non-cratering events. The magnitude bias was calculated for three yields, 60, 125, and 300 kt, in two different ways:

$$\Delta m_b = m_b(n-cr) - m_b(cr) = \log \left[ \frac{A_{c,n-cr}}{A_{c,cr}} \right] \quad (6)$$

$$\Delta m_b = \log \left[ \frac{A_c}{A_a} \right]_{n-cr} - \log \left[ \frac{A_c}{A_a} \right]_{cr} \quad (7)$$

where  $A_a$  and  $A_c$  are the "a" phase and "c" phase amplitudes, respectively, and  $cr$  and  $n-cr$  refer to cratering and non-cratering events, respectively. The results are shown in Figure 16, and  $\Delta m_b(n-cr - cr) \sim 0.09$  to 0.22 magnitude units. It is interesting that the results from using Equation (7) appear more robust than those from using Equation (6). This may be because the yield differences for the events, which were only partly corrected for by normalizing each trace, are in a sense "factored out" when the ratios of the "a" and "c" phase amplitudes are used.

The deconvolved site terms are a by product of the deconvolution process in the sense that we are mostly interested in the source time functions in this study. The site terms are shown in Figures B1 to B4 of Appendix B; they are "wrapped around" because the deconvolution uses finite time series. There are substantial variations in the site terms, even among stations near to each other (such as those in the NORSAR and EKA arrays), and all of the site terms appear to be the source of some of the P wave coda. To show the effect of the site terms on seismic waves in more detail, Figures 17 to 19 show site terms that have been

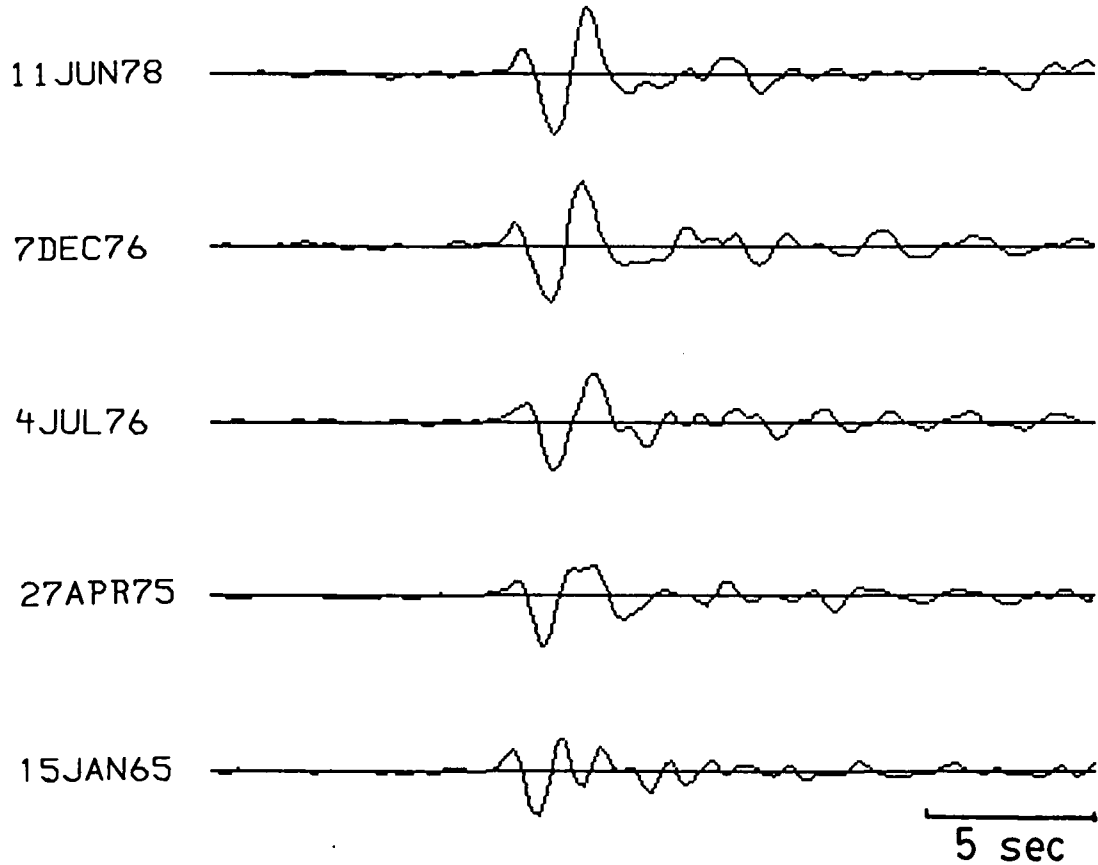


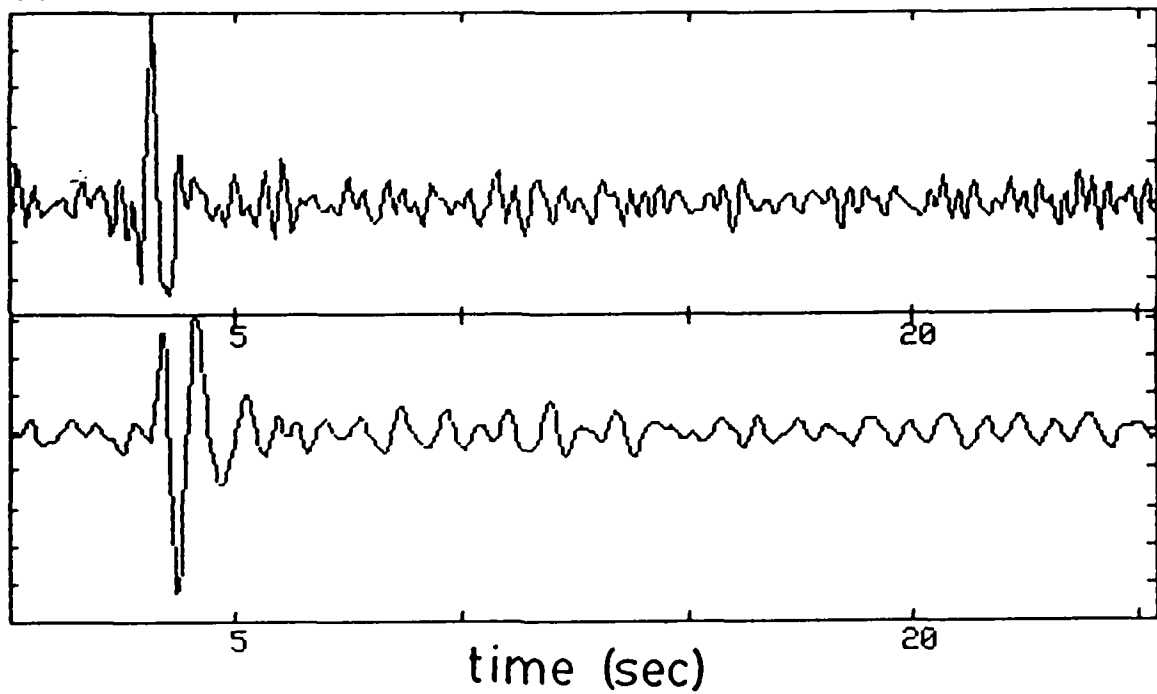
**Figure 15.** Deconvolved source terms from the set of eastern KTS data recorded at EKA which have been filtered with a wavelet consisting of a von Seggern and Blandford pulse of yield 125 kt, a  $t^* = 0.15$  sec, and an EKA instrument response. The bottom trace is from the eastern KTS cratering shot.

## Non-Cratering - Cratering Magnitude Difference Estimates

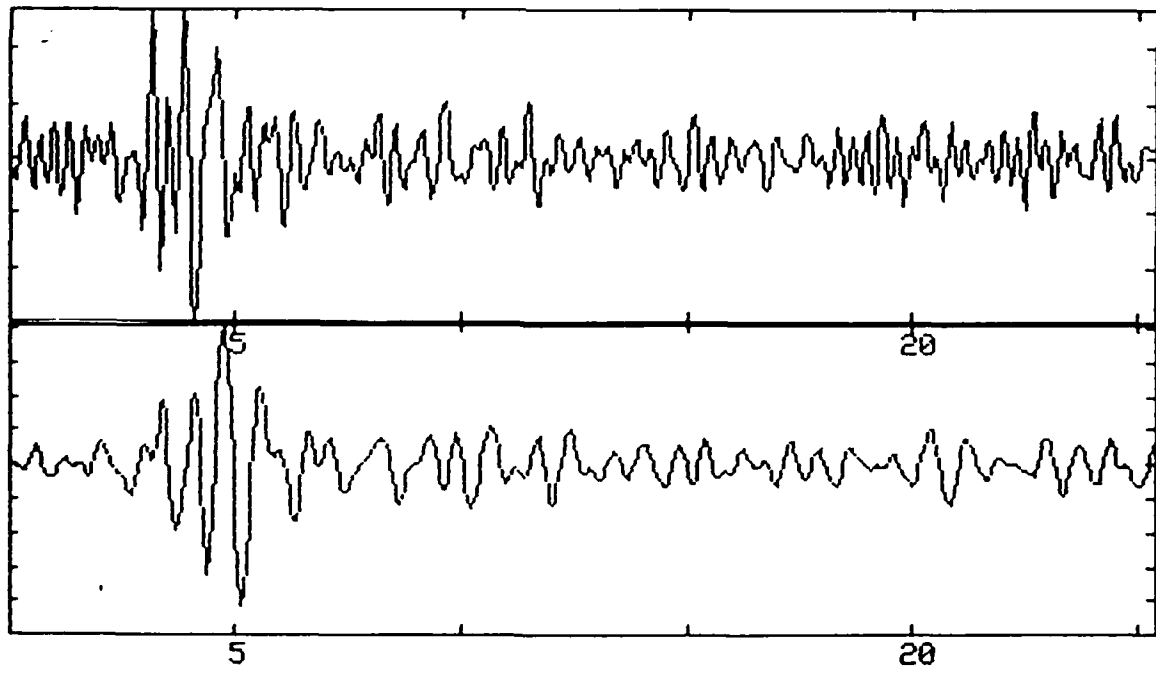
	yield = 60kt	125kt	300kt
$\log\left(\frac{A_{c,n-cr}}{A_{c,cr}}\right)$	0.09±0.09	0.13±0.10	0.22±0.08
$\log\left(\frac{A_c}{A_a}\right)_{n-cr} - \log\left(\frac{A_c}{A_a}\right)_{cr}$	0.15±0.04	0.15±0.02	0.18±0.05

Figure 16. Magnitude difference estimates between the presumed cratering event at eastern KTS and four buried eastern KTS explosions for yields of 60, 125, and 300 kt. The magnitude differences were calculated from equations (6) and (7) in the text.  $A_a$  and  $A_c$  are the "a" phase and "c" phase amplitudes, respectively, and cr and n-cr refer to cratering and non-cratering events, respectively.

NB2



NB4



**Figure 17.** Examples of filtered site terms for the set of NTS data recorded at NORSAR. In each pair, the top trace is the deconvolved site term, which has been filtered in the bottom trace with a von Seggern and Blandford wavelet assuming a yield of 500 kt,  $t^* = 0.45$  sec, and a NORSAR instrument response.

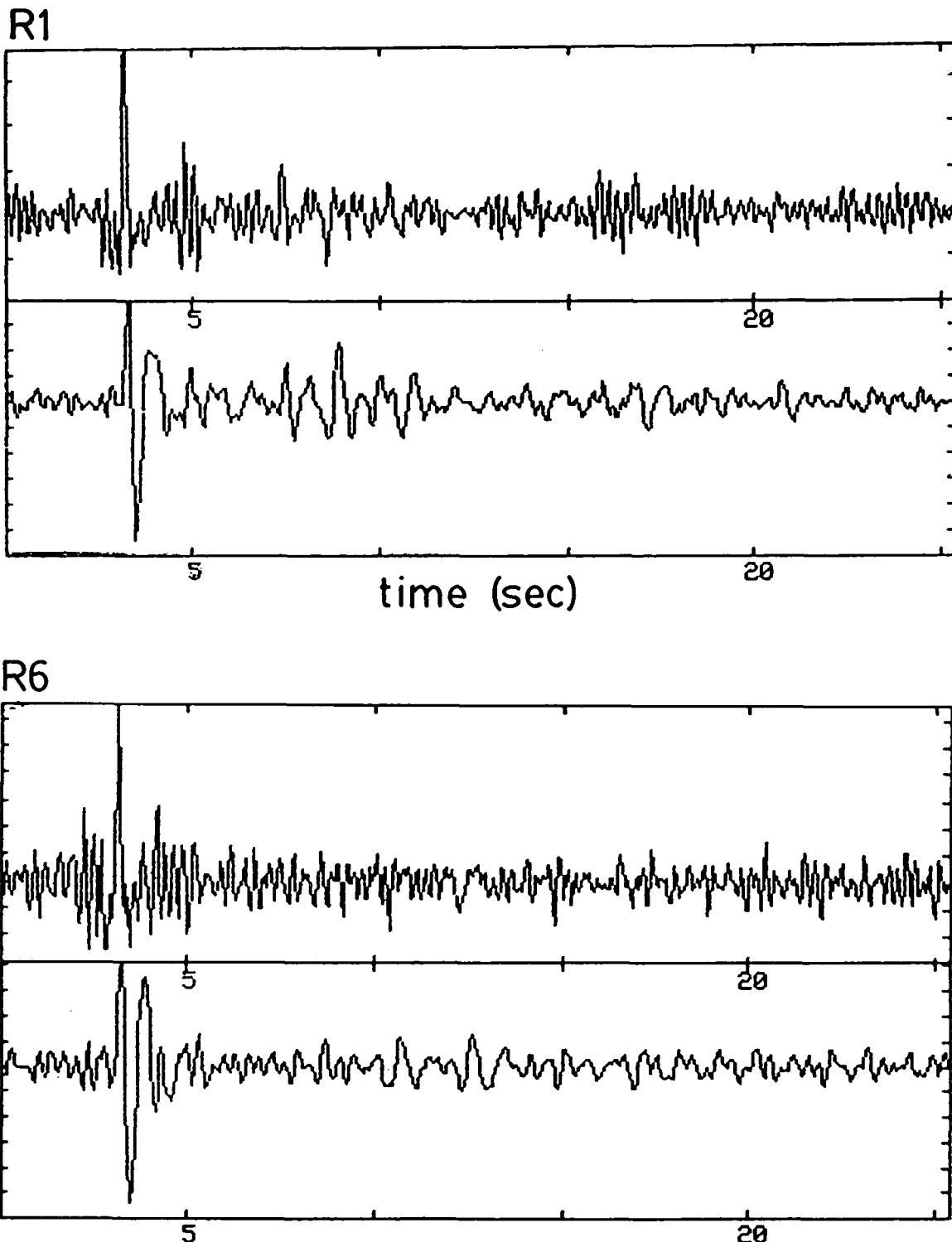
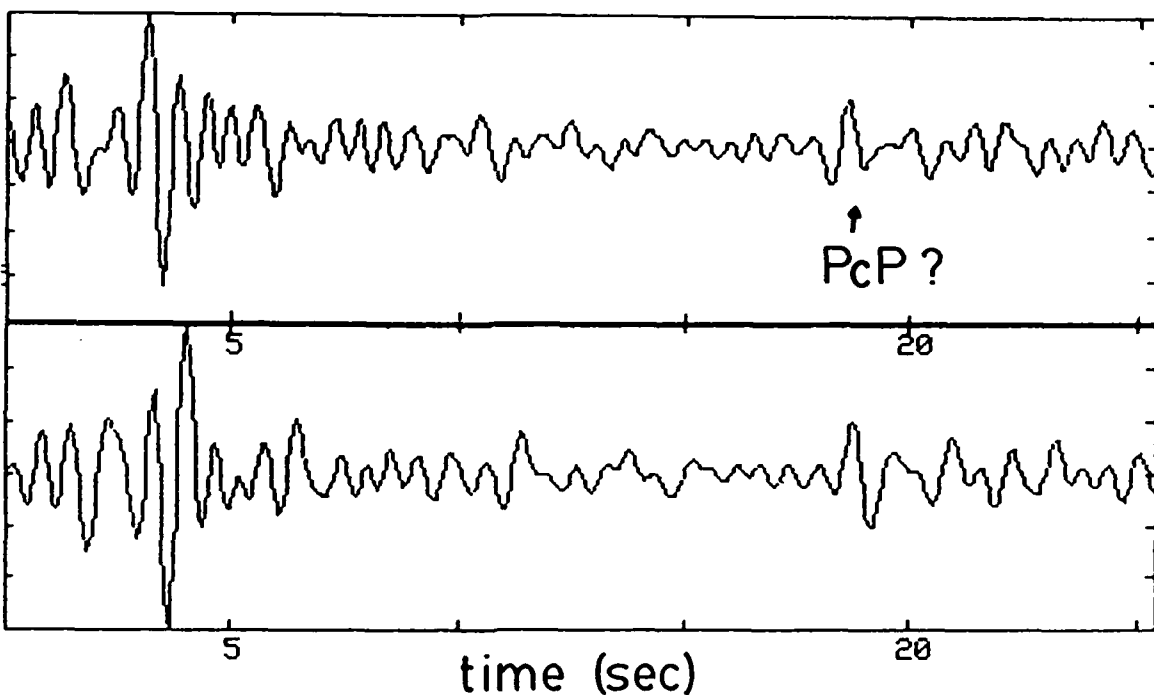


**Figure 18.** Examples of filtered site terms for the set of KTS data recorded at EKA. In each pair, the top trace is the deconvolved site term, which has been filtered in the bottom trace with a von Seggern and Blandford wavelet assuming a yield of 130 kt,  $t^* = 0.15$  sec, and an EKA instrument response.

RSNY



RSSD

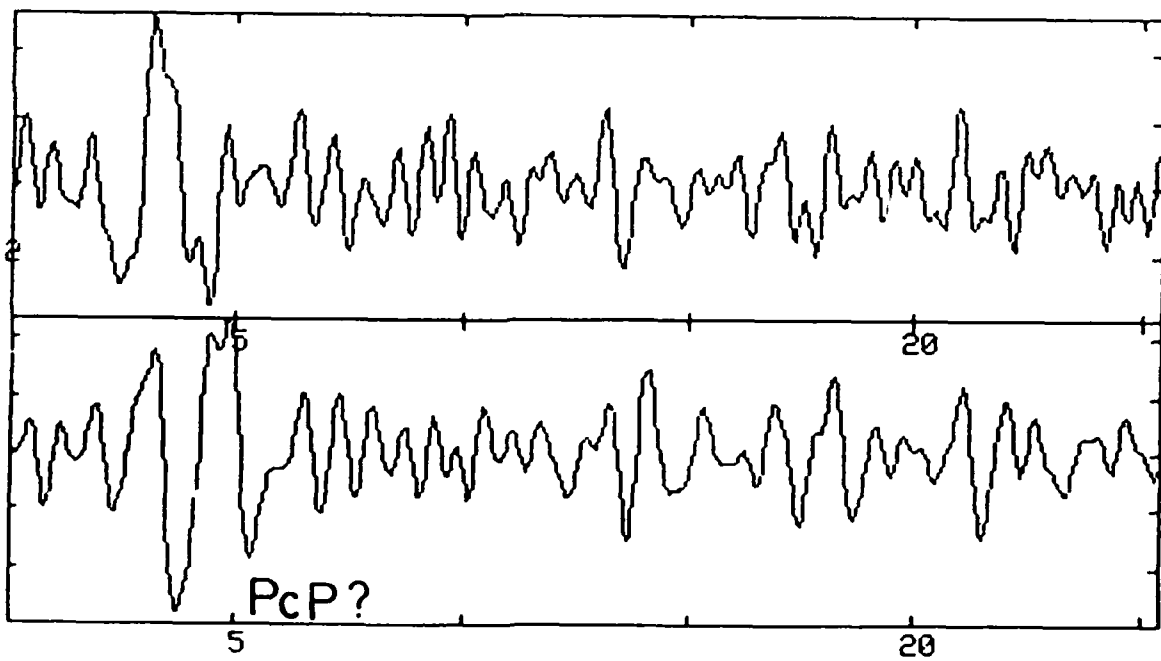


**Figure 19.** Examples of filtered site terms for the set of Astrakhan data recorded at the RSTN. In each pair, the top trace is the deconvolved site term, which has been filtered in the bottom trace with a von Seggern and Blandford wavelet assuming a yield of 22 kt,  $t^* = 0.15$  sec, and an RSTN instrument response. The predicted location of the PcP arrival is also marked.

convolved with von Seggern and Blandford wavelets including  $t^*$  and an appropriate instrument response. In Figure 19, the predicted arrival time of PcP from Astrakhan has been marked. The influence of the site function on the coda is clearly seen, as is the difference between sites that are closely located geographically. Also, three NORSAR sites were used in studies of data from events at two different azimuths (NTS and KTS). The site terms for these receivers from the two azimuths are shown in Figure 20. The initial response of each site function is similar for the events from different azimuths, while there is more variation in the coda, especially in NB5 (bottom of Figure 20).

The resolution kernels for the deconvolutions are shown in Figures B5 to B8 of Appendix B. The width of the resolution kernels depends on the frequency bandwidth of the deconvolutions; for the source-receiver pairs studied in this report, the width is about 0.15 sec at half maximum.

As one check on the results, reconstructions were calculated by convolving the appropriate source wavelet, deconvolved source time function, and deconvolved site time function. All of the original traces are in Appendix C, shown for comparison with the reconstructions in Appendix D. Figures 21 and 22 show examples of traces from an NTS event and a KTS event along with their reconstructions. The similarity of the observed and reconstructed traces is very good, better in fact than some reported reconstructions made with "relative receiver functions", probably because we use an array of small areal extent rather than widely spaced stations. Moreover, the correlation coefficients between the original and reconstructed traces are commonly above 0.9 for the *whole* 25.6 second length of the samples chosen (12.8 sec for the Astrakhan data). Also note how well the details of the coda have been preserved in the reconstructions. The reconstructions prove, at least, that the observed waveforms are not inconsistent with some plausible pP parameters coupled with low  $t^*$  that, unlike values used in pre-

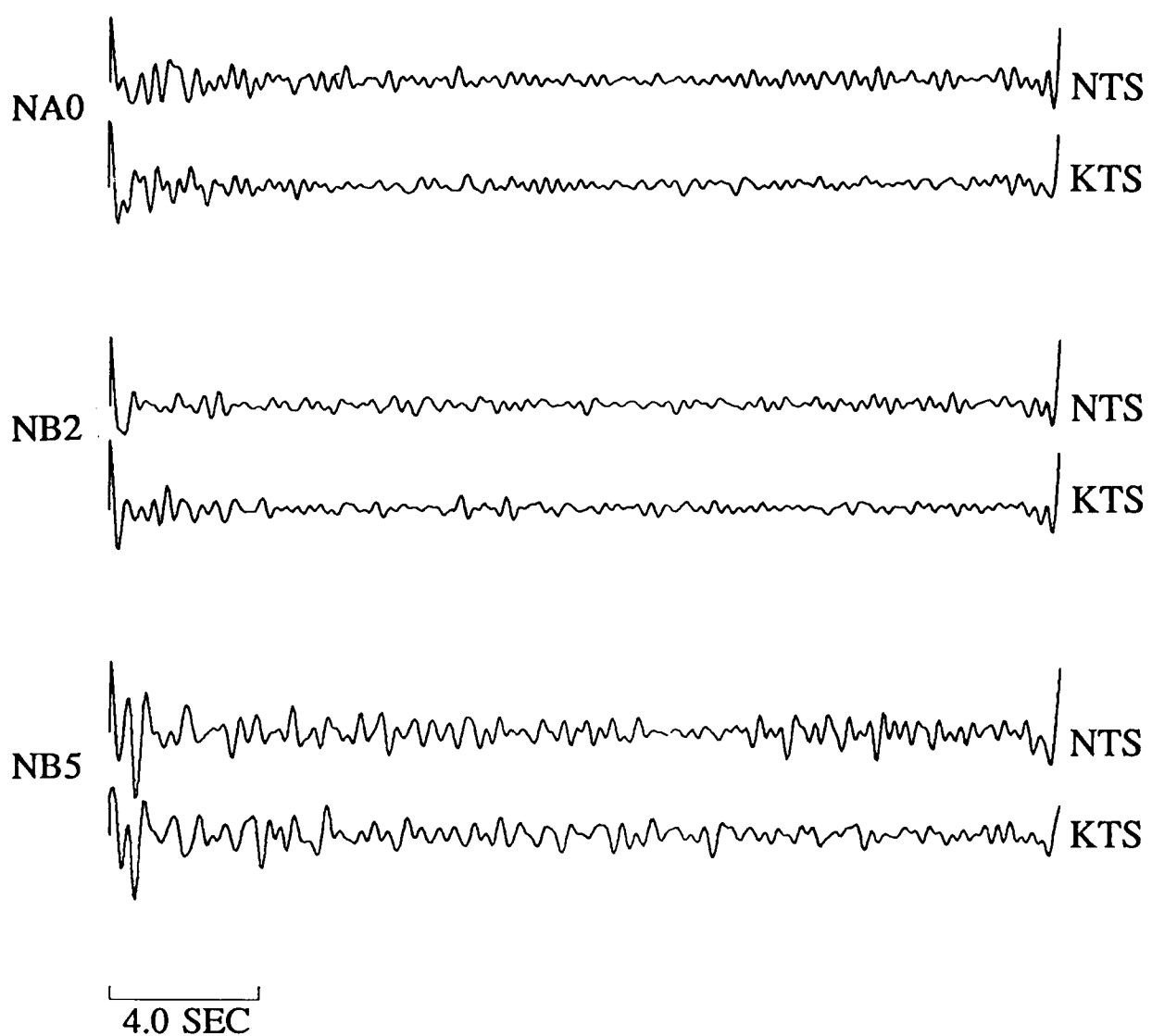


**Figure 20.** Deconvolved site terms for NOKSAR receivers used in studies of data from both NTS and KTS. Both the NTS and KTS data sets were deconvolved separately in the 0.4 to 3.5 Hz frequency band. There appear to be some azimuthal dependencies in these site terms.

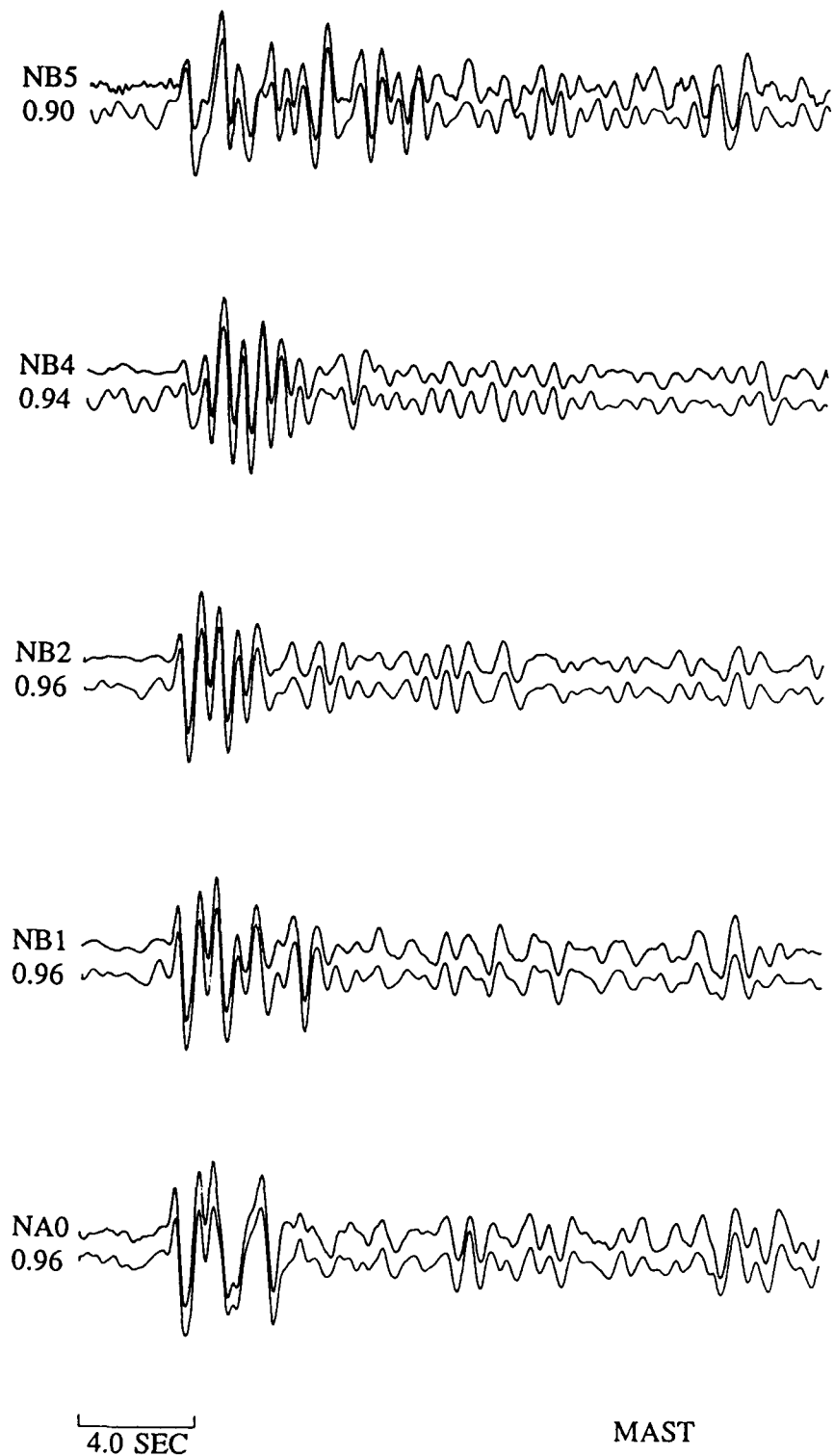
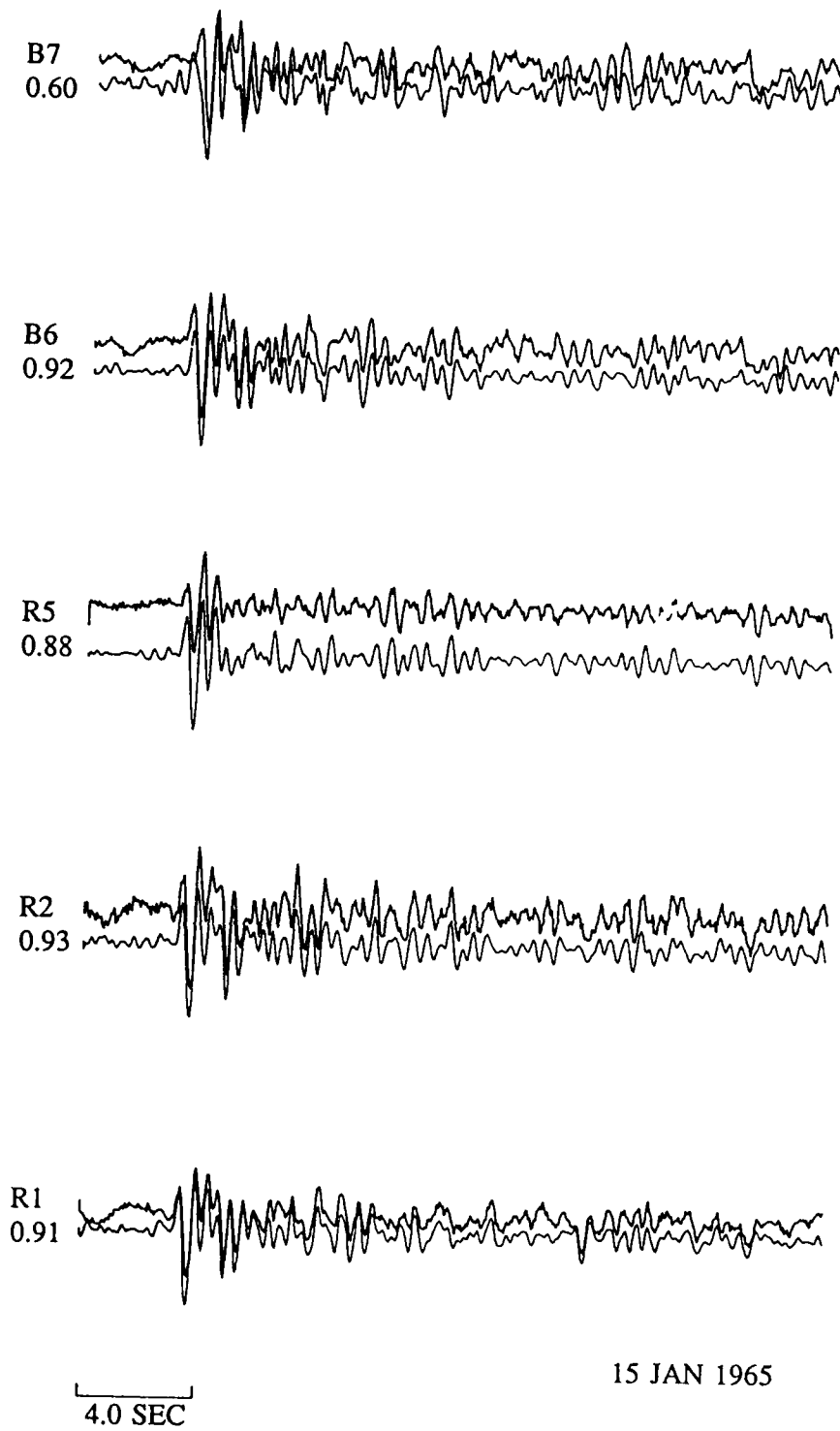


**Figure 21.** Five traces from the NTS explosion Mast as recorded at NORSAR (top of each pair of traces), along with their reconstructions (bottom of each pair of traces). The receiver names are given to the left of each pair of traces, as is the correlation coefficient between each original trace and its reconstruction.



15 JAN 1965

**Figure 22.** Five traces from the eastern KTS cratering shot of 15 January 1965 as recorded at EKA (top of each pair of traces), along with their reconstructions (bottom of each pair of traces). The receiver names are given to the left of each pair of traces, as is the correlation coefficient between each original trace and its reconstruction.

vious synthetic simulations, also agree with spectral data.

### Conclusions

Most of the ambiguities associated with the pP estimation methods proposed in the past are associated with the fact that, for most explosions, the simple P+pP model is not valid. This can be verified by analyses of interevent spectral ratios and the results of our multichannel deconvolutions. In addition, for single channels the site effects will also disguise any spectral modulation due to P-pP interference even if the P+pP model is valid. Finite difference simulations of P waves from explosion sources emplaced in laterally heterogeneous structures also support the idea that complex arrival patterns, rather than simple P+pP sequences, should be common.

Multichannel deconvolutions of four data sets consisting of array recordings of suites of events at several test sites gave the following results:

- \* NTS events deconvolved at NORSAR show, in general complex source functions not easily interpretable in terms of the P+pP model.
- \* Eastern Kazakh explosions deconvolved at EKA and NORSAR appear to have simpler source functions with an identifiable pP arrival with a time delay in the 0.3-0.6 sec range.
- \* The deconvolved source function of a presumed cratering explosion at Eastern Kazakh is visibly different from the deconvolved source functions for buried explosions at the same test site. Assuming the first positive spike to be direct P, the effect of the cratering on  $m_b$  was estimated as a reduction of 0.09 to 0.22 magnitude units.
- \* For a set of Astrakhan events deconvolved using the RSTN stations we see a late arriving pP 1 sec after the direct P, as well as other late arrivals.
- \* Reconstructions from the site and source time series and the source wavelets show excellent agreement with the original traces including fine details in the coda. The coda is partially due to both near site and source scattering.

These results have profound implications to the study of scattering of seismic waves near the sources and receivers. Since most, but not all, of the source factors are associated with relatively simple time series compared to the site factors, the associated events must have generated little scattered energy near the source. If this were not true we would not have been able to reconstruct the associated time series. We cannot think of any conceivable physical mechanism that would generate complex and similar source wavetrains for explosions at various locations within the same test site.

#### Suggested Future Work

Although in the work presented we attempted to ensure the uniqueness of our results by using reasonable starting assumptions, much more can be done to reduce the uncertainties in the final results. There are several possible constraints, all based on common sense arguments that have not been as yet used in our processing of the data. For instance, one might use the expectation that the time domain representations of site factors be uncorrelated beyond the initial few seconds. Similarly one might constrain the later parts of the source time functions to be uncorrelated. One might also exploit the fact that some sites show waveforms that are more coherent with each other, shorter and simpler than at some "anomalous" sites. This does not mean however that, similar to the "transparent" station concept, there is no site distortion at these sites. Rather it may simply mean that the effects of the scattering operator are similar in the first second and less severe at later times. We must also point out that the iterative, frequency domain algorithm for this process is by no means essential and other algorithms may be just as viable. Successive time domain deconvolutions with one-sided causal filters may also be performed iteratively, although such filters may be less effective in removing complex site effects. On the other hand, causal outputs are more appealing and appear more realistic.

Despite the fact that the process we have applied is not constrained to be causal, the source and site time series as well as the reconstructions do not show appreciable precursors. A better understanding of the convergence properties of the iterative method would also be desirable. We prefer the iterative approach because it allows us to change constraints as we go along, but the idea of factoring can be exploited without any iteration. Most of the effort in this study was expended in developing, implementing and testing the algorithm and little time was left for "fine tuning" and optimization. The results shown here are probably inferior to the best that can be produced by the method after optimizing the weighting of frequencies and the initial conditions.

After testing out and optimizing the method, the implementation of an intelligent, adaptive scheme for routine determination of source time functions at seismic arrays becomes a practical possibility. The deconvolution process also easily lends itself for incorporation into "intelligent" learning systems which adapt themselves as new data are added. For instance, if we are satisfied with the previous estimates of the site factors we can "freeze" these and the process can be used for routine estimation of the source time functions from the same test site. If we have, from other sources or methods, "true" values of pP parameters then we can keep the associated source function constant and rerun the process to obtain estimates of site and source factors conditional to such constraints. Improvements in  $t^*$ , explosion source models etc. can be naturally incorporated in the scheme, and the results produced in this report must thus not be considered as to be the best that can be obtained. The algorithm could be installed permanently in a computer and all data originating from selected test sites may be processed. Instead of retaining all the past data only the updated site factors would be kept for the processing of new signals along various azimuths. These may take the place of stored beam parameters. It would be possible, using multiple arrays, to look for effects of strain release along various azimuths and similarly to the comparison of cratering and noncratering events in

this study, compare source functions of events with and without strain release.

## References

- Bakun, W.H. and L.R. Johnson (1973). The deconvolution of teleseismic P waves from explosions MILROW and CANNIKIN, *Geophys. J. R. astr. Soc.*, 34, 321-342.
- Blandford, R.R., T.J. Cohen, and J.W. Woods (1973). An iterative approximation to the mixed-event processor, *SDAC-TR-73-7*, Teledyne Geotech, Alexandria, Virginia.
- Cohen, T.J. (1970). Source depth determinations using spectral estimation and cepstral analysis, *Geophys. J. R. astr. Soc.*, 20, 223-231.
- Cohen, T.J. (1975). Ps and pP phases from seven Pahute Mesa events, *Bull. Seism. Soc. Am.*, 65, 1029-1032.
- Cormier, V.F. (1982). The effect of attenuation on seismic body waves, *Bull. Seism. Soc. Am.*, 72, S169-S200.
- Dahlman, O. and H. Israelson (1977). *Monitoring Underground Nuclear Explosions*, Elsevier Scientific Publishing Company, Amsterdam.
- Der, Z.A., R.H. Shumway, L.M. Anderson, T.W. McElfresh, and J.A. Burnett (1983). Analysis of estimators for pP times and amplitudes, *VSC-TR-83-17*, Teledyne Geotech, Alexandria, Virginia.
- Der, Z.A., T.W. McElfresh, R. Wagner, and J.A. Burnett (1985). Spectral characteristics of P waves from nuclear explosions and yield estimation, *Bull. Seism. Soc. Am.*, 75, 379-390.
- Filson, J. and C.W. Frasier (1972). Multisite estimation of explosive source parameters, *J. Geophys. Res.*, 77, 2045-2061.
- Frankel, A. and R.W. Clayton (1984). A finite difference simulation of wave propagation in two-dimensional random media, *Bull. Seism. Soc. Am.*, 74, 2167-2186.
- Hart, R.S., D.M. Hadley, G.R. Mellman, and R. Butler (1979). Seismic amplitude and waveform search, *SGI-P-70-002*, Sierra Geophysics, Arcadia, California.
- Kemerait, R.C. and A.F. Sutton (1982). A multidimensional approach to seismic event depth estimation, submitted to a special issue of *Seismic Analysis and Discrimination*, Elsevier Publishing Co.
- Israelson, H. (1983). Deconvolution based on source scaling applied to teleseismic signals, *FOA Rapport C 20514-T1*, Forsvarets Foskningsanstalt, Huvudavdelning 2, Stockholm, Sweden.
- Jurkevics, A. and R. Wiggins (1984). A critique of seismic deconvolution methods, *Geophysics*, 49, 2109-2116.

- Lay, T., Helmberger, D.V. and D.G. Harkrider (1984a). Source models and yield scaling relations for underground nuclear explosions at Amchitka Island. *Bull. Seism. Soc. Am.*, 74., 843-862.
- Lay, T., Arvesen, C.G., Burger, R.W. and L.J. Burdick (1984b). Estimating seismic yield and defining distinct test sites using complete waveform information, *WCCP-R-84-04*, Woodward-Clyde Consultants, Pasadena, CA.
- Levy, S. and P.K. Fullagar (1981). Reconstruction of sparse spike train from a portion of its spectrum and application to high resolution deconvolution, *Geophysics*, 46, 1235-1243.
- Lundquist, G.M., G.R. Mellman and D.M. Hadley (1980). Relative receiver functions for three different array concepts, *SGI-R-80-021*, Sierra Geophysics, Inc., Arcadia, California.
- Marshall, P.D. (1972). Some seismic results from a worldwide sample of large underground explosions, *AWRE Report O 49/72*, Aldermaston, Berkshire, England.
- McLaughlin, K.L., L.M. Anderson, Z.A. Der, T.W. McElfresh, and A.C. Lees (1986). Effects of local geologic structure on Yucca Flats, NTS waveforms - 2-dimensional finite difference calculations, *TGAL-86-4*, Teledyne Geotech, Alexandria, Virginia.
- Mellman G.R. and S.K. Kaufman (1981). Relative waveform inversion, *SGI-R-81-048*, Sierra Geophysics, Redmond, WA.
- Mellman, G.R., Kaufman, S.K. and W.C. Tucker (1984). Depth corrections for yield estimation of underground nuclear explosions, In *Basic Research in the VELA program*, AFOSR review meeting, Santa Fe, NM, May 7-9, 1984.
- Mueller, R.A. and J.R. Murphy (1971). Seismic characteristics of underground nuclear detonations: Part I. Seismic spectrum scaling, *Bull. Seism. Soc. Am.*, 61, 1575-1692.
- Murphy, J.R. and S.Day (1984). Source spectrum, DARPA sponsored "Workshop on attenuation effects on body waves", October 23-24, Rosslyn, Virginia.
- Oldenburg, D.W. (1981). A comprehensive solution of the linear deconvolution problem, *Geophys. J. R. astr. Soc.*, 65, 331-358.
- Oldenburg, D.W., Levy, S. and K.P. Whittal (1981). Wavelet estimation and deconvolution, *Geophysics*, 46, 1528-1542.
- Robinson, E.A. and S. Treitel (1980). *Geophysical Signal Analysis*, Prentice Hall, Englewood Cliffs, New Jersey.
- Shumway, R.H. (1984). Deconvolution of multiple time series, In *Statistical Analysis of Time Series*, Japan-U.S. joint seminar, Tokyo.
- Shumway, R.H. and R.R. Blandford (1978). On detecting and estimating multiple arrivals from underground nuclear explosions, *SDAC-TR-77-8*, Teledyne-Geotech, Alexandria, VA.

Shumway, R.H. and Z.A. Der (1985). Deconvolution of multiple time series, *Tech-nometrics*, 27, 385-393.

von Seggern, D.H. and R.R. Blandford (1972). Source time functions and spectra for underground nuclear explosions, *Geophys. J. R. astr. Soc.*, 31, 83-97.

Wiggins, R.A. (1978). Minimum entropy deconvolution, *Geoexploration*, 16, 21-35.

## **Appendix A**

Spectral ratios of pairs of NTS events at NORSAR stations.  
Spectral ratios of NTS events at pairs of NORSAR stations.

**Table A1**

Parameters used in Forming Synthetic Spectral Ratios			
Event	pP-P (sec)	pP/P	Yield (kt)
Camembert	1.15	0.9	1003
Inlet	0.95	1.0	315
Kasseri	1.05	0.9	1272
Mast	0.9	0.9	579
Muenster	1.25	0.8	1133
Stilton	0.85	0.9	222
Tybo	0.9	1.3	386

From Lay *et al* (1984a). pP-P and pP/P are from Mast as the master event; the yields are the average of the yields from the four different master events.

# INLET / KASSERI

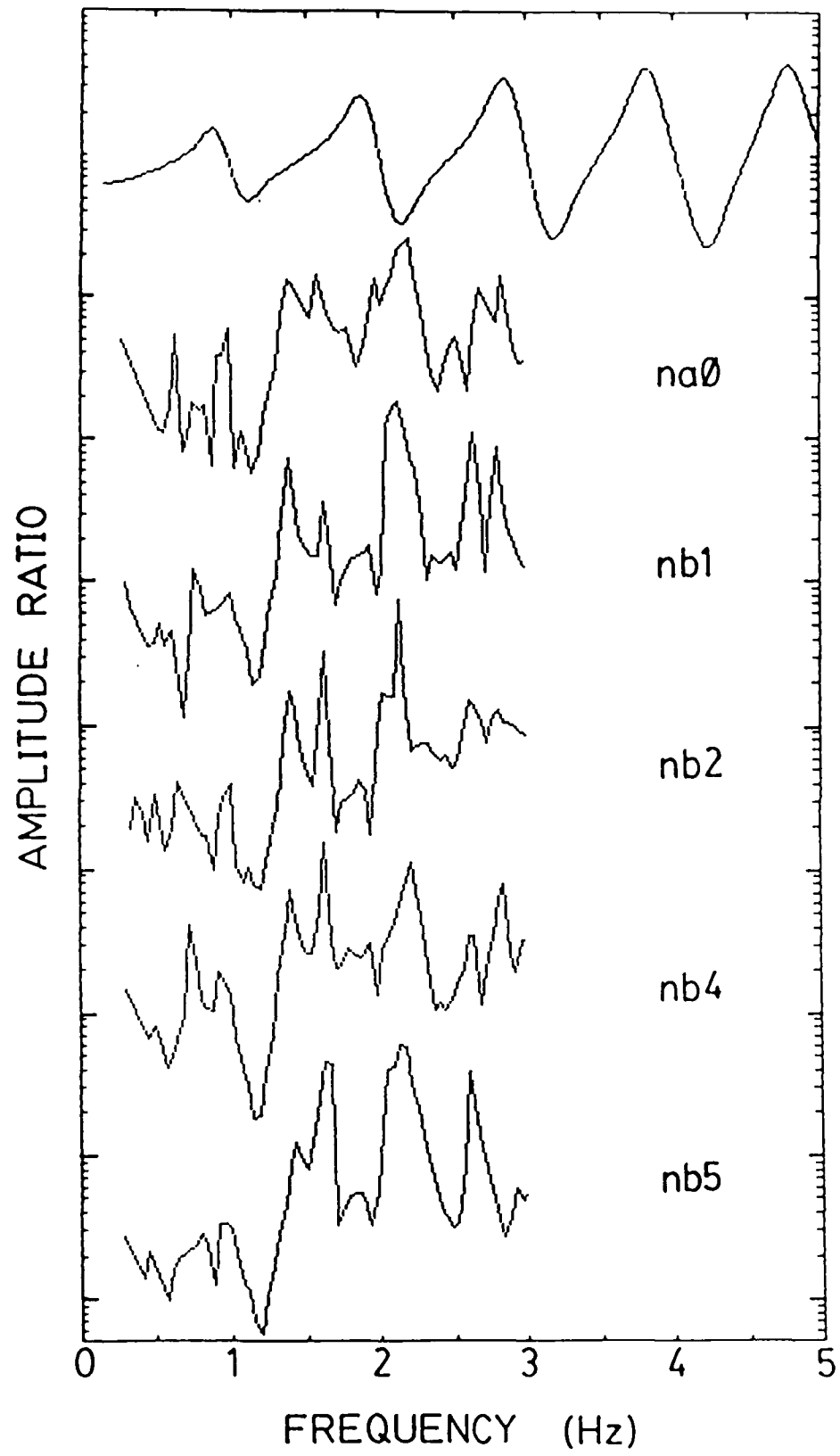


Figure A1. Spectral ratios between NTS events Inlet and Kasseri at NORSAR stations.

INLET / MAST

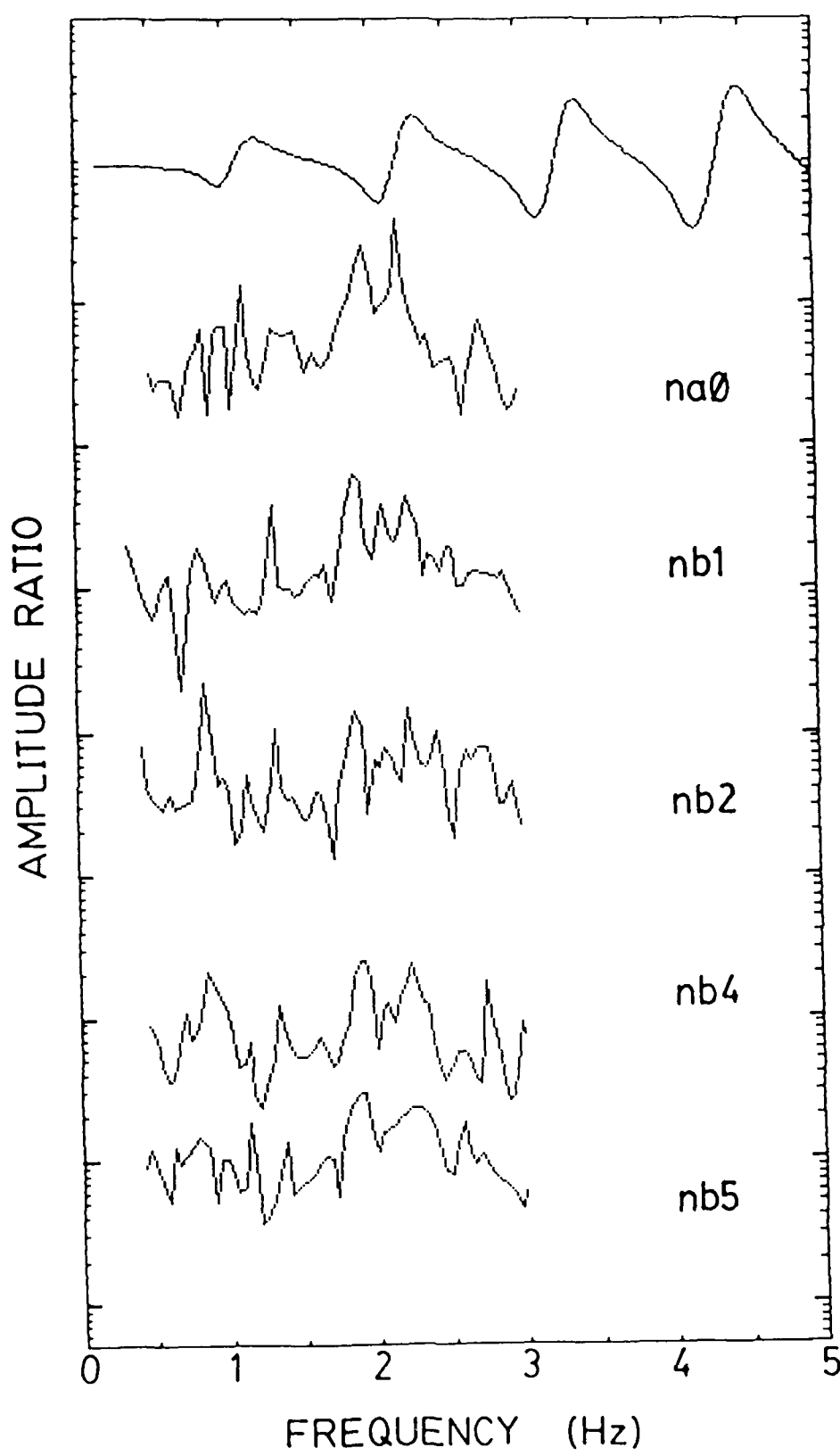


Figure A2. Spectral ratios between NTS events Inlet and Mast at NORSAR stations.

MAST / KASSERI

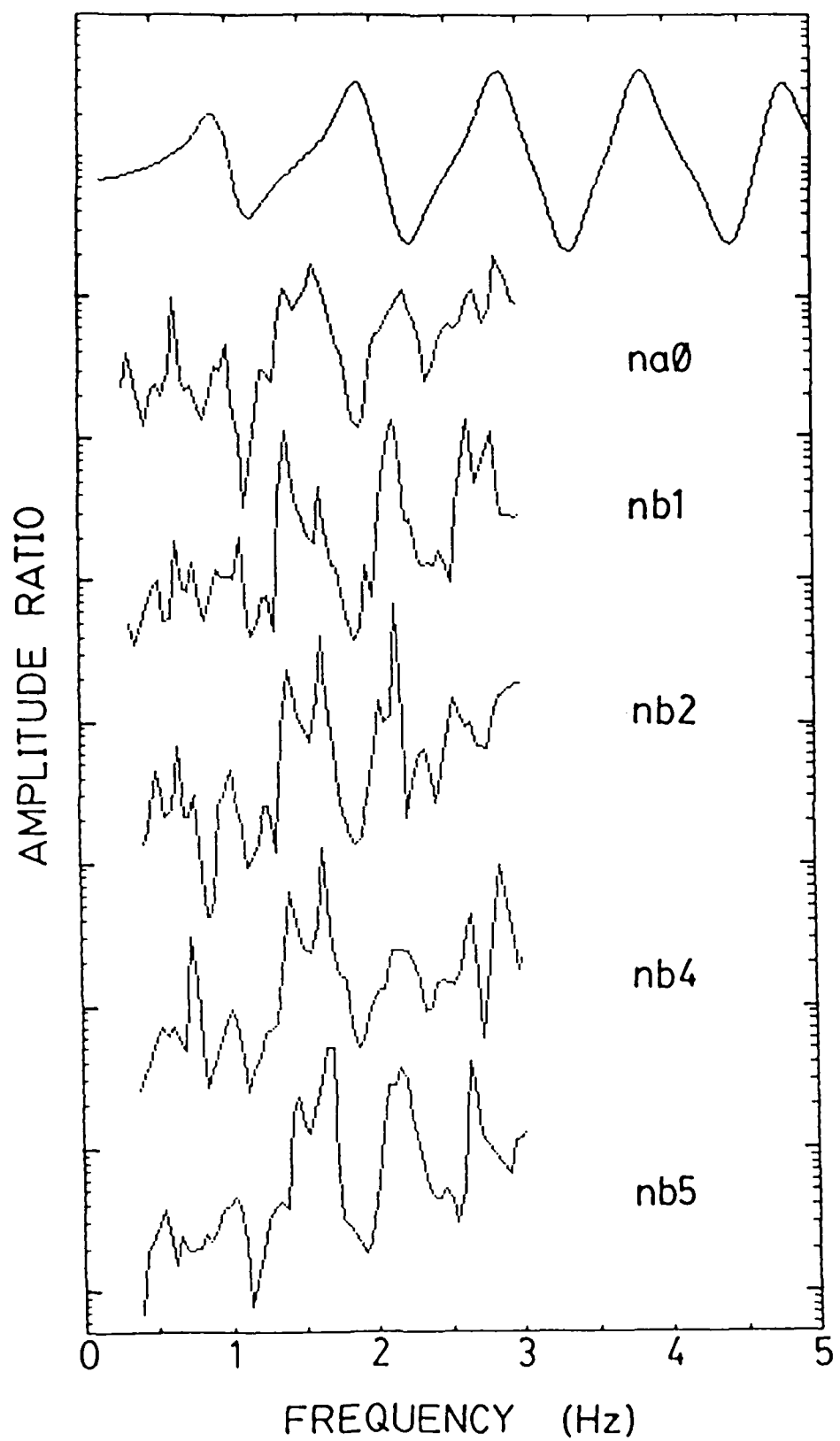


Figure A3. Spectral ratios between NTS events Mast and Kasseri at NORSAR stations.

# STILTON/ INLET

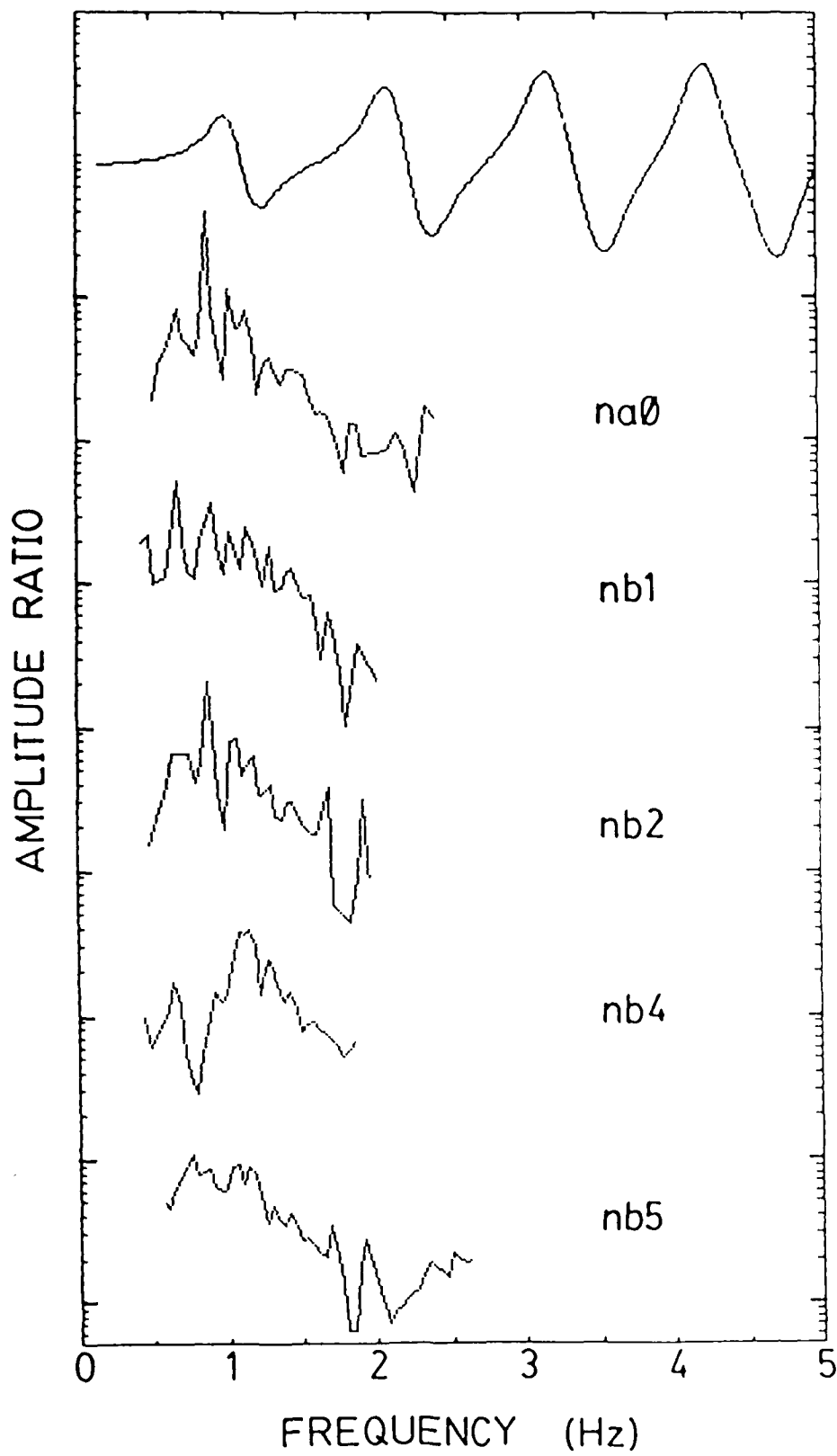


Figure A4. Spectral ratios between NTS events Stilton and Inlet at NORSAR stations.

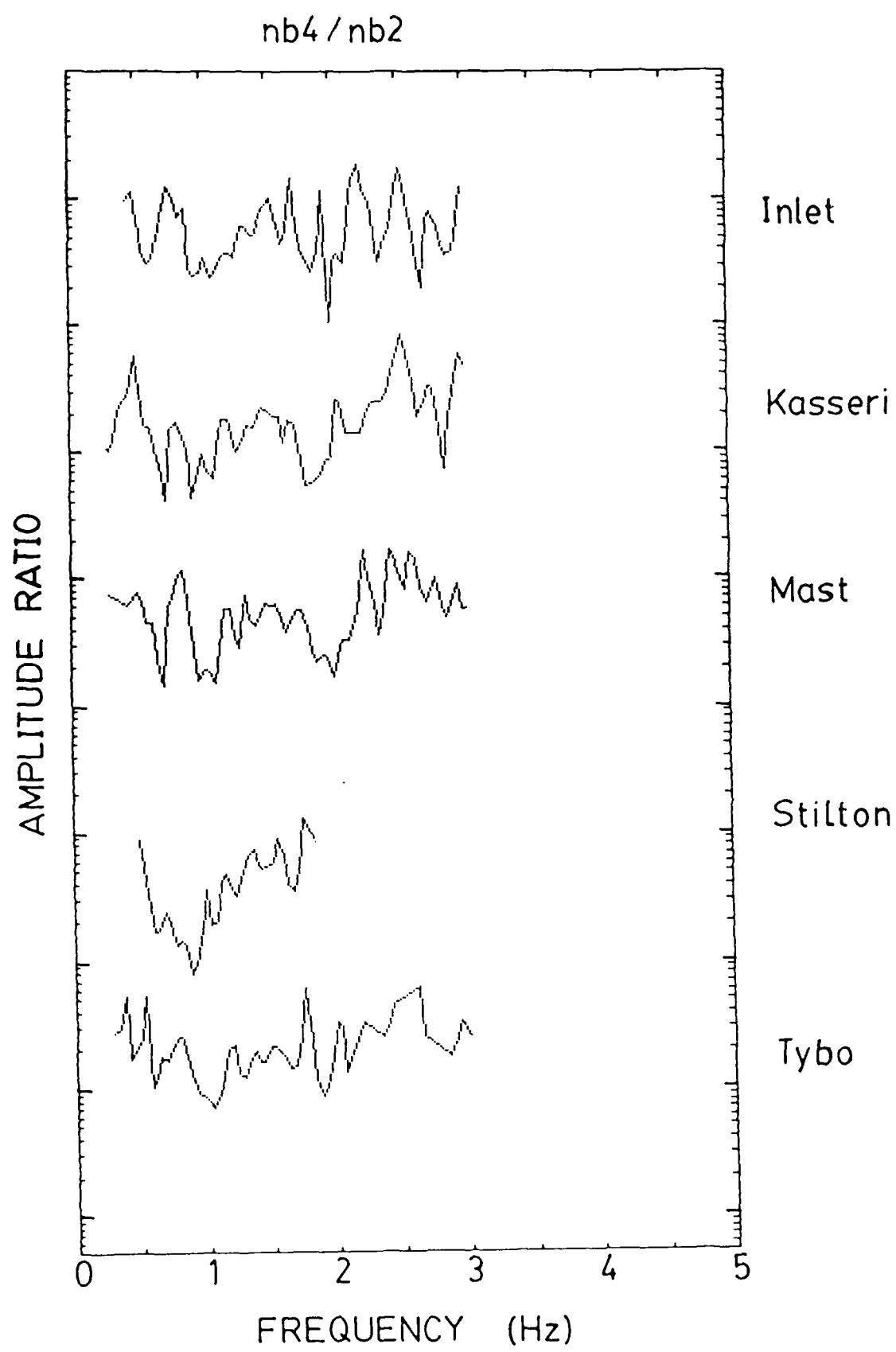


Figure A5. Spectral ratios between NORSAR receivers NB4 and NB2 at NTS events.

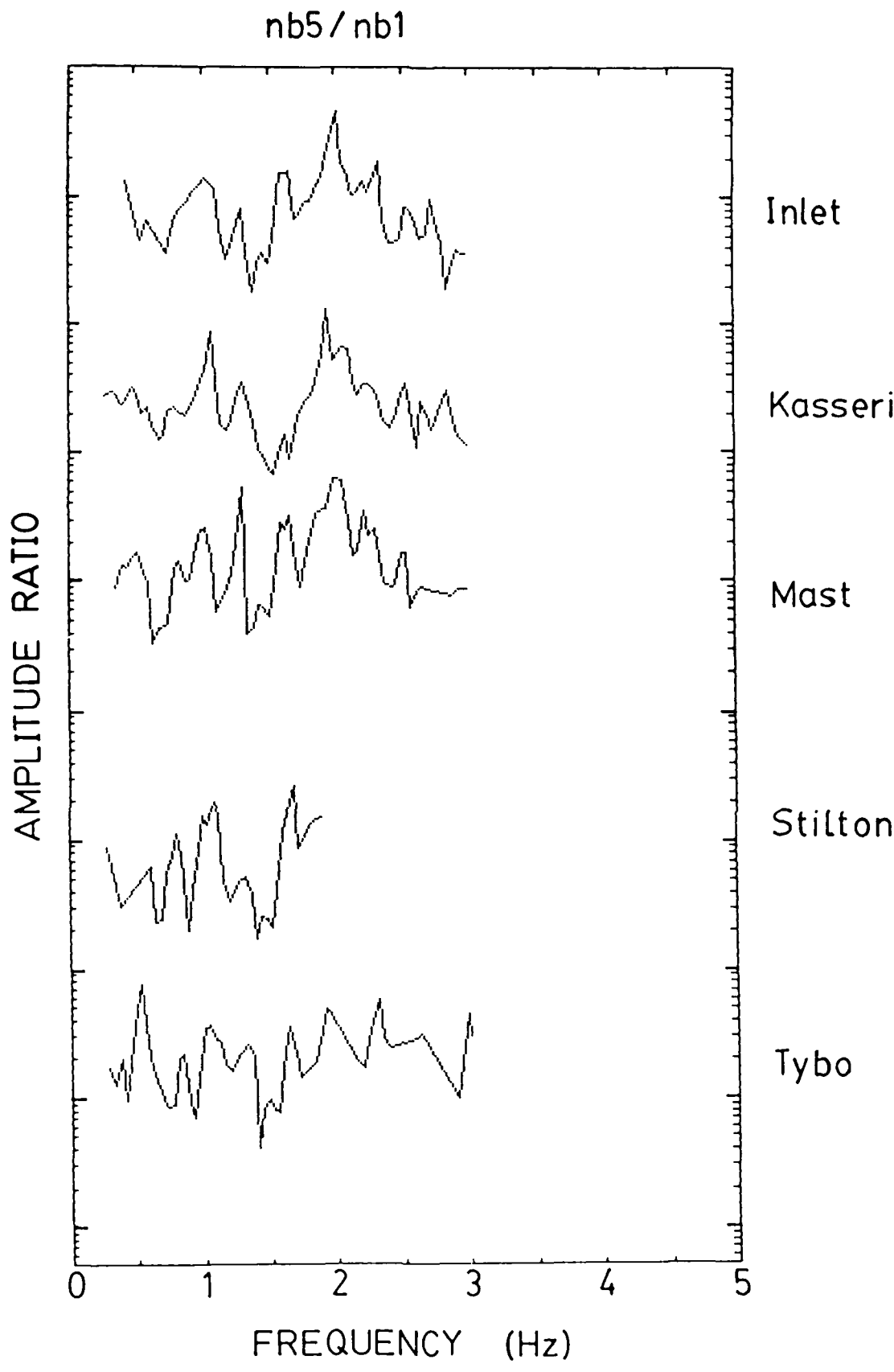


Figure A6. Spectral ratios between NORSAR receivers NB5 and NB1 at NTS events.

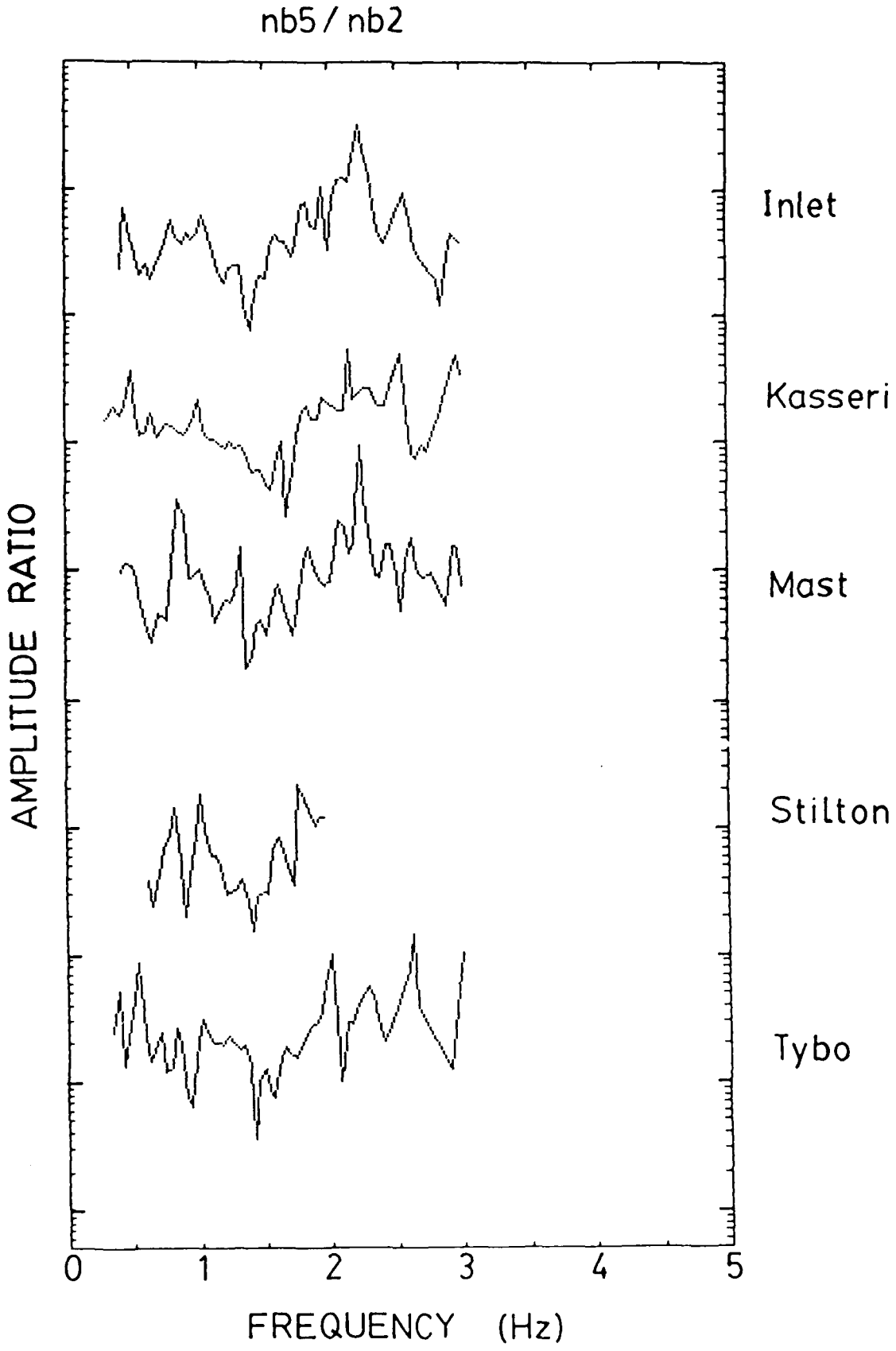


Figure A7. Spectral ratios between NORSAR receivers NB5 and NB2 at NTS events.

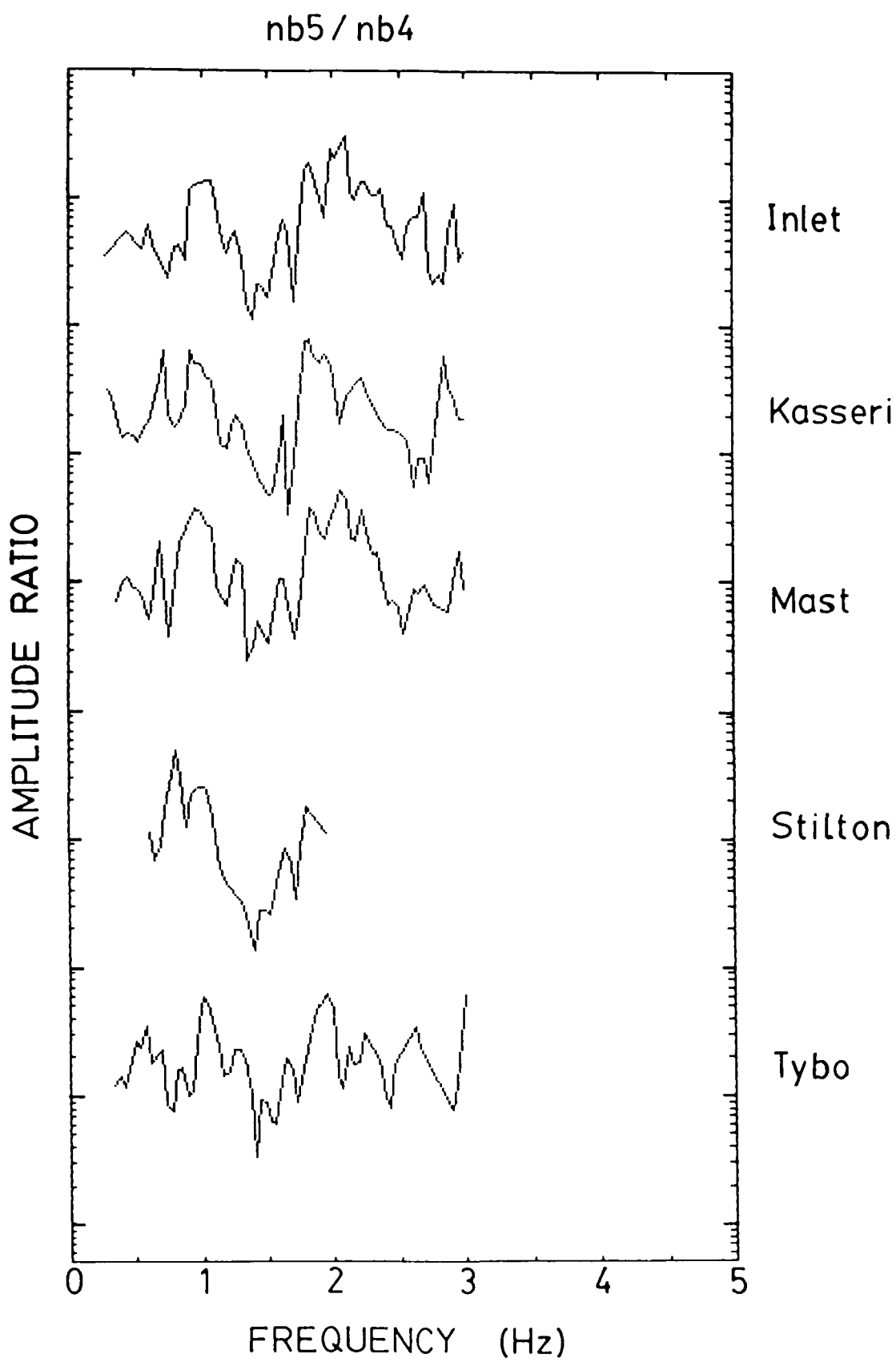
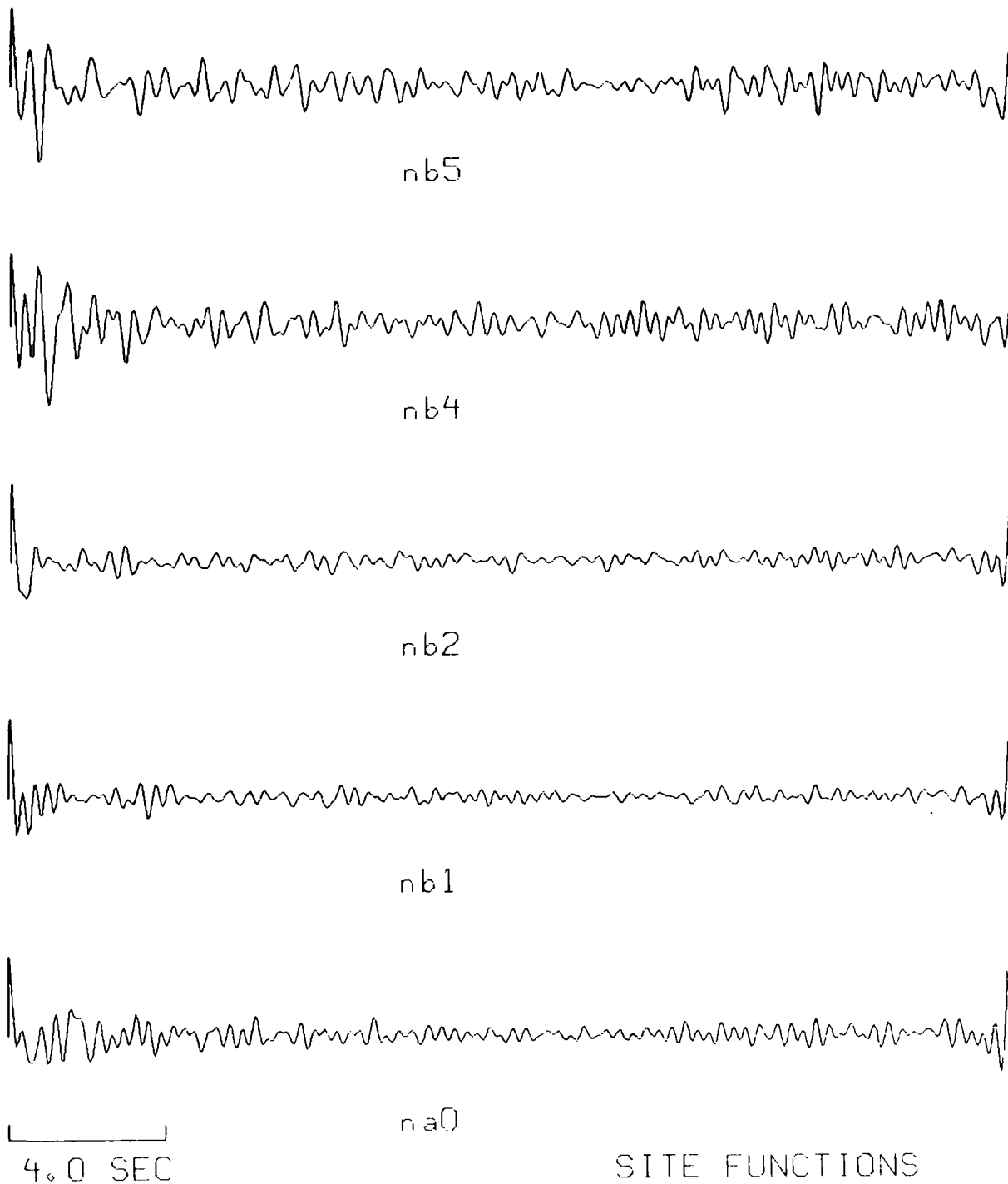


Figure A8. Spectral ratios between NORSAR receivers NB5 and NB4 at NTS events.

## **Appendix B**

Deconvolved site time functions.  
Resolution kernels from deconvolutions.



**Figure B1.** Deconvolved site terms for NTS events recorded at NORSAR.



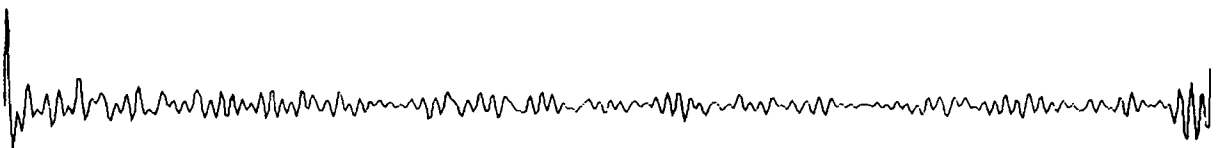
N06B



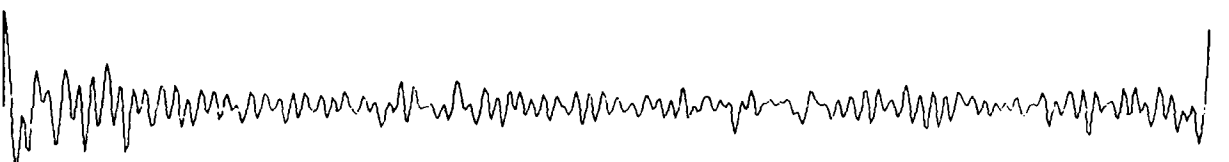
N05B



N03B



N02B



N01A

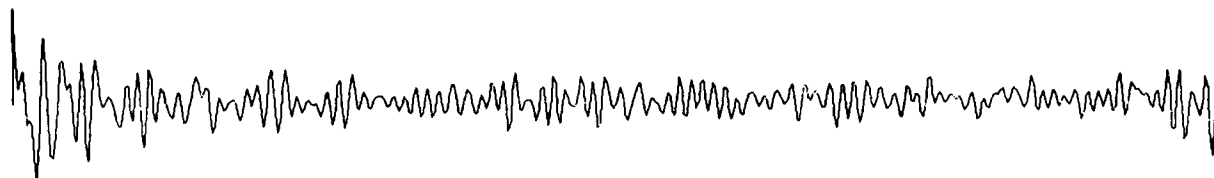
4.0 SEC

SITE FUNCTIONS

**Figure B2.** Deconvolved site terms for KTS events recorded at NORSAR.



NO2C



NO7B

4.0 SEC

SITE FUNCTIONS

**Figure B2 (continued).**

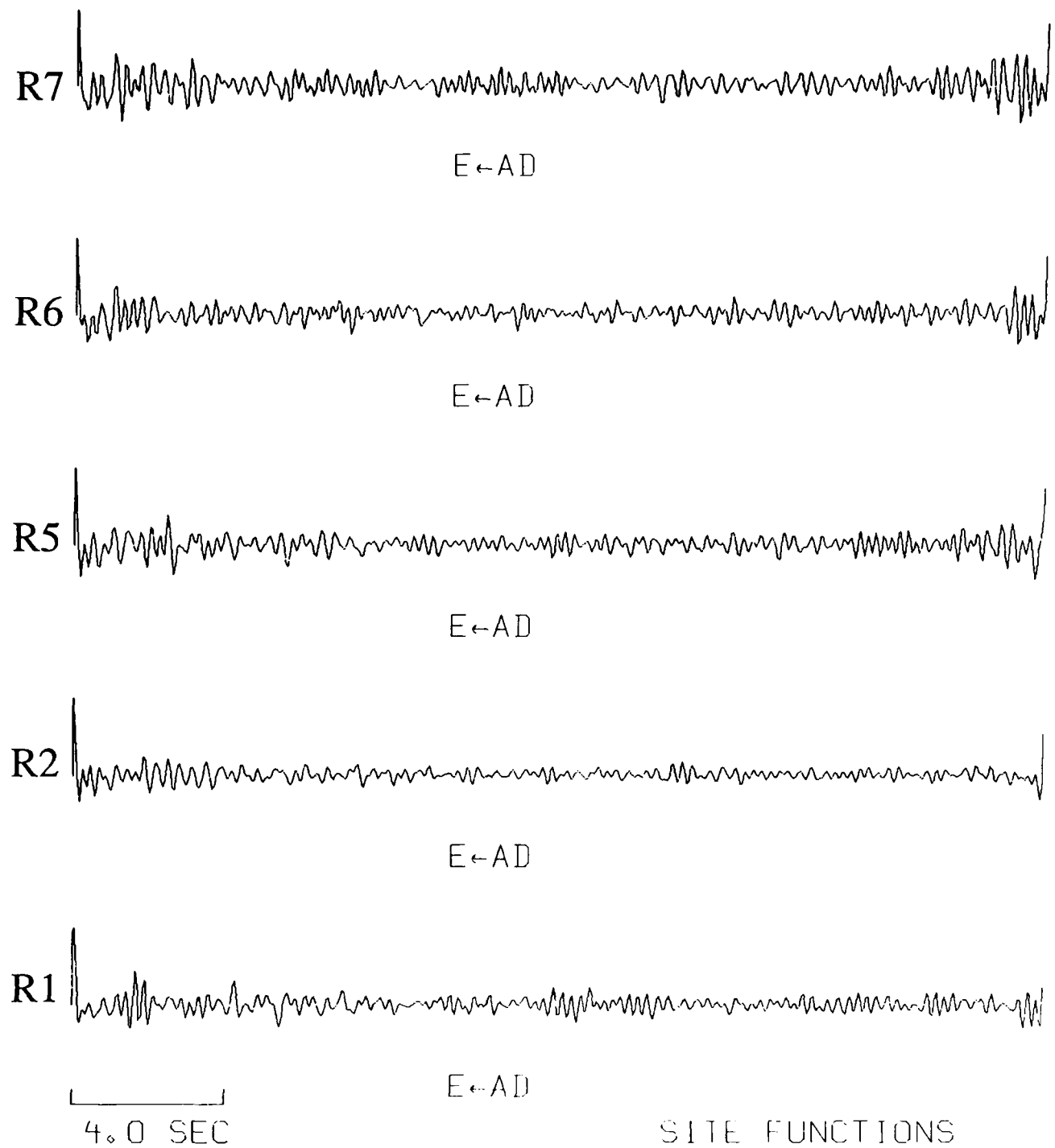
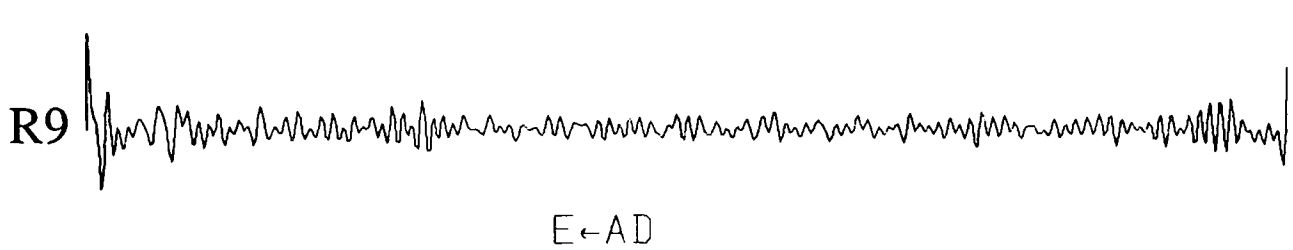
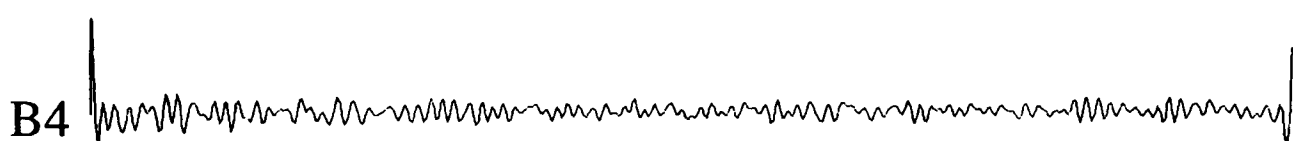


Figure B3. Deconvolved site terms for KTS events recorded at EKA.



4.0 SEC

SITE FUNCTIONS

Figure B3 (continued).

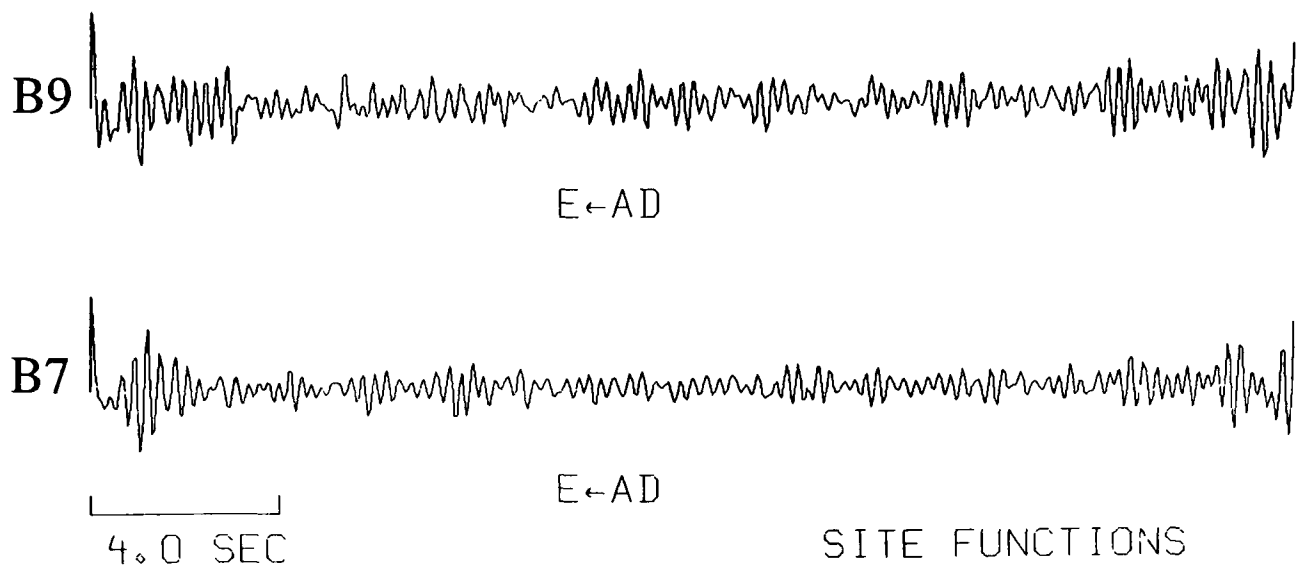
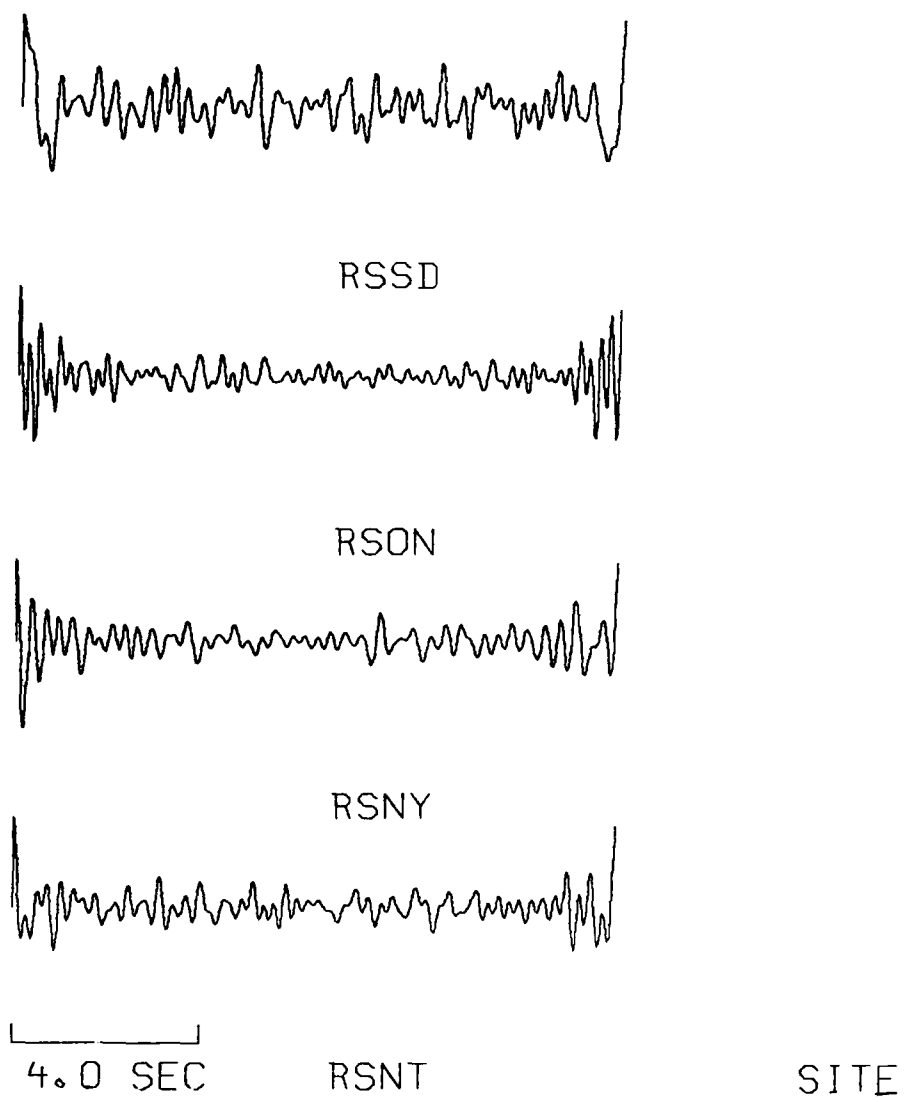
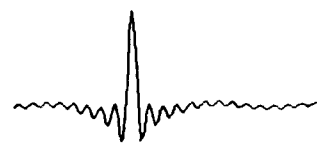


Figure B3 (continued).



**Figure B4.** Deconvolved site terms for Astrakhan events recorded at the RSTN.



KASSERI



TYBO



MAST



INLET



STILTON

4.0 SEC

RESOLUTION KERNELS

Figure B5. Resolution kernels for NTS events recorded at NORSAR.



27DEC74



16FEB73



29NOV71



30JUN71



22MAR71

4.0 SEC

RESOLUTION KERNELS

Figure B6. Resolution kernels for KTS events recorded at NORSAR.



7AUG75



30JUN75



11MAR75

4.0 SEC

RESOLUTION KERNELS

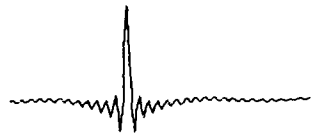
**Figure B6** (continued).



11 JUN78



7DEC76



4JUL76



27APR75



15JAN65

4.0 SEC

RESOLUTION KERNELS

Figure B7. Resolution kernels for KTS events recorded at EKA.



Event 4



Event 3



Event 2



Event 1

4.0 SEC

Figure B8. Resolution kernels for Astrakhan events recorded at the RSTN.

**(THIS PAGE INTENTIONALLY LEFT BLANK)**

## **Appendix C**

Original traces of explosion data.

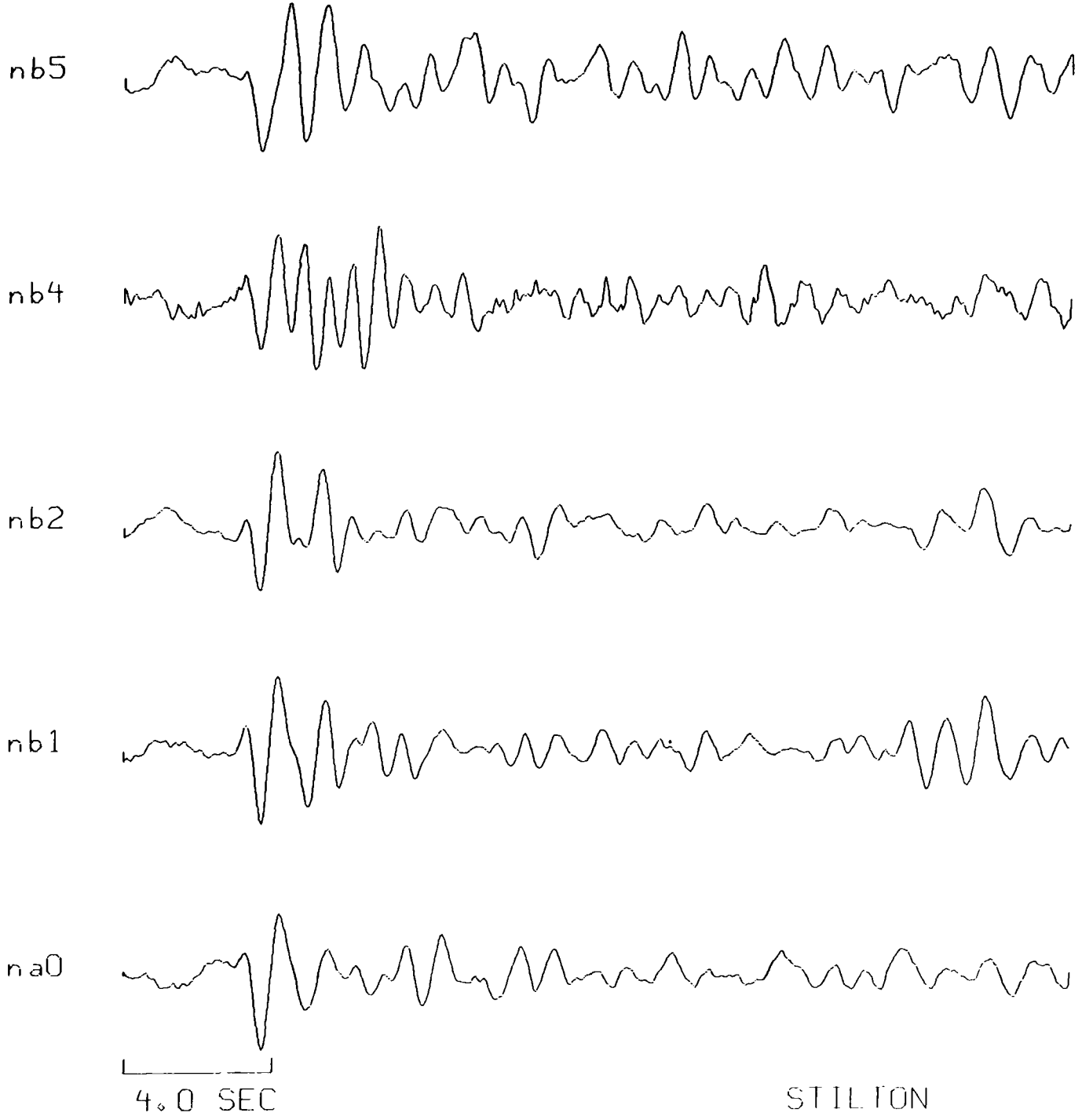
NTS data recorded at NORSAR.

Kazakh data recorded at NORSAR.

Kazakh data recorded at EKA.

Azgir data recorded at the RSTN.

**NTS data recorded at NORSAR.**



nb5



nb4



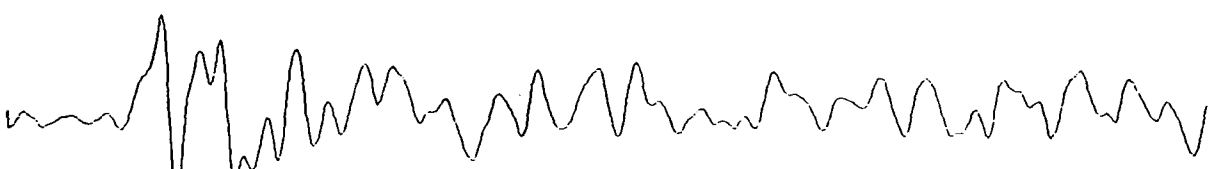
nb2



nb1

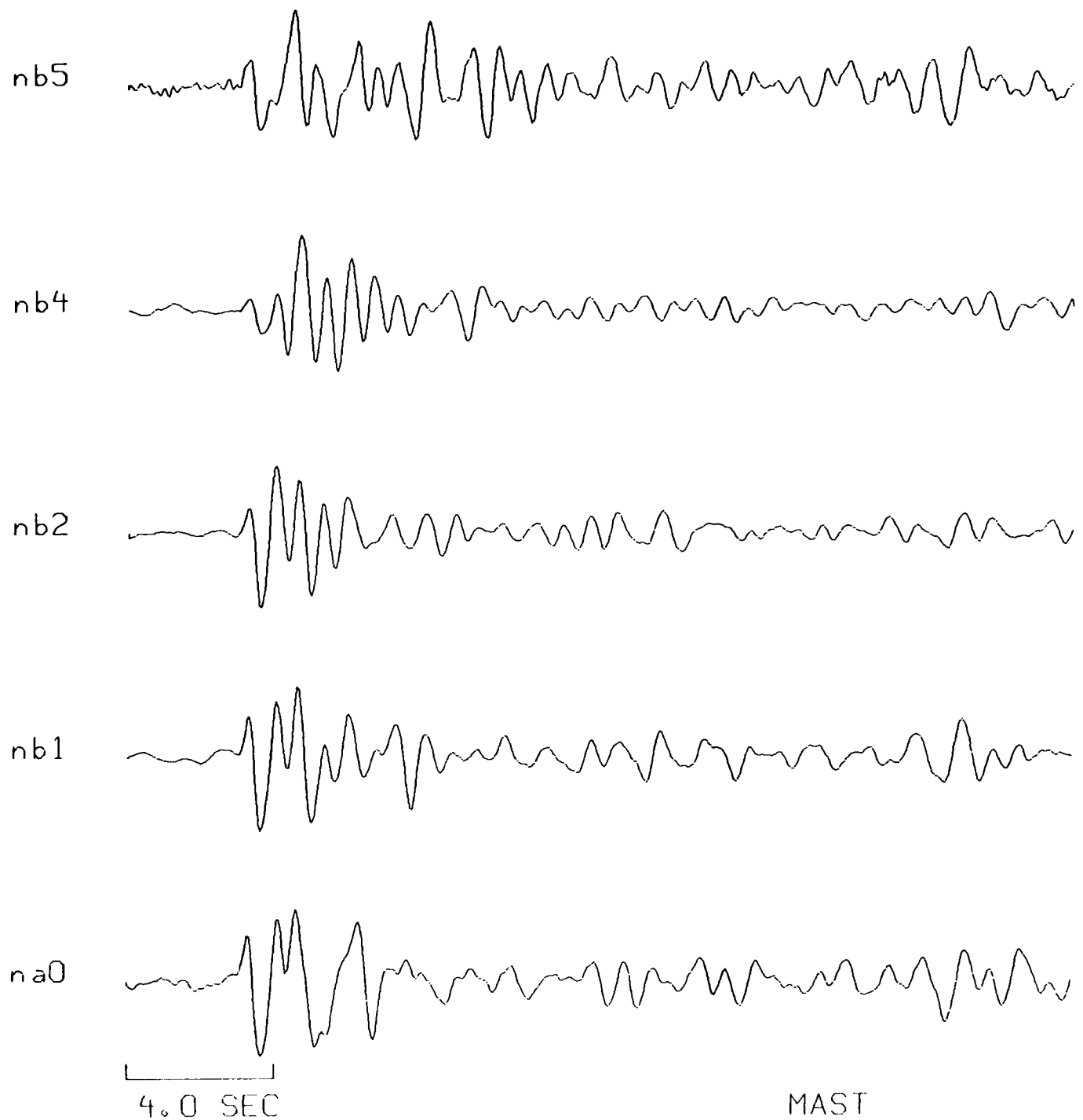


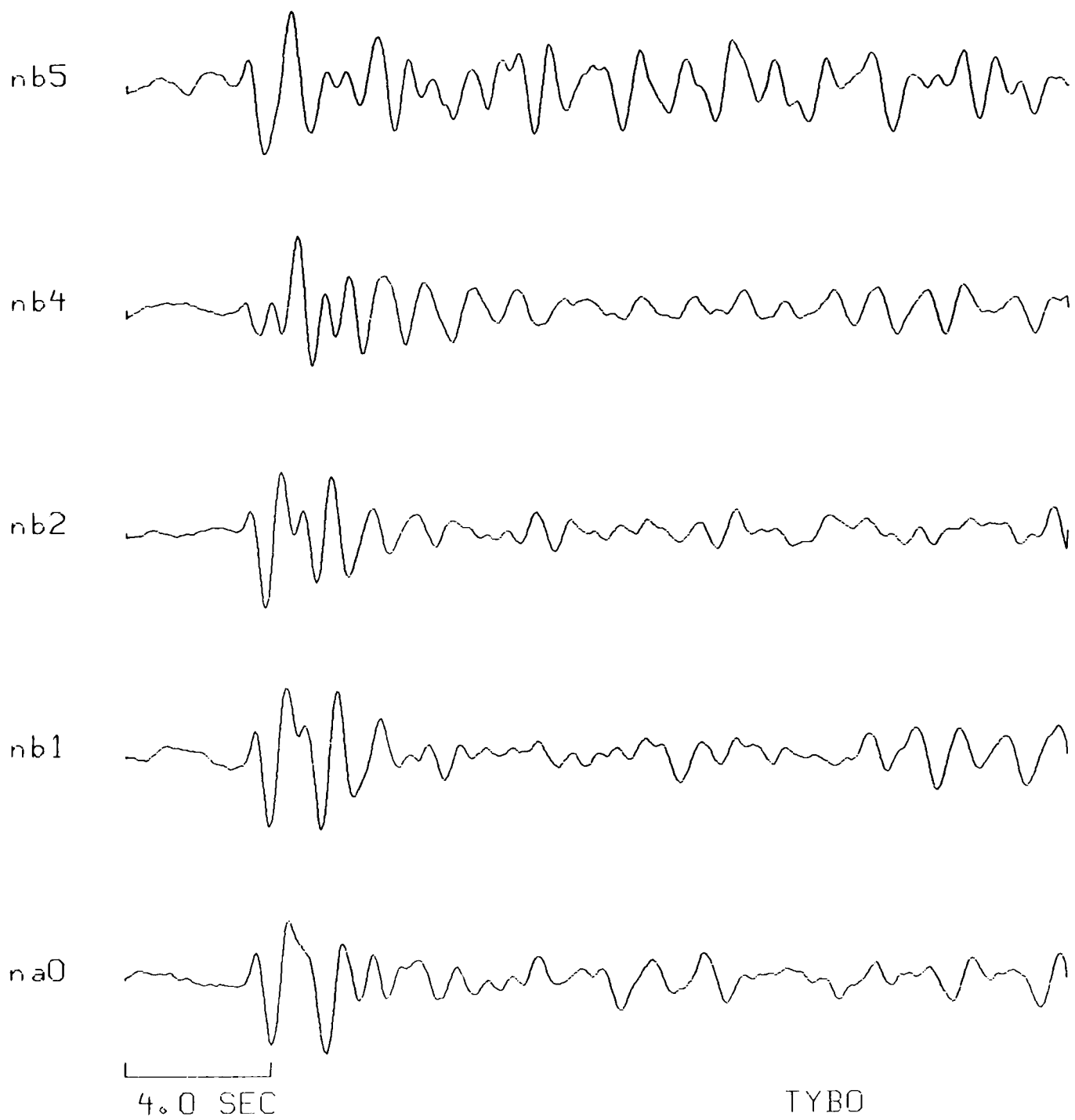
na0

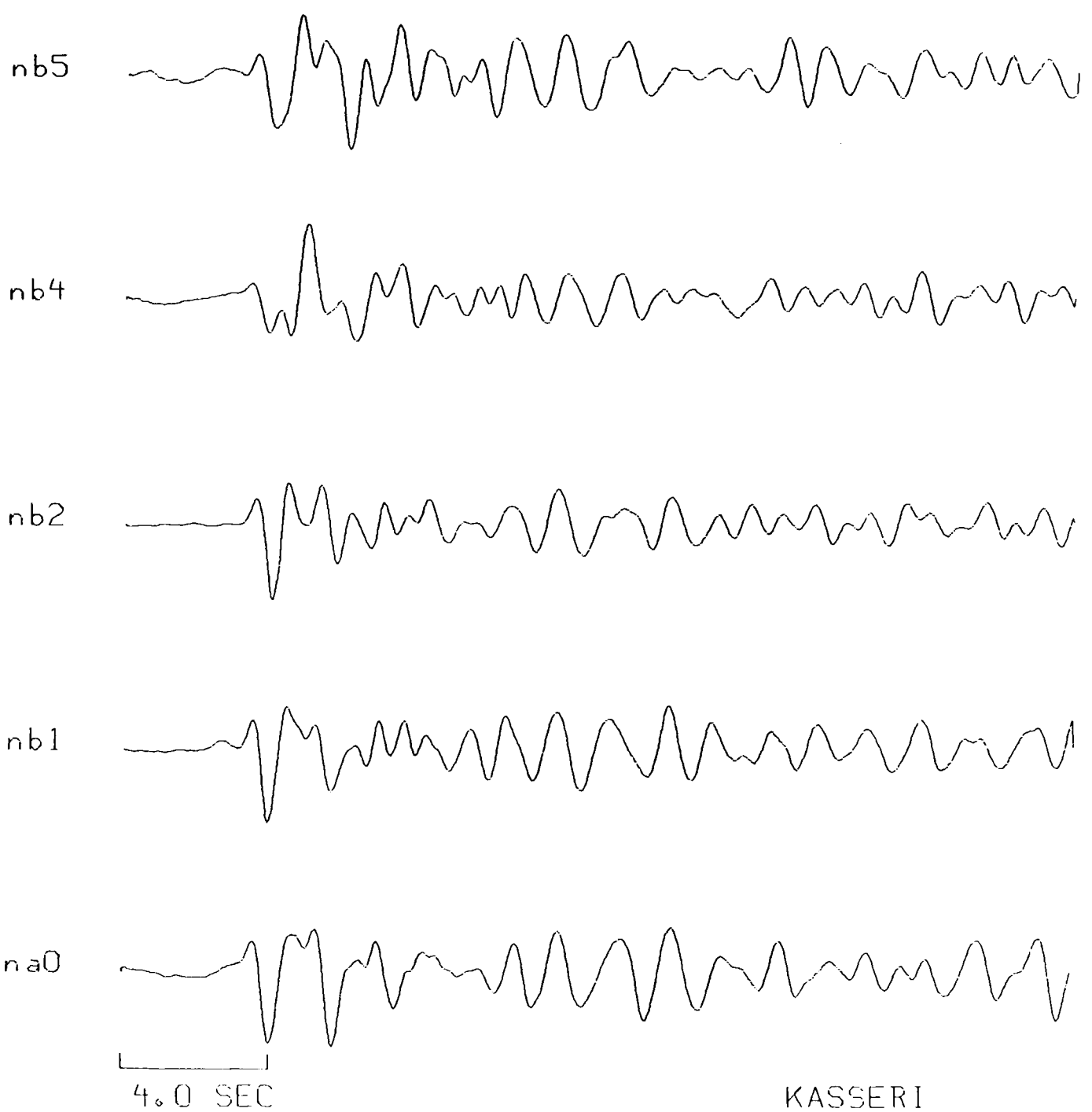


4.0 SEC

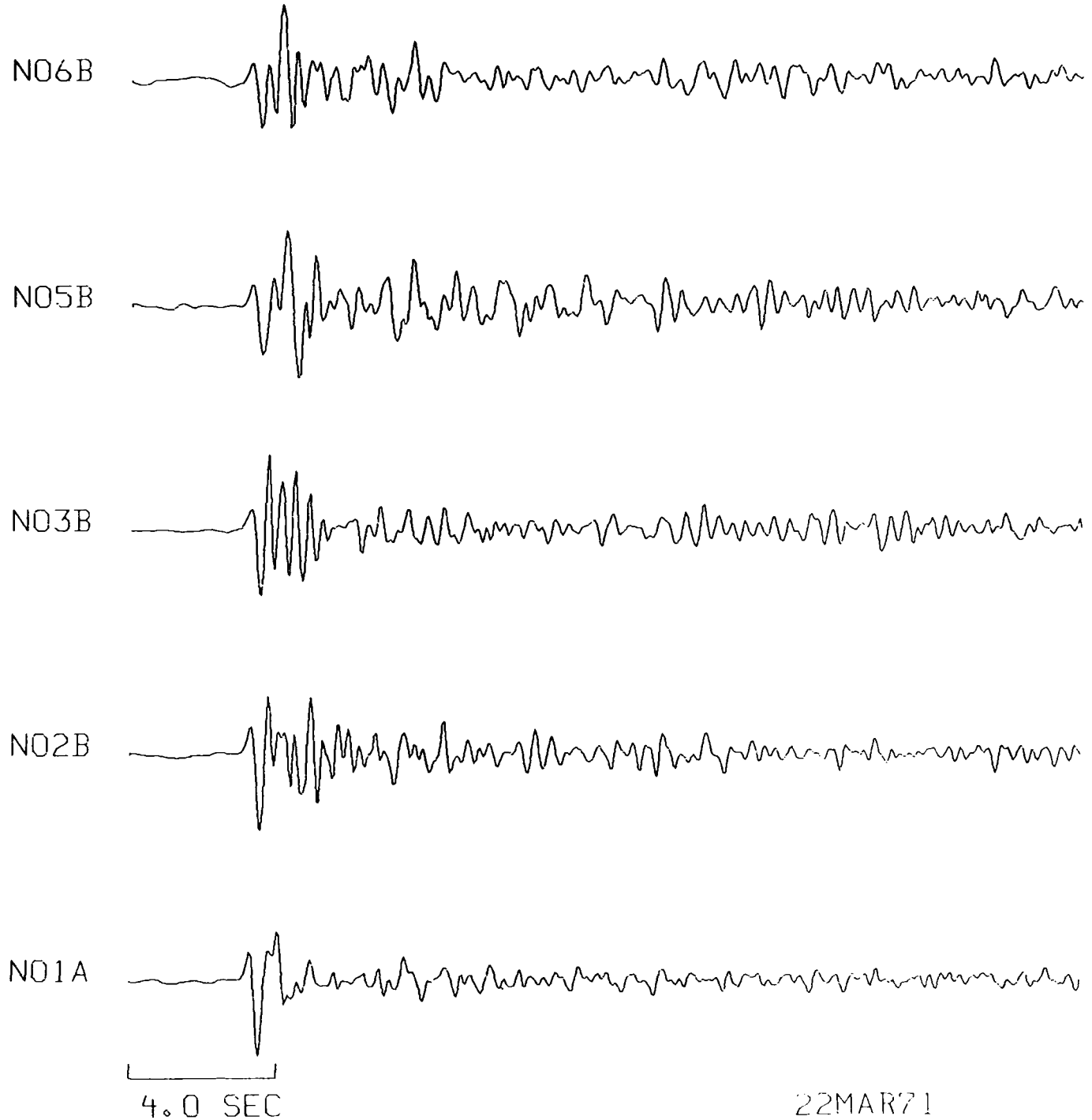
INLET







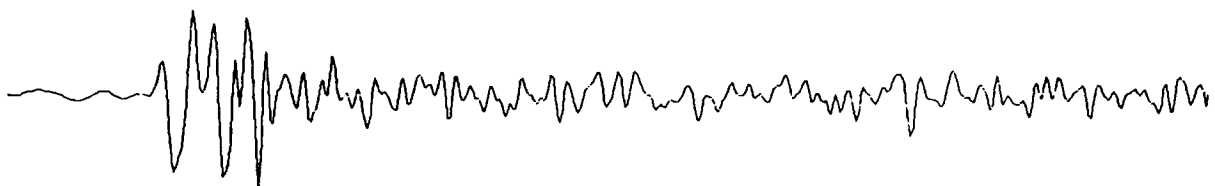
**Kazakh data recorded at NORSAR.**



NO2C

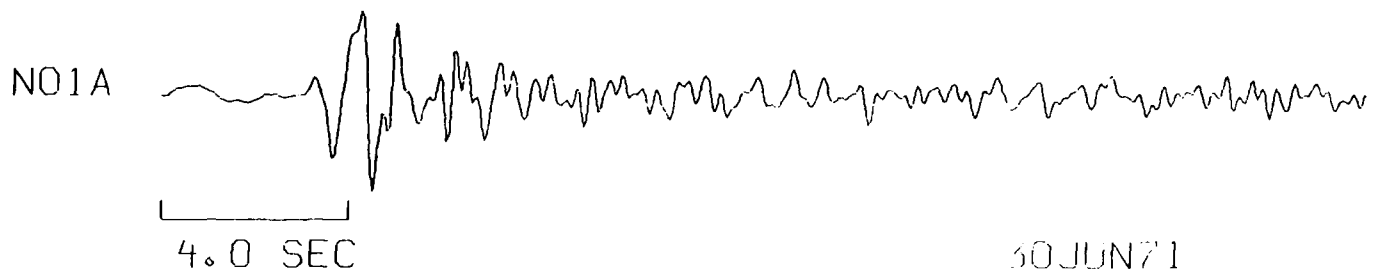
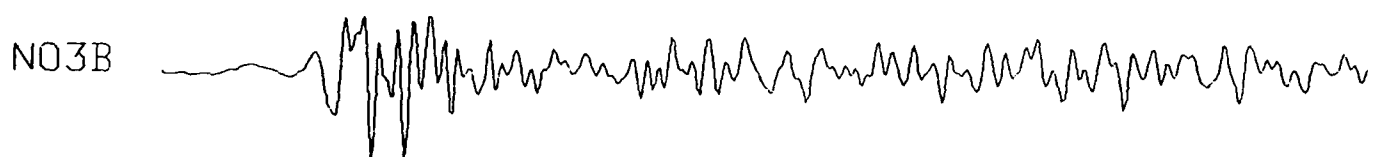


NO7B

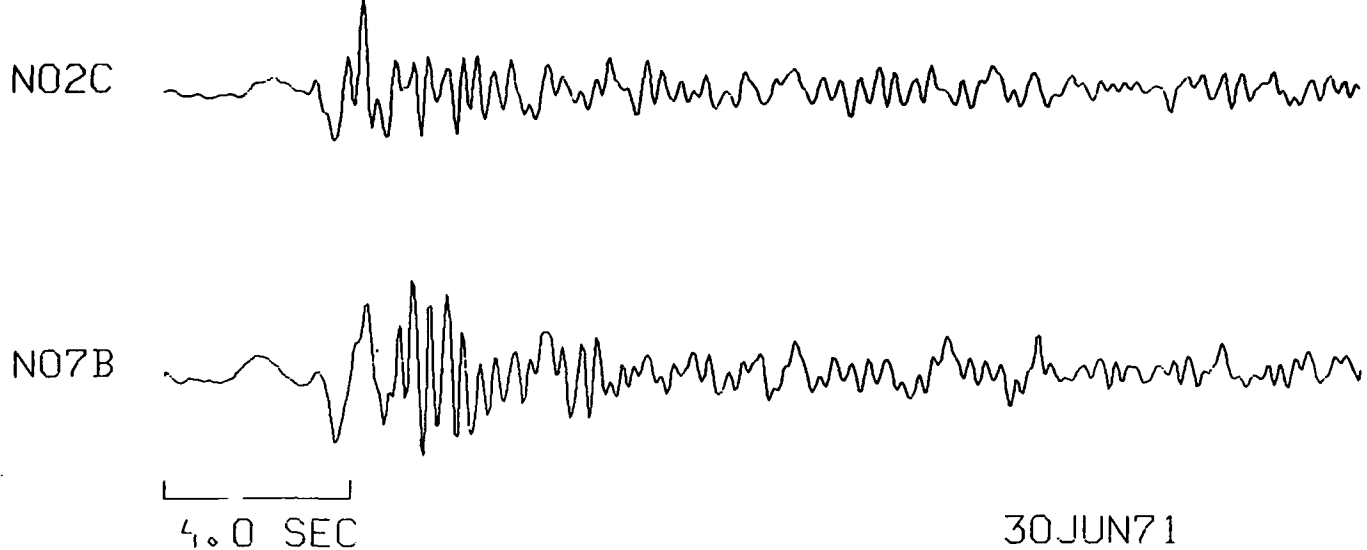


4.0 SEC

22MAR71

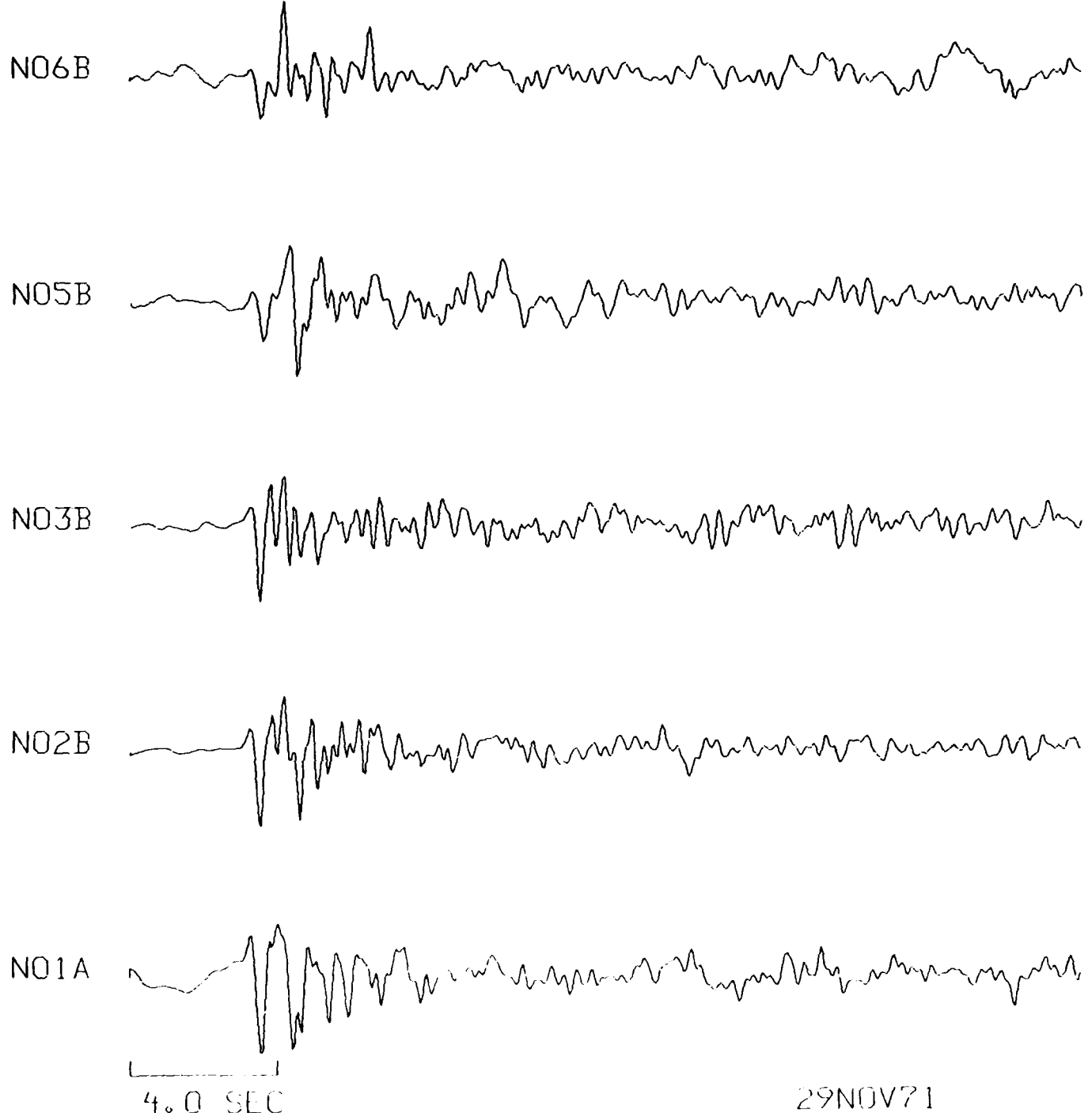


30 JUN 71



4.0 SEC

30 JUN 71



N02C

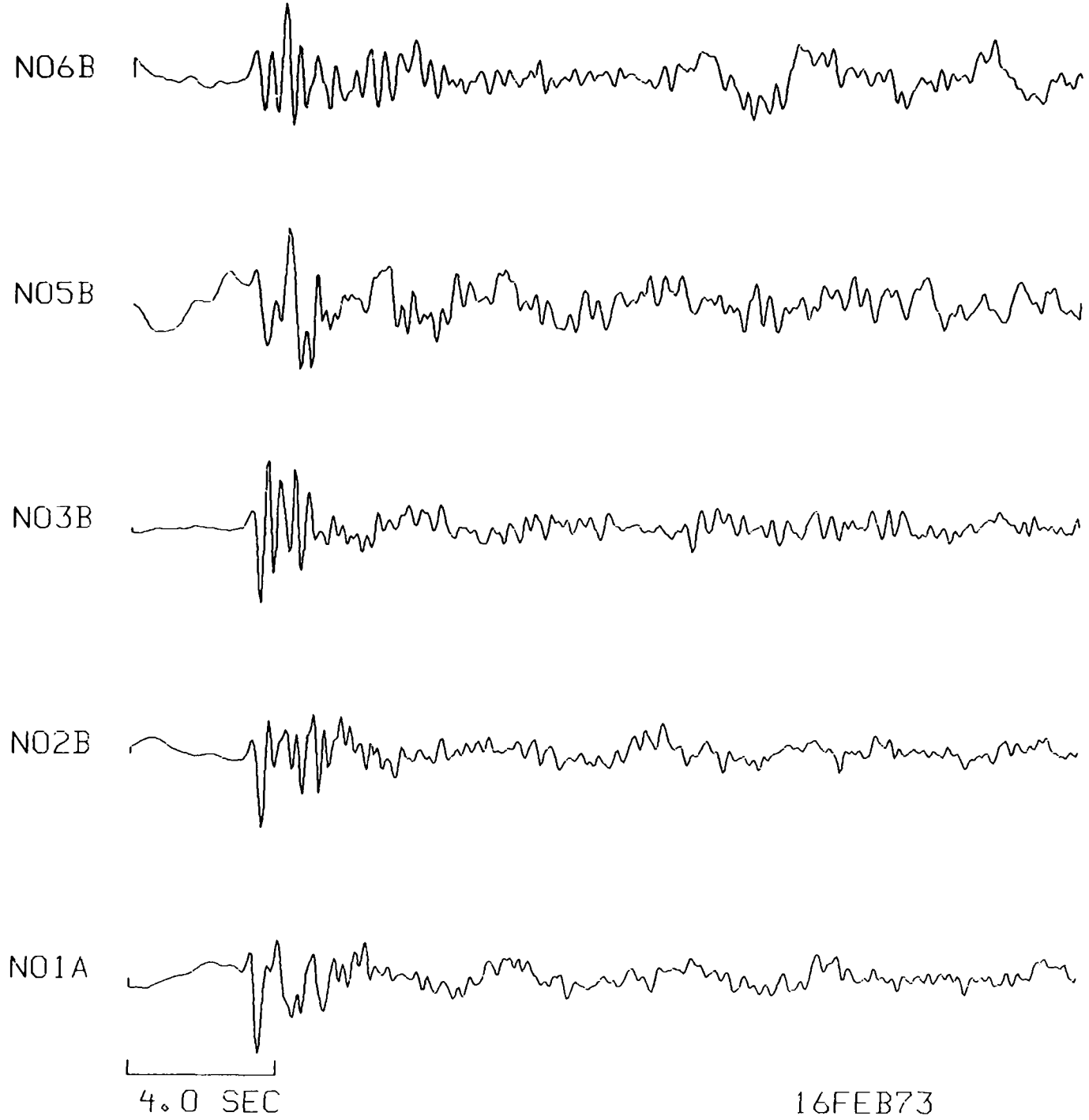


N07B

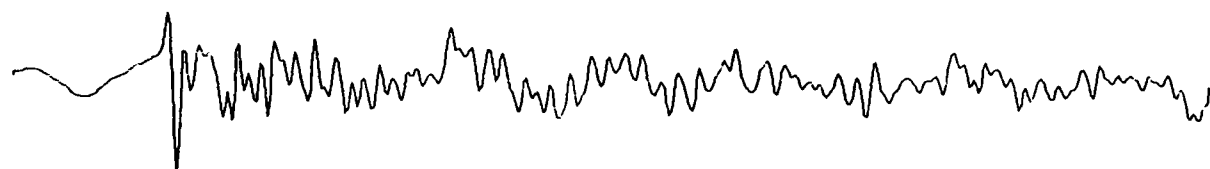


4.0 SEC

29NOV71



N02C

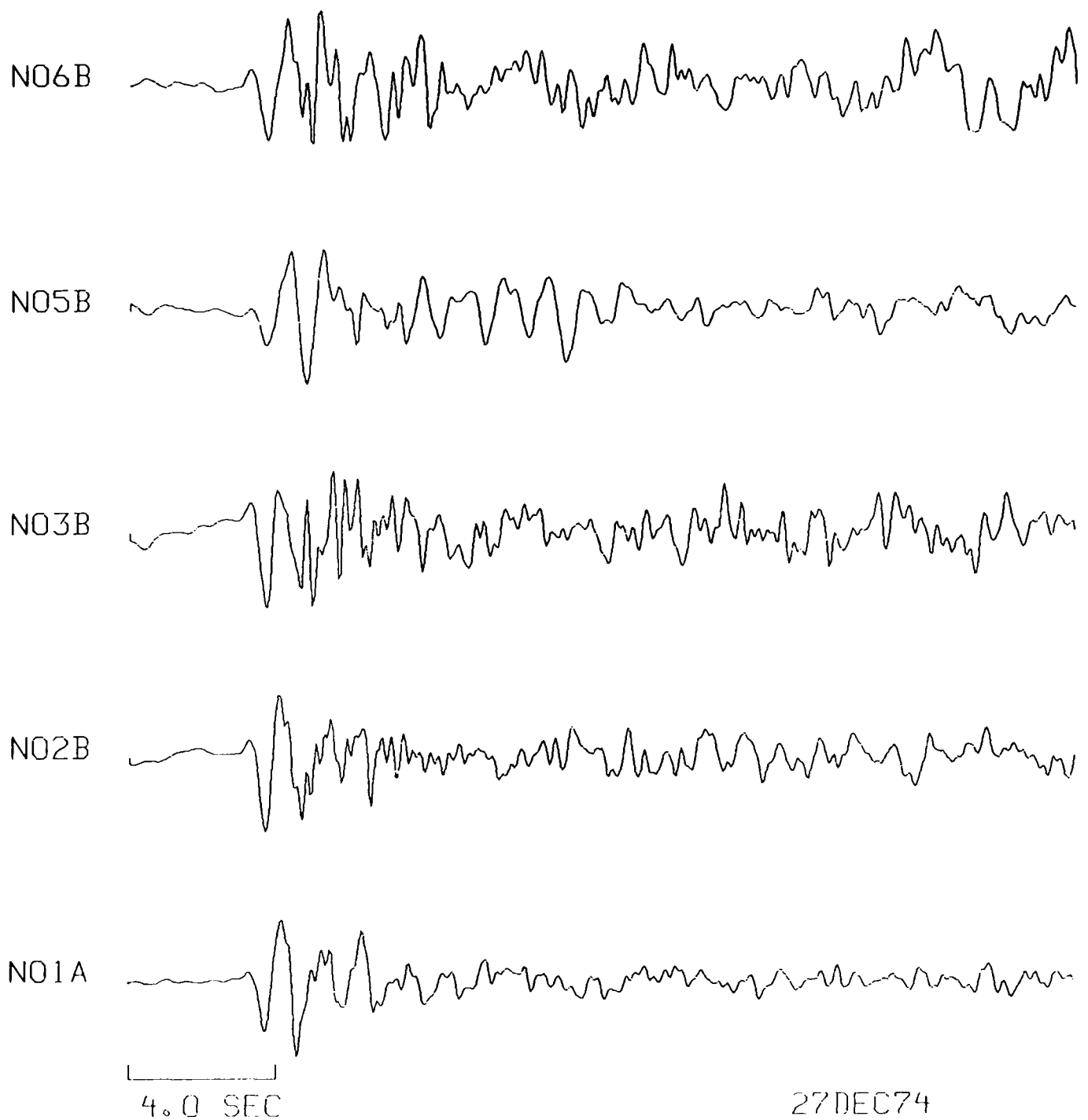


N07B



4.0 SEC

16FEB73



NO2C

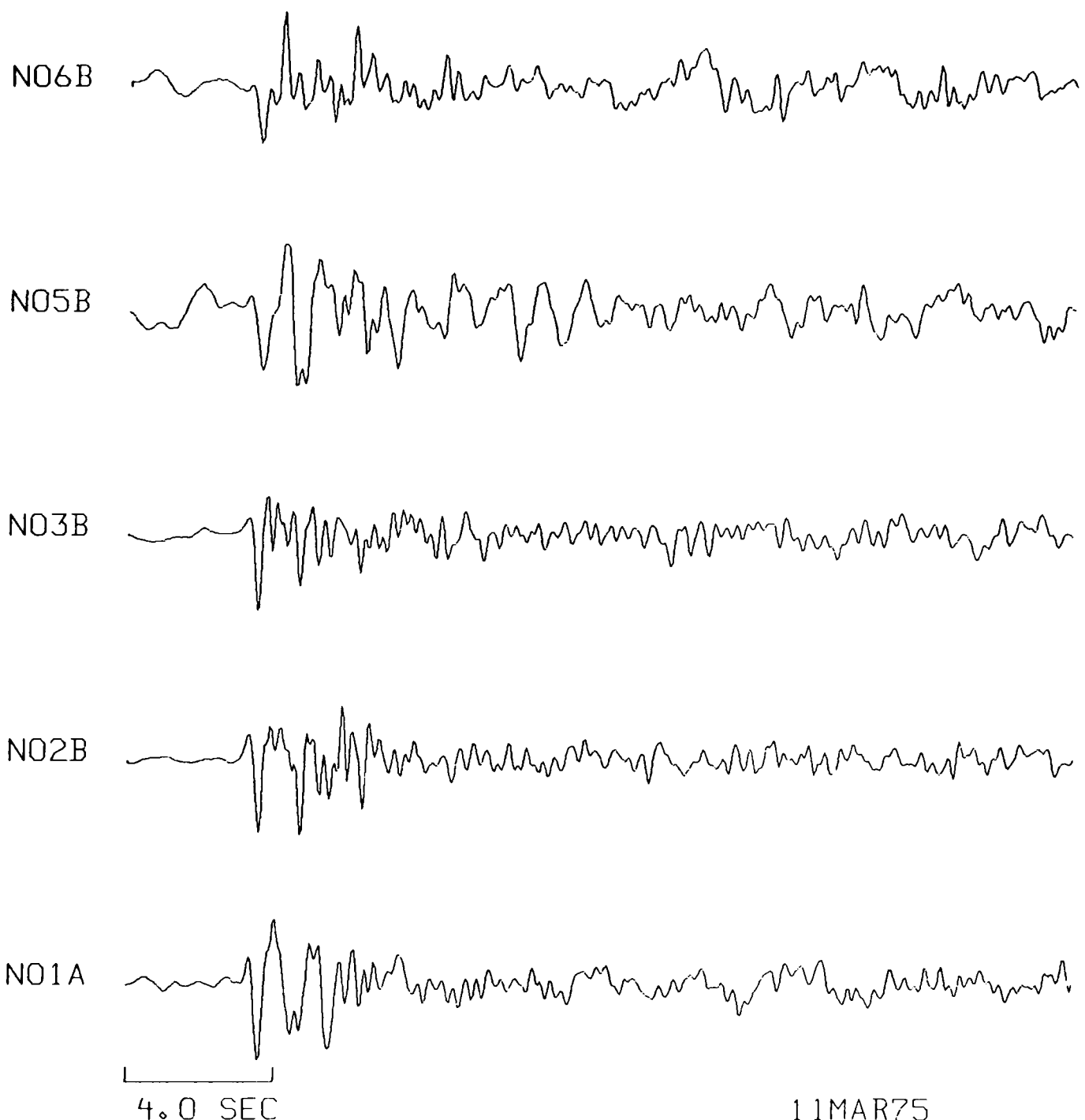


NO7B



4.0 SEC

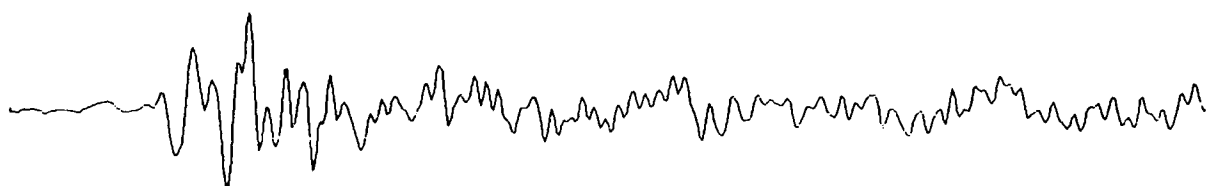
27DEC74



NO2C

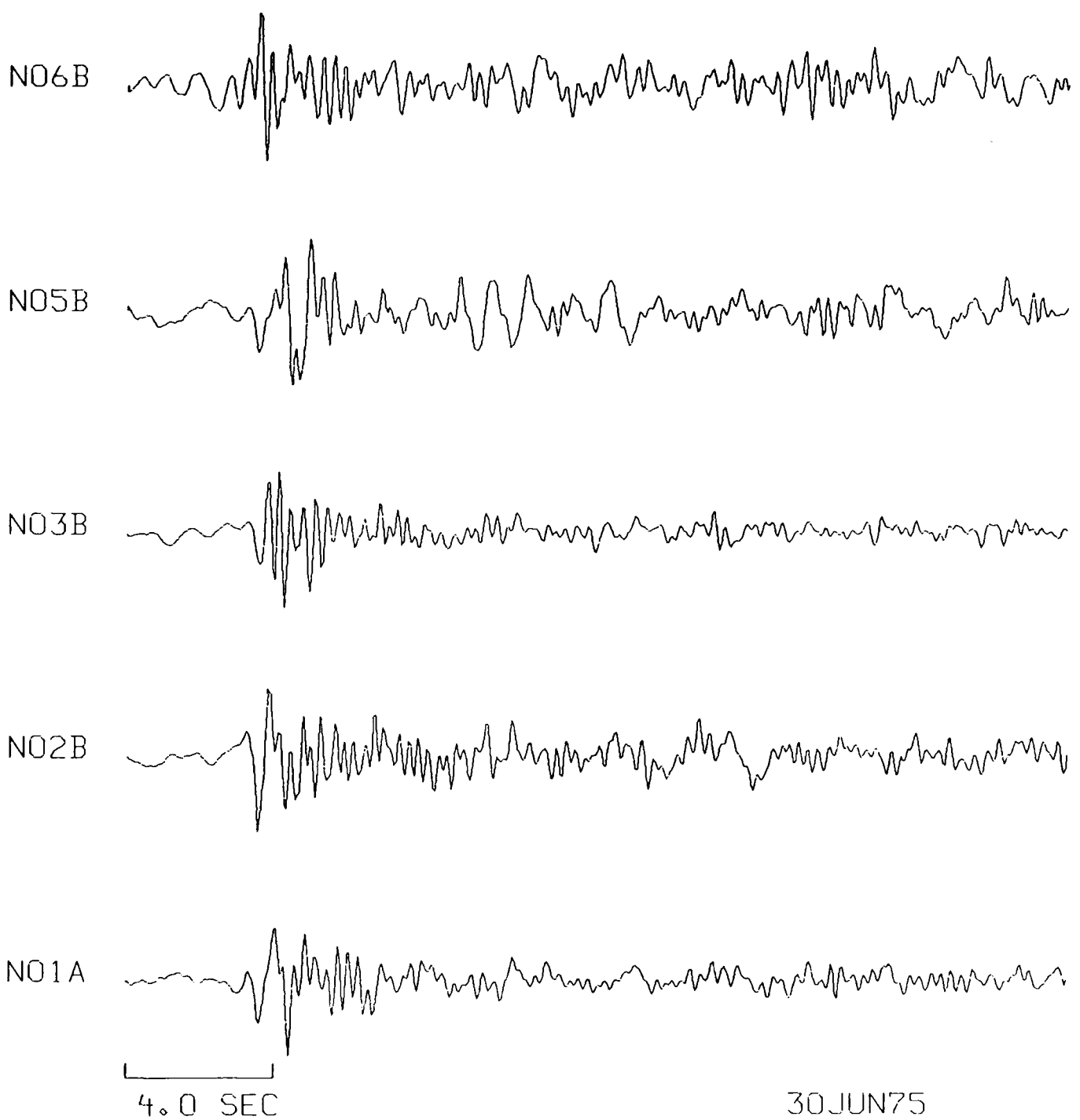


NO7B



4.0 SEC

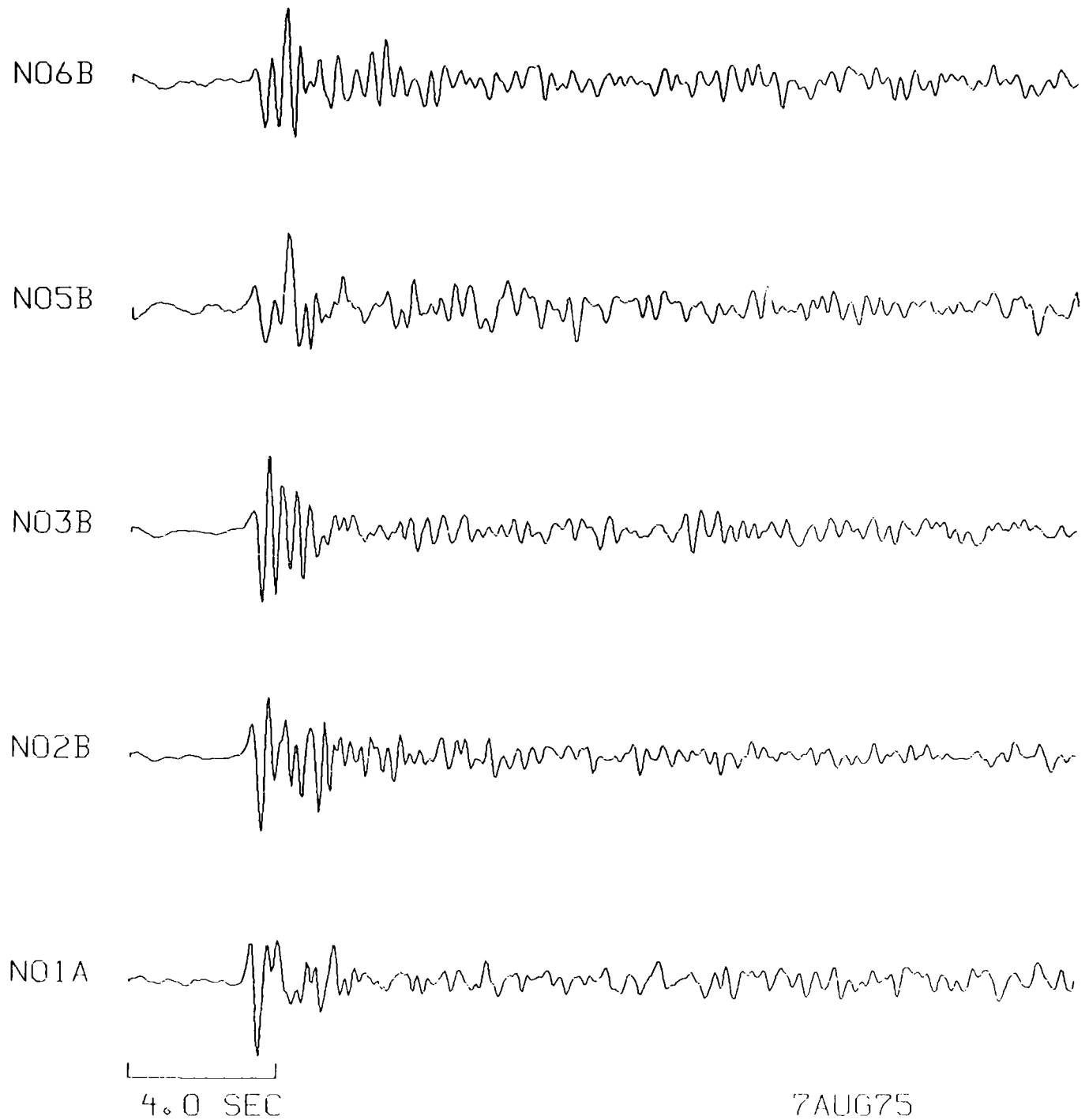
11 MAR 75

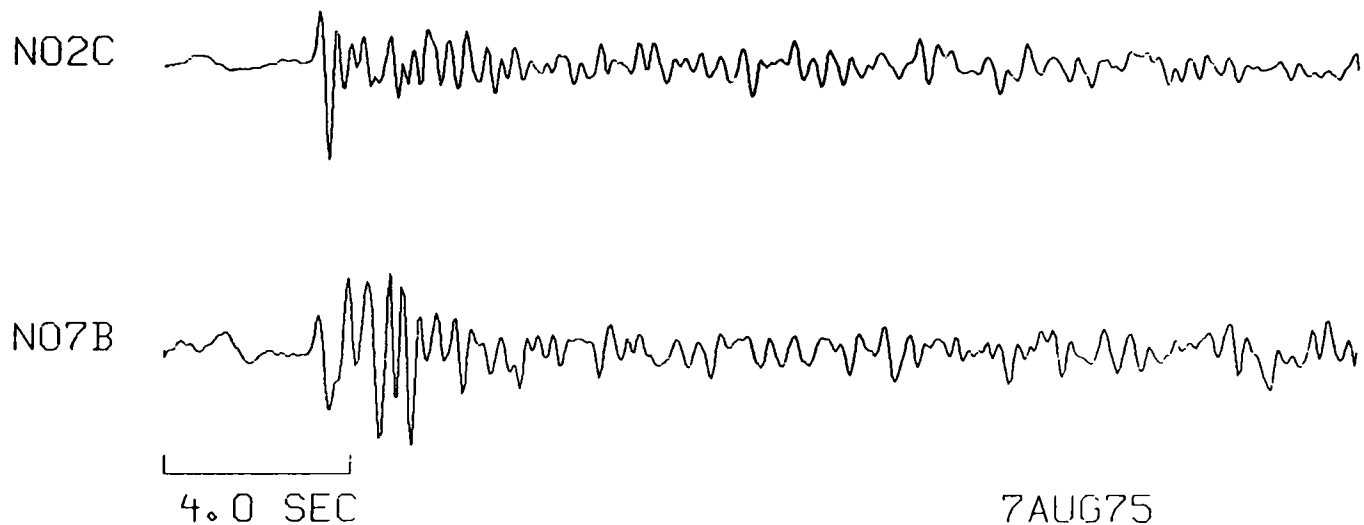




[ ]  
4.0 SEC

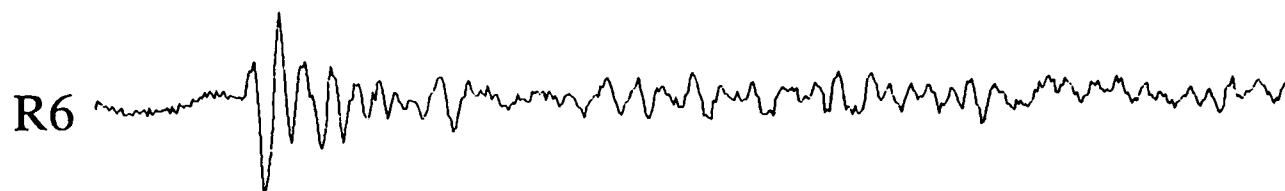
30JUN75





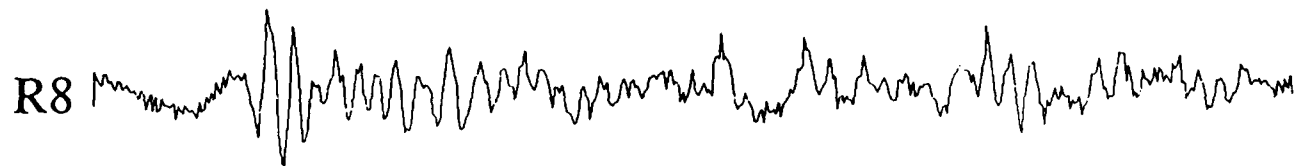
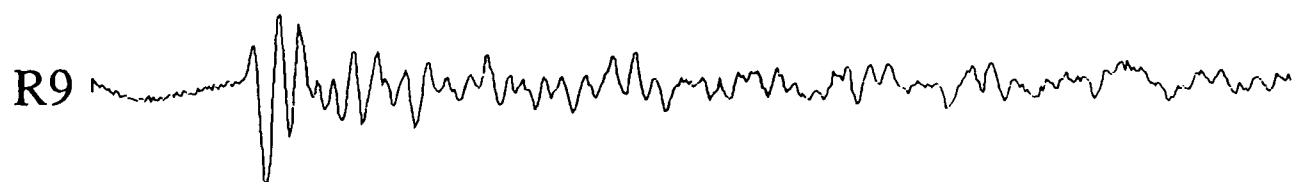
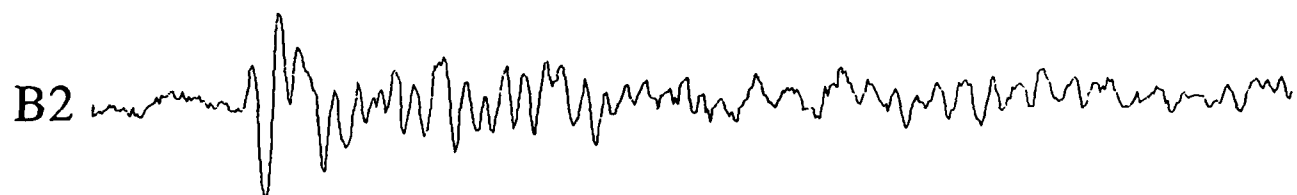
7AUG75

**Kazakh data recorded at EKA.**



4.0 SEC

15JAN65



4.0 SEC

15JAN65

B9



B7



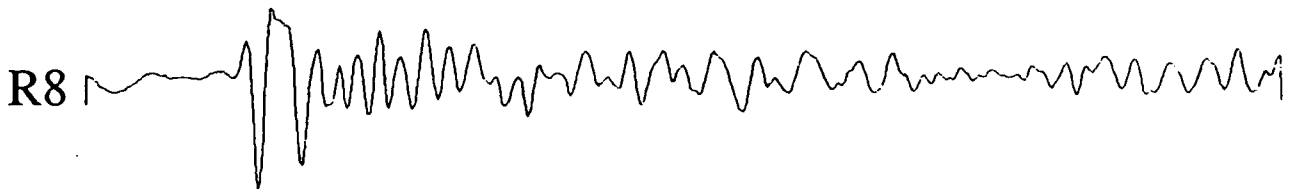
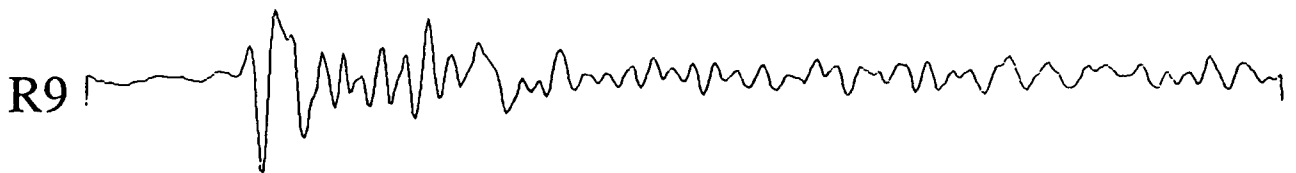
4.0 SEC

15JAN65



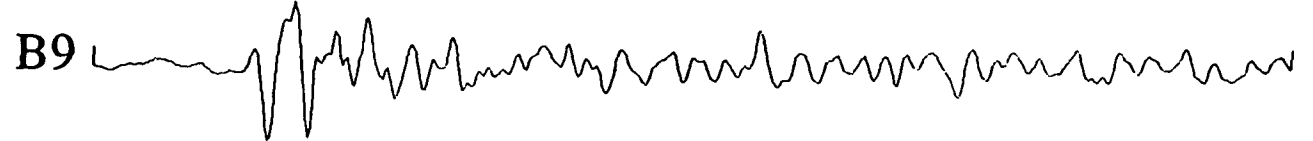
4.0 SEC

27APR75



4.0 SEC

27 APR 75



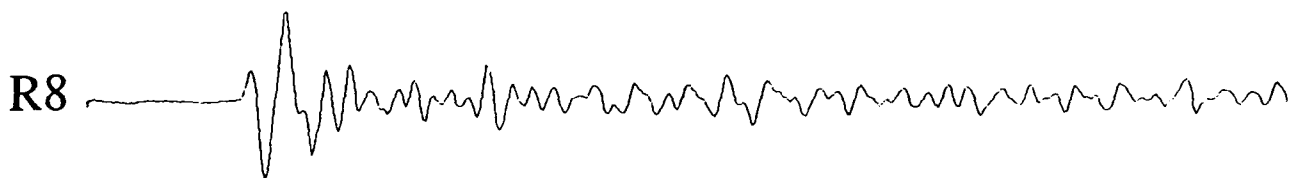
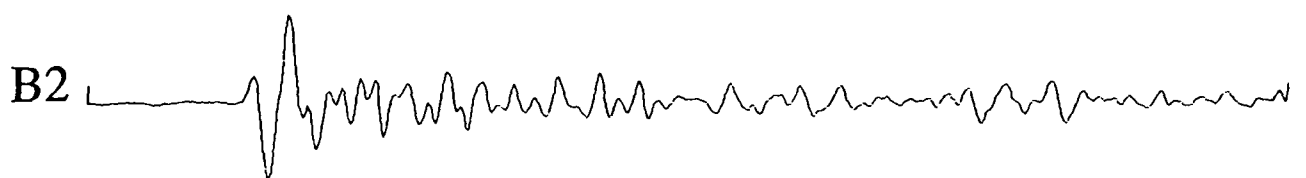
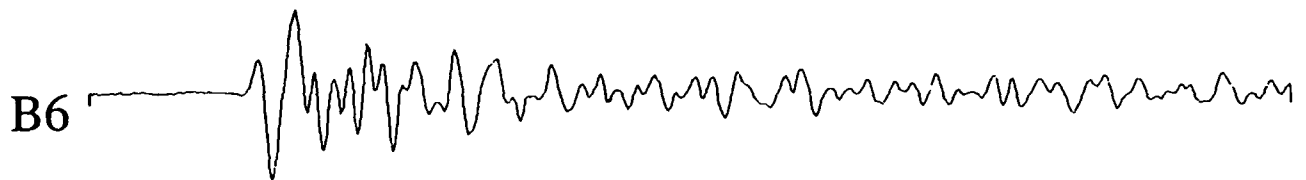
4.0 SEC

27APR75



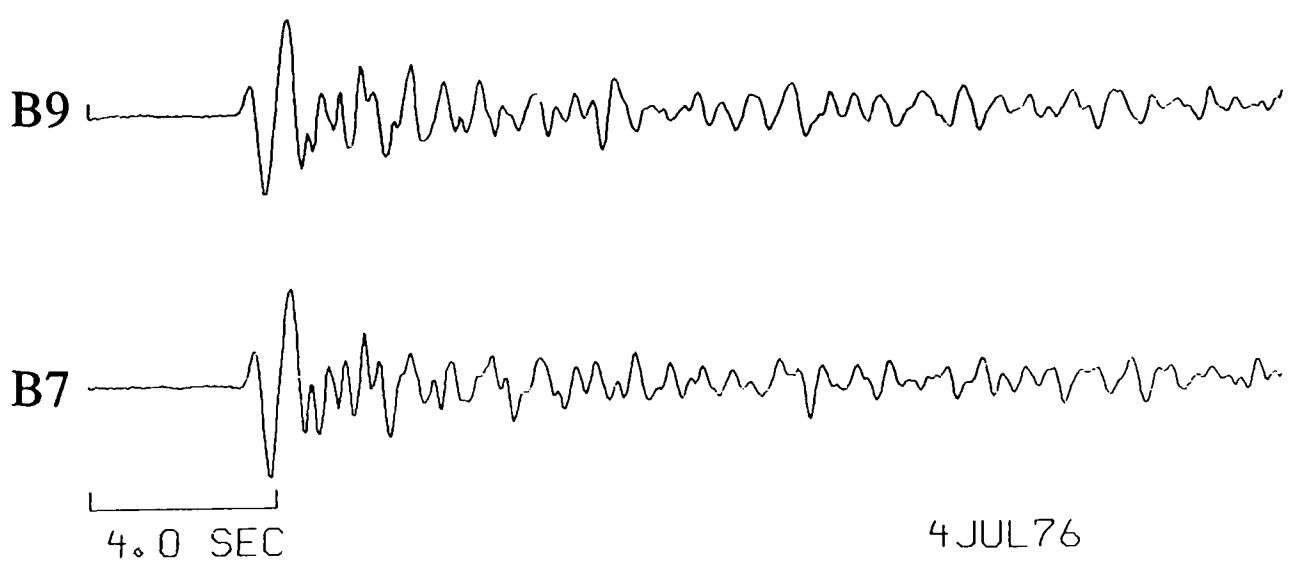
4.0 SEC

4 JUL 76

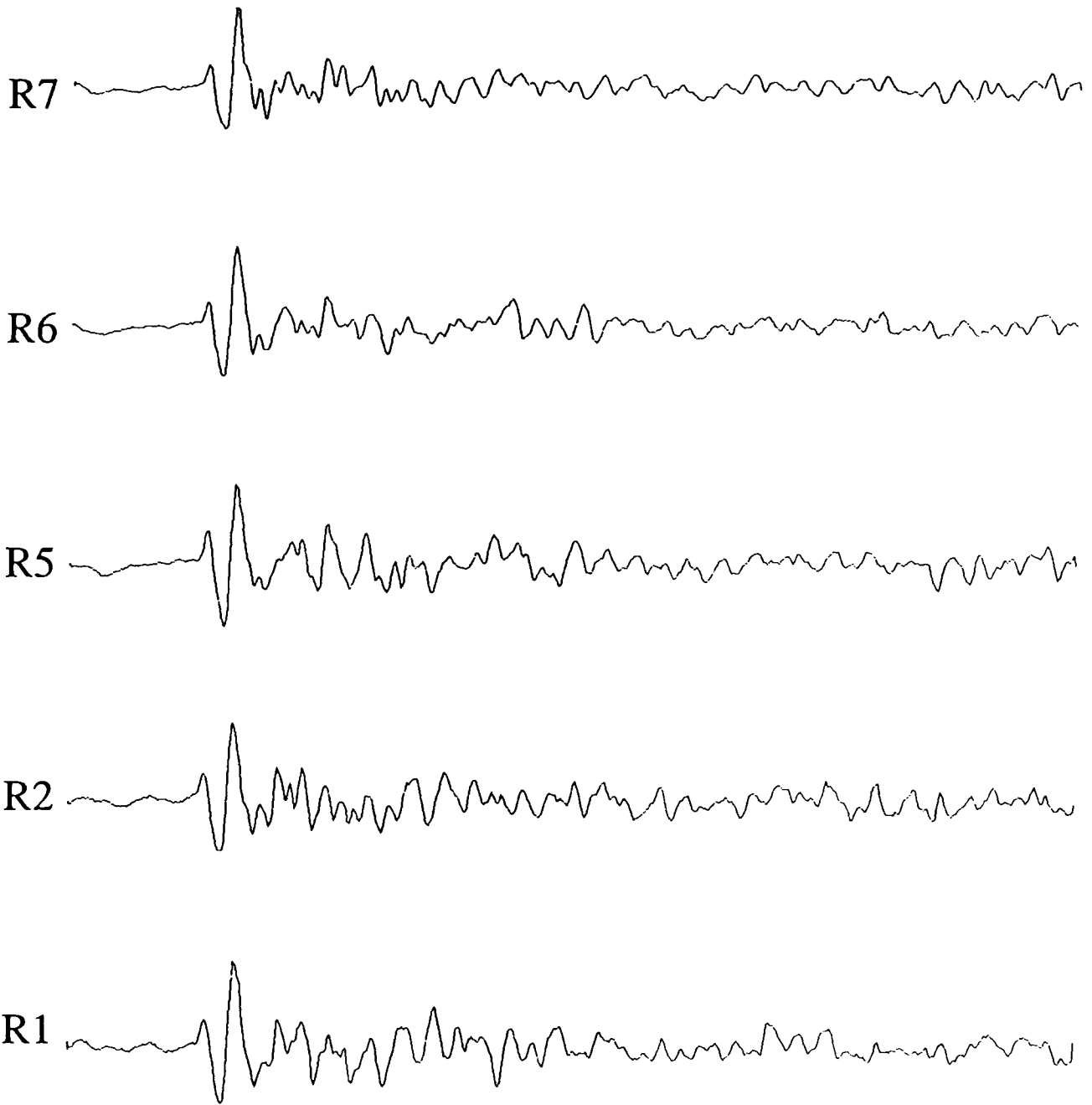


[ ]  
4.0 SEC

4 JUL 76

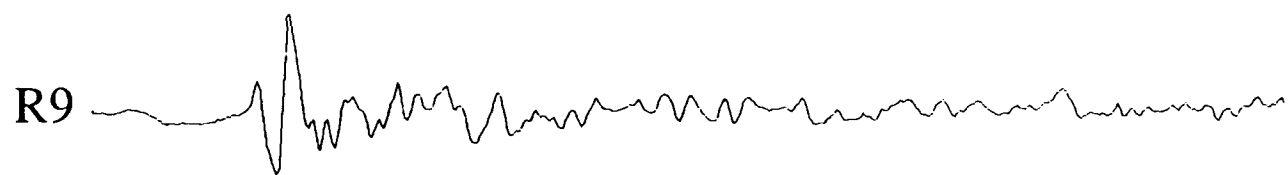
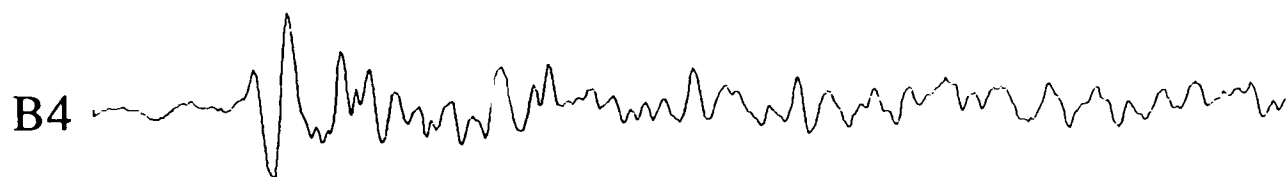


4 JUL 76



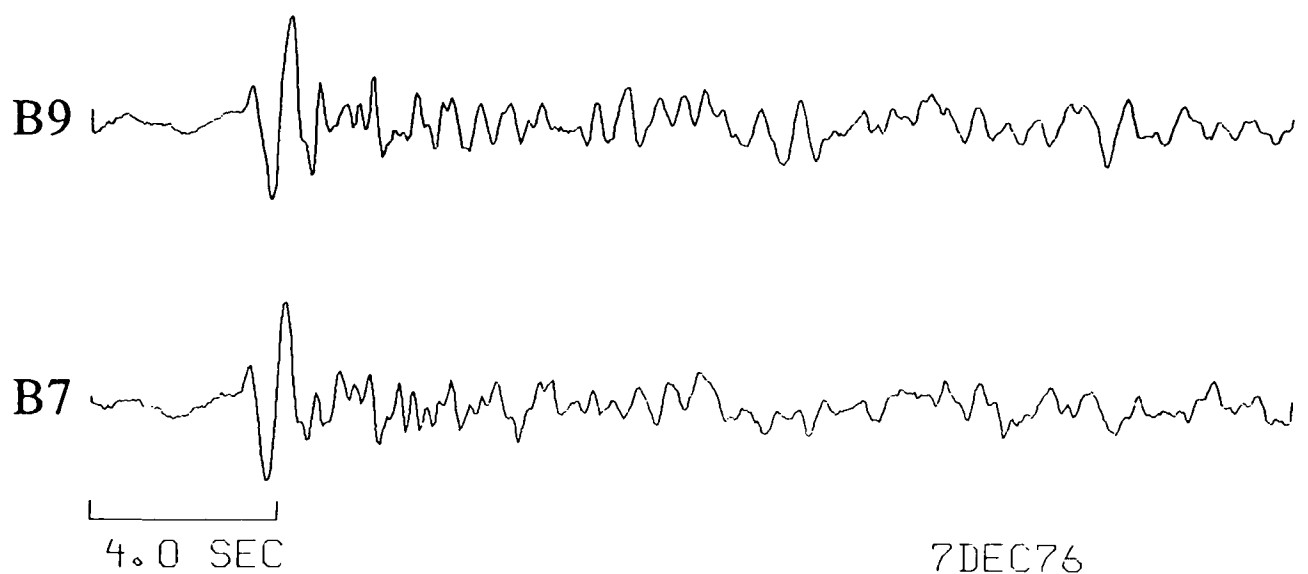
[ ]  
4.0 SEC

7DEC76

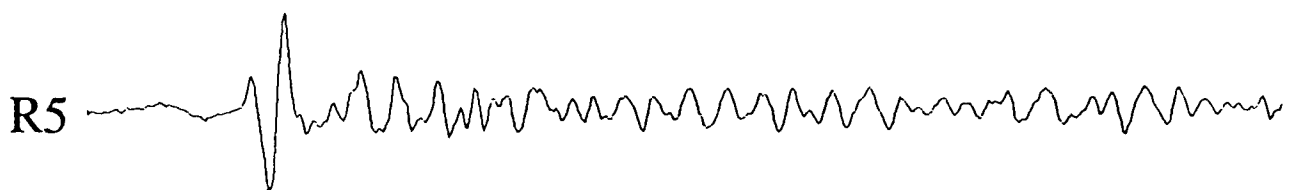
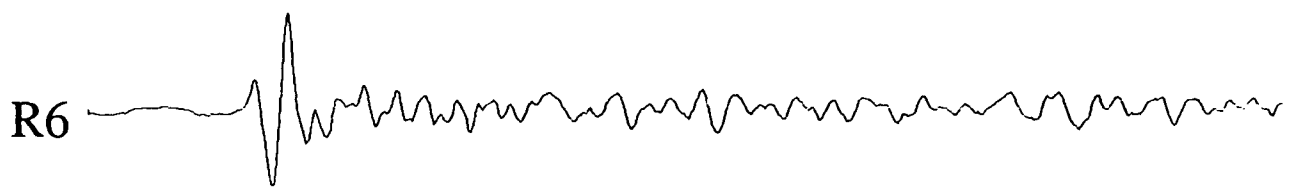
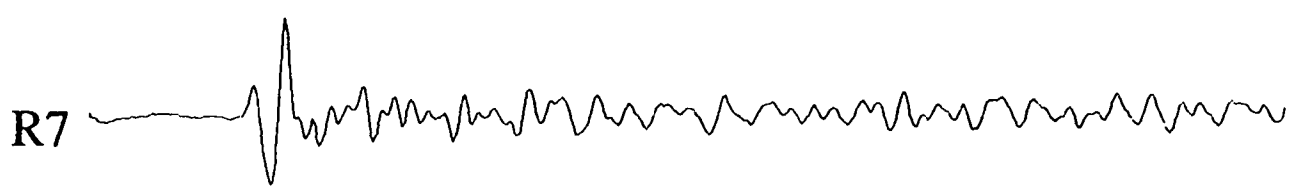


[ ]  
4.0 SEC

7 DEC 76

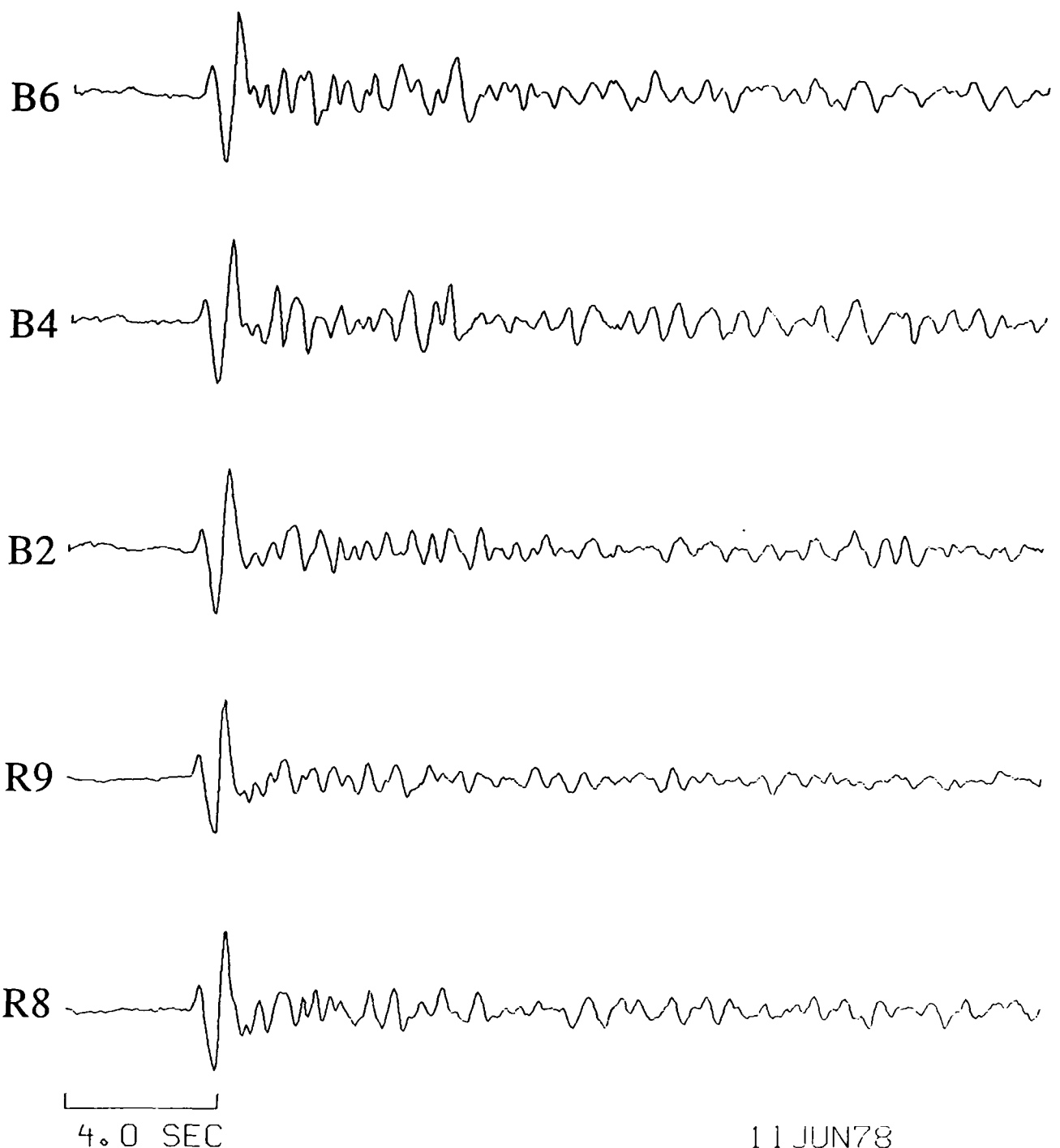


7DEC76

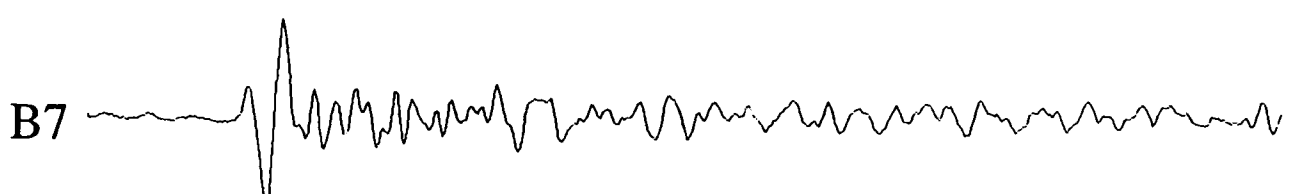


4.0 SEC

11 JUN 78



11 JUN78



4.0 SEC

11 JUN 78

**Azgir data recorded at the RSTN.**

RSSD



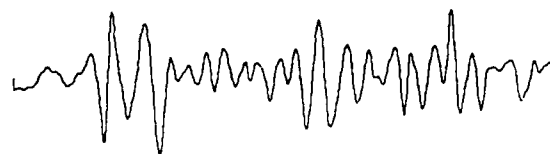
RSON



RSNY



RSNT



4.0 SEC

Event 1

RSSD



RSON



RSNY



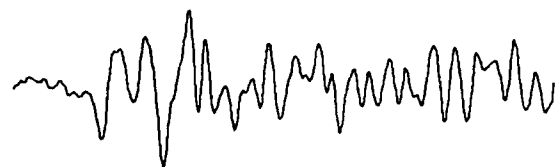
RSNT



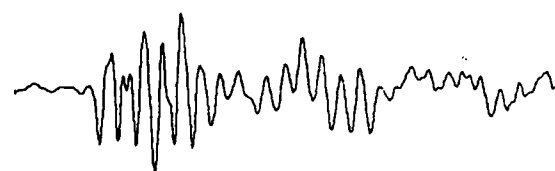
4.0 SEC

Event 2

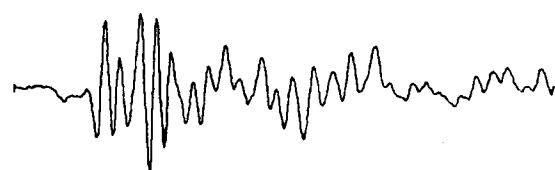
RSSD



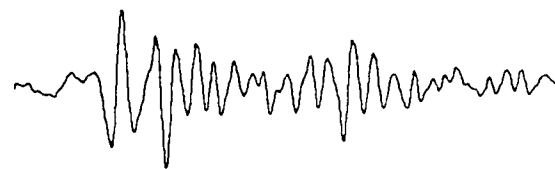
RSON



RSNY



RSNT



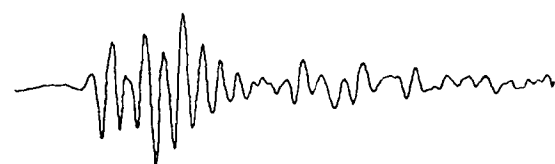
4.0 SEC

Event 3

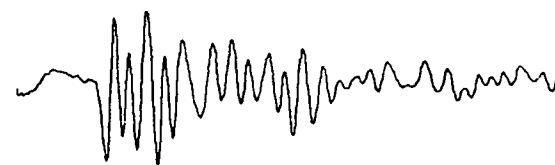
RSSD



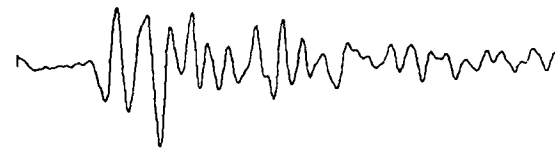
RSON



RSNY



RSNT



4.0 SEC

Event 4

**(THIS PAGE INTENTIONALLY LEFT BLANK)**

## **Appendix D**

Reconstructed traces of explosion data.

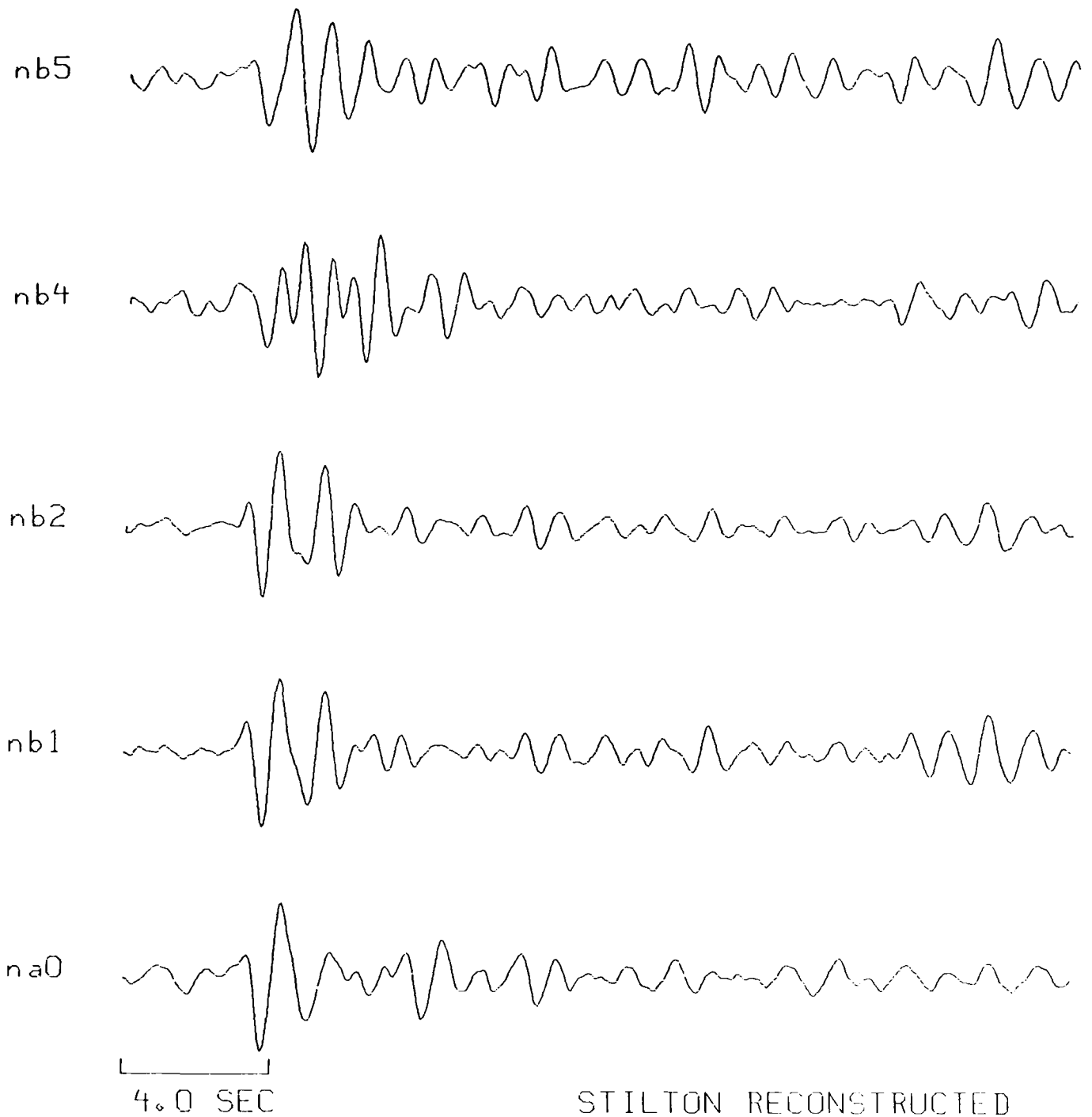
NTS data recorded at NORSAR.

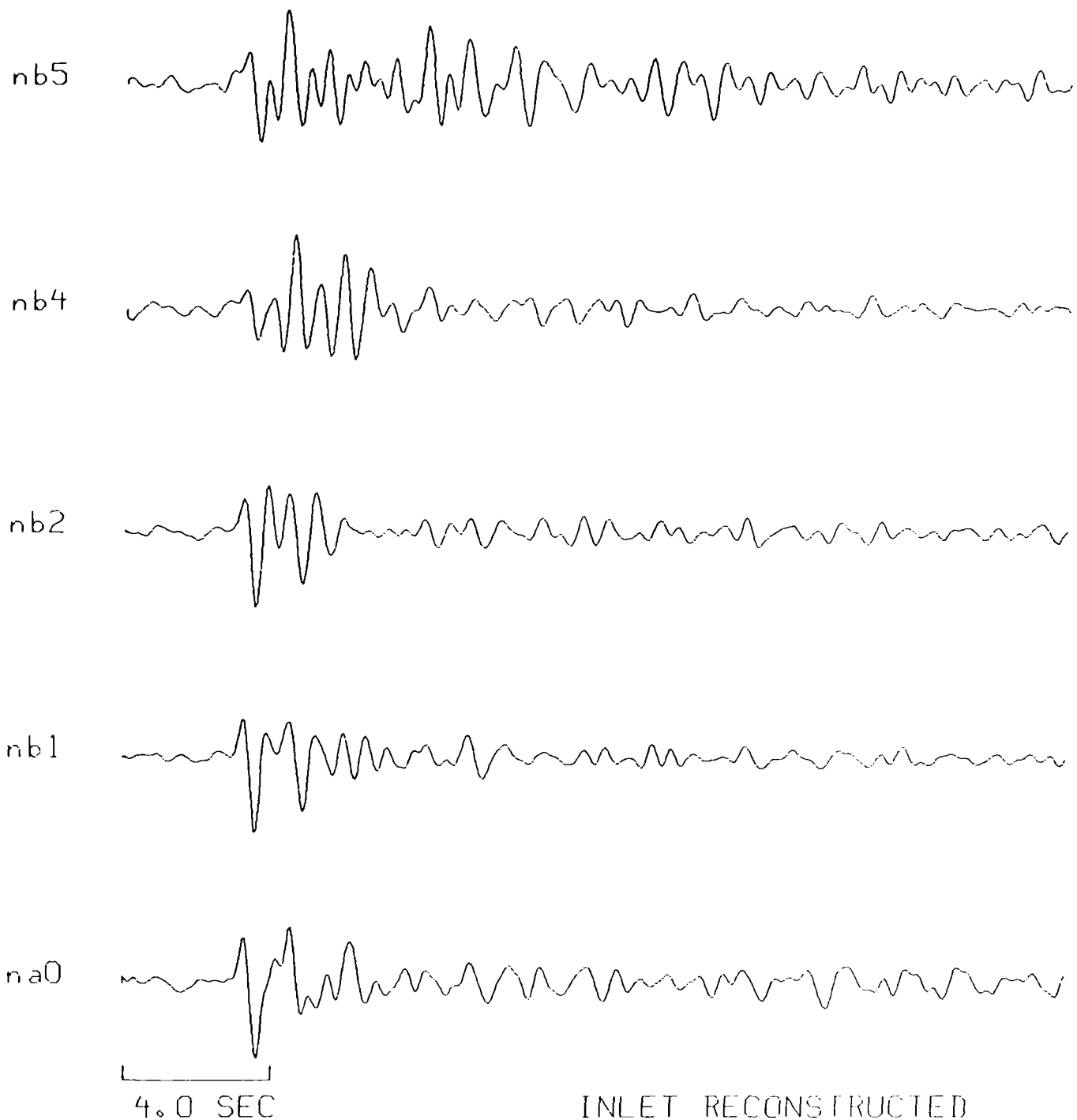
Kazakh data recorded at NORSAR.

Kazakh data recorded at EKA.

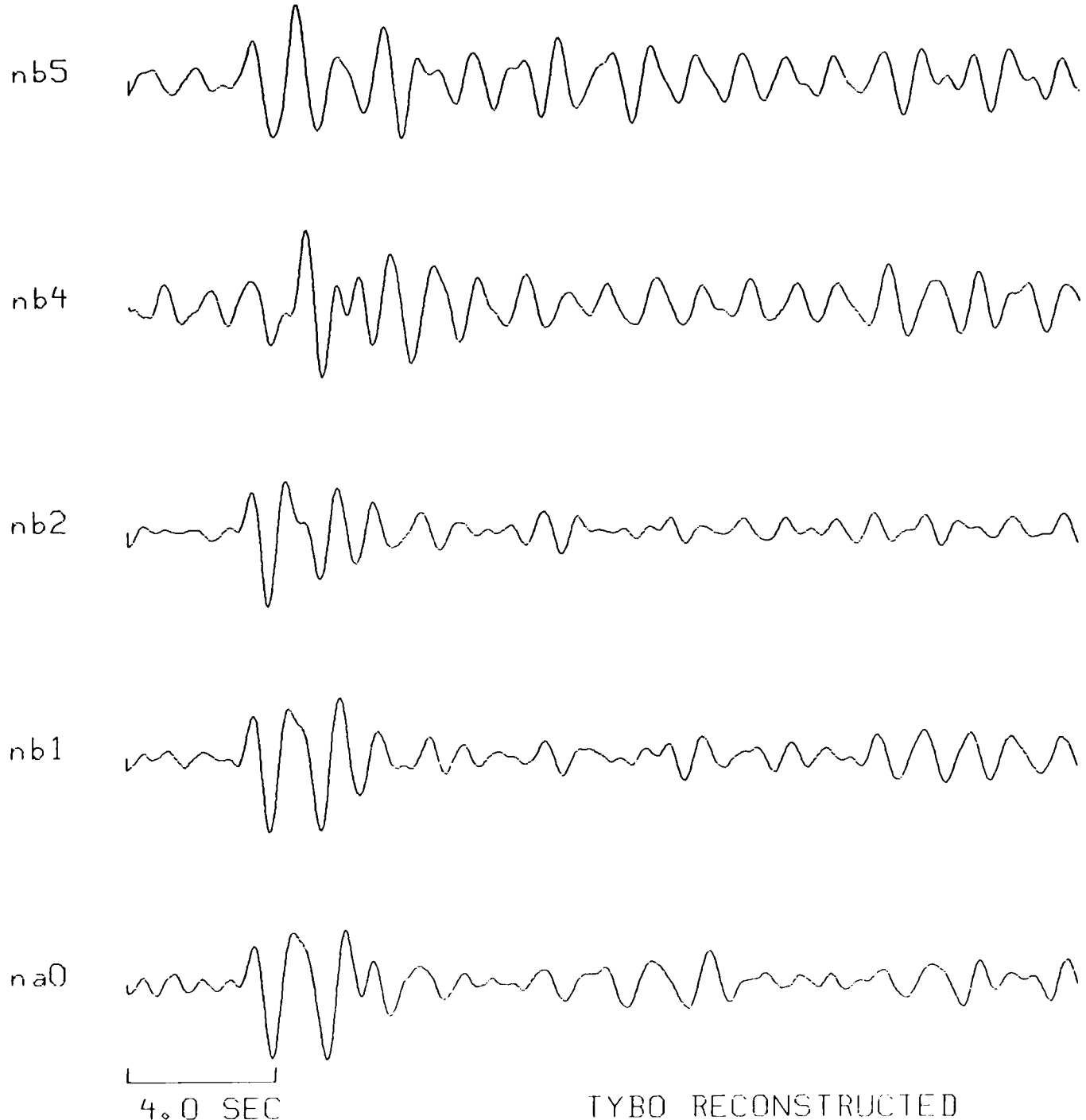
Azgir data recorded at the RSTN.

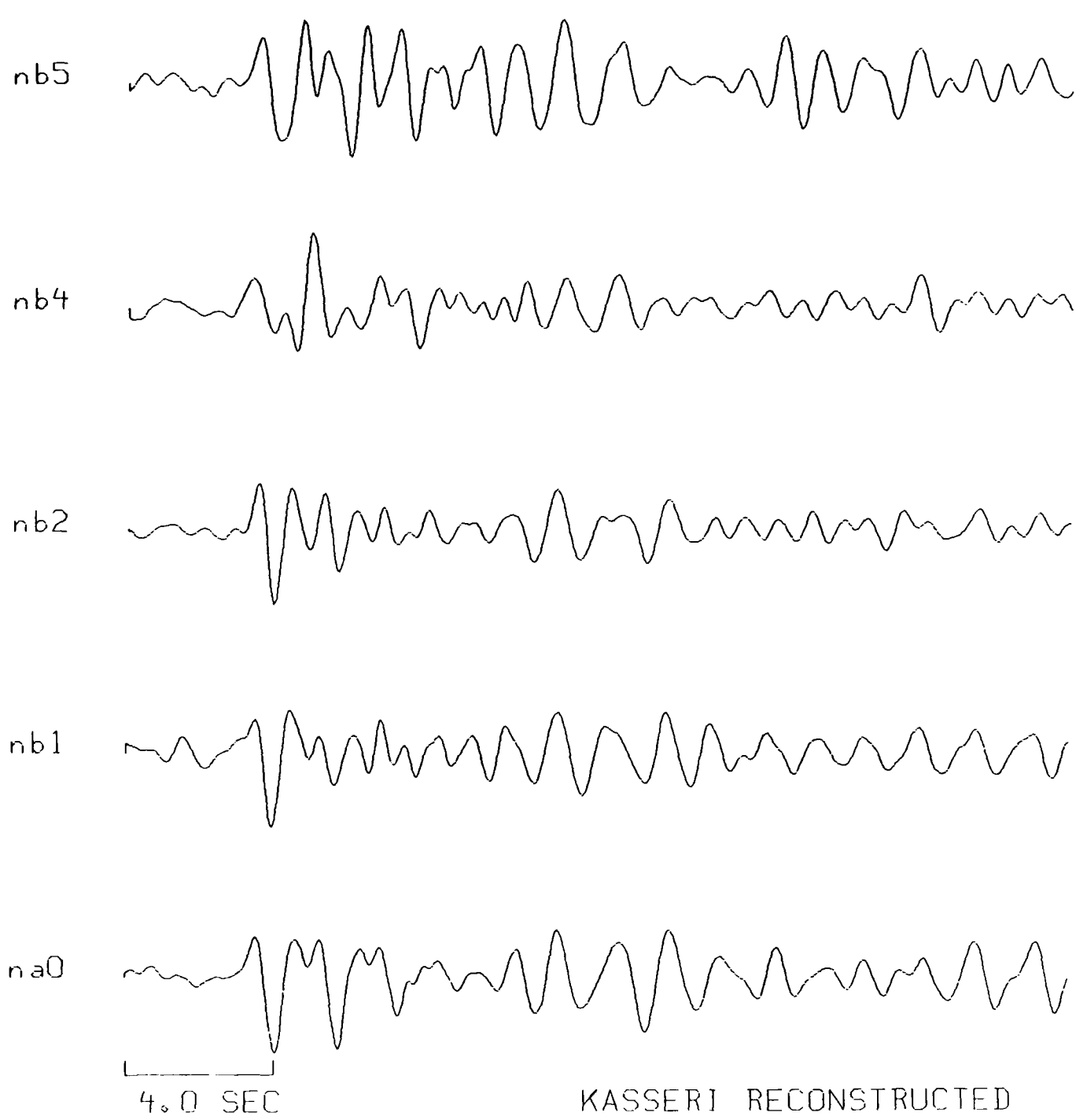
**NTS data recorded at NORSAR.**



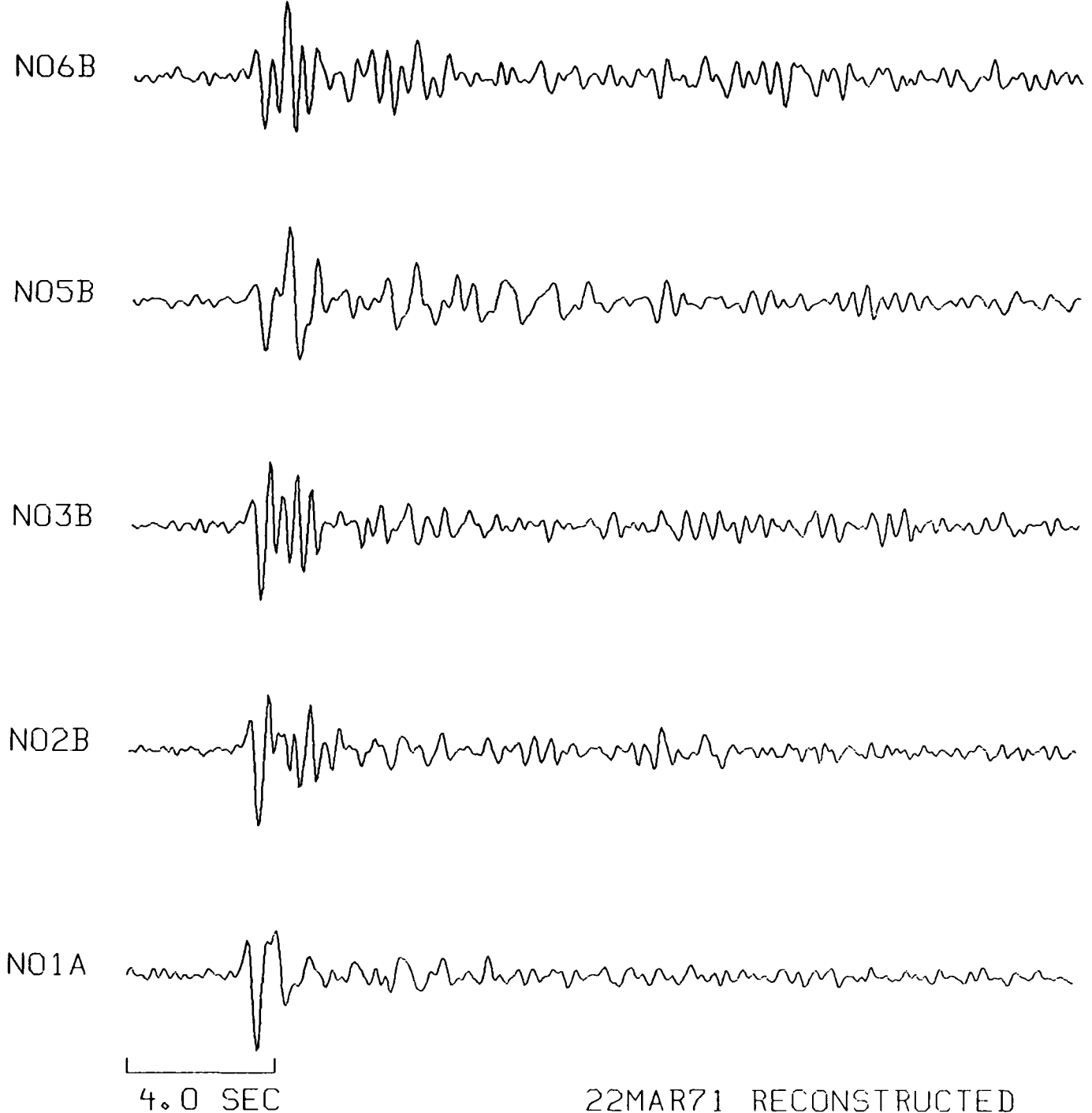




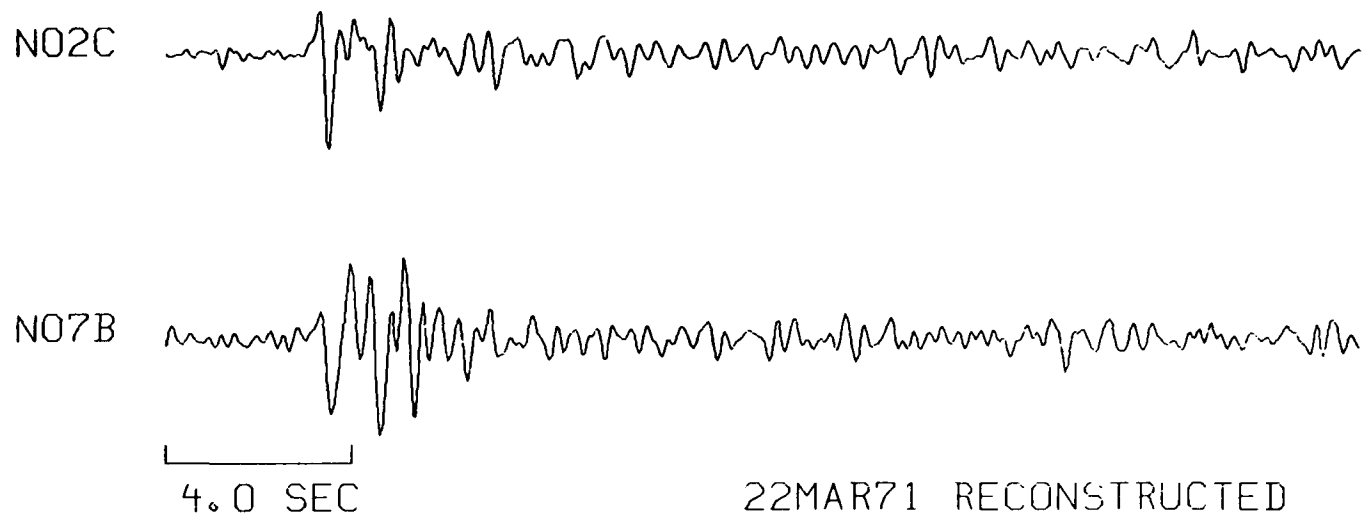




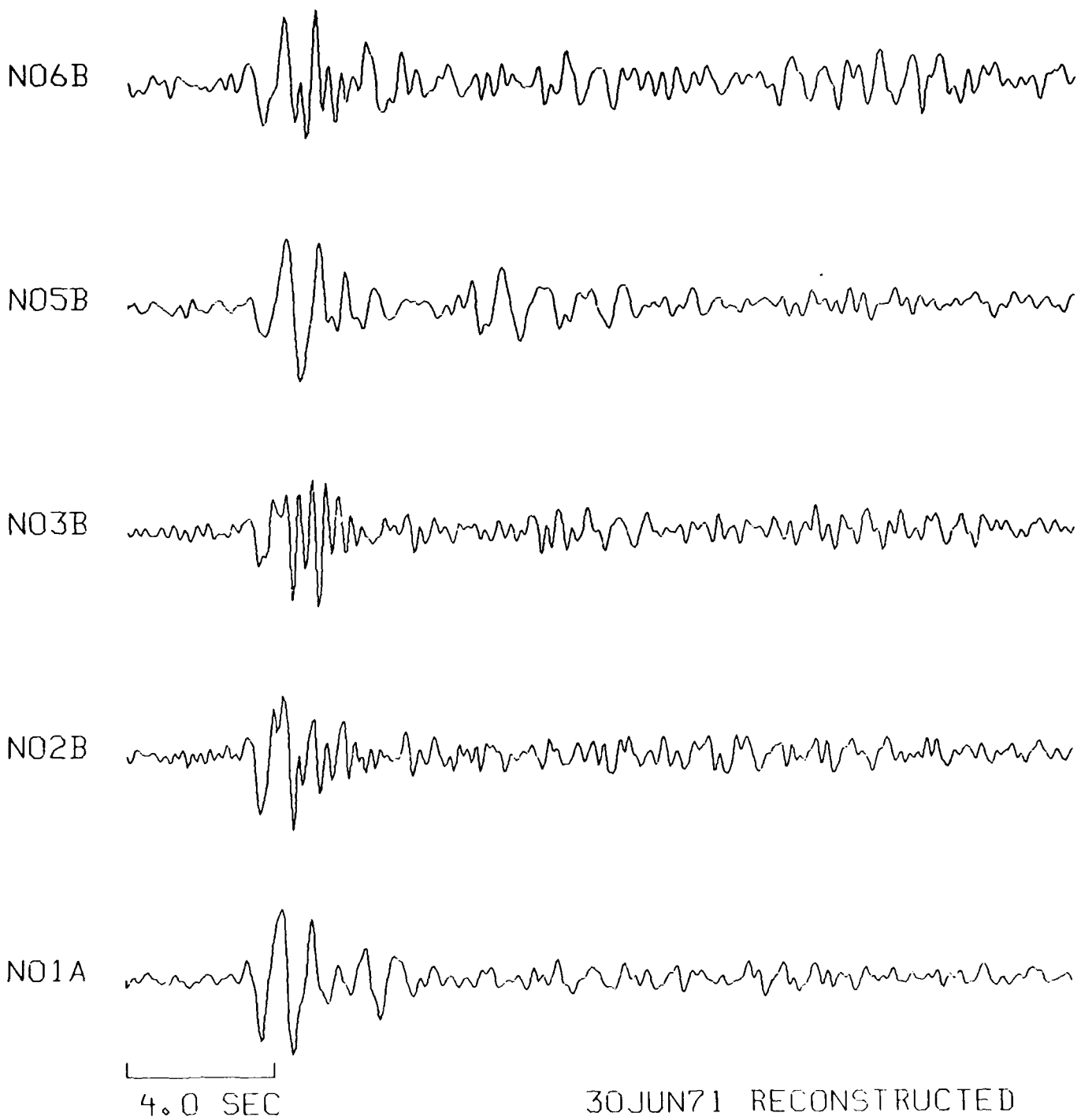
**Kazakh data recorded at NORSAR.**

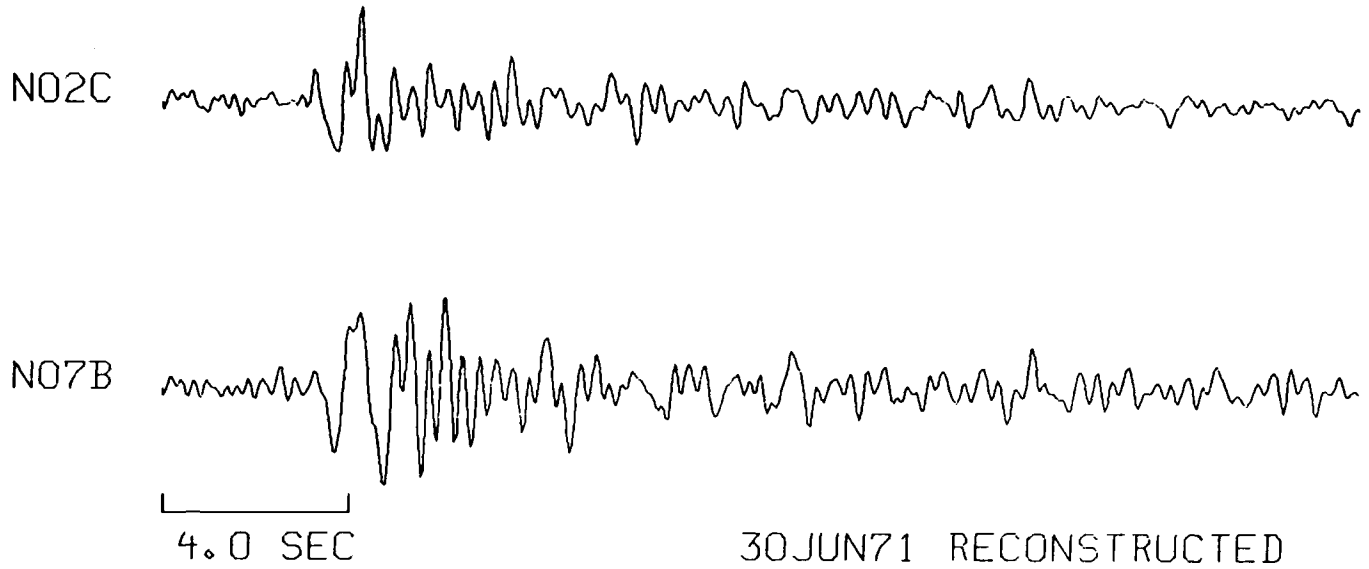


22MAR71 RECONSTRUCTED



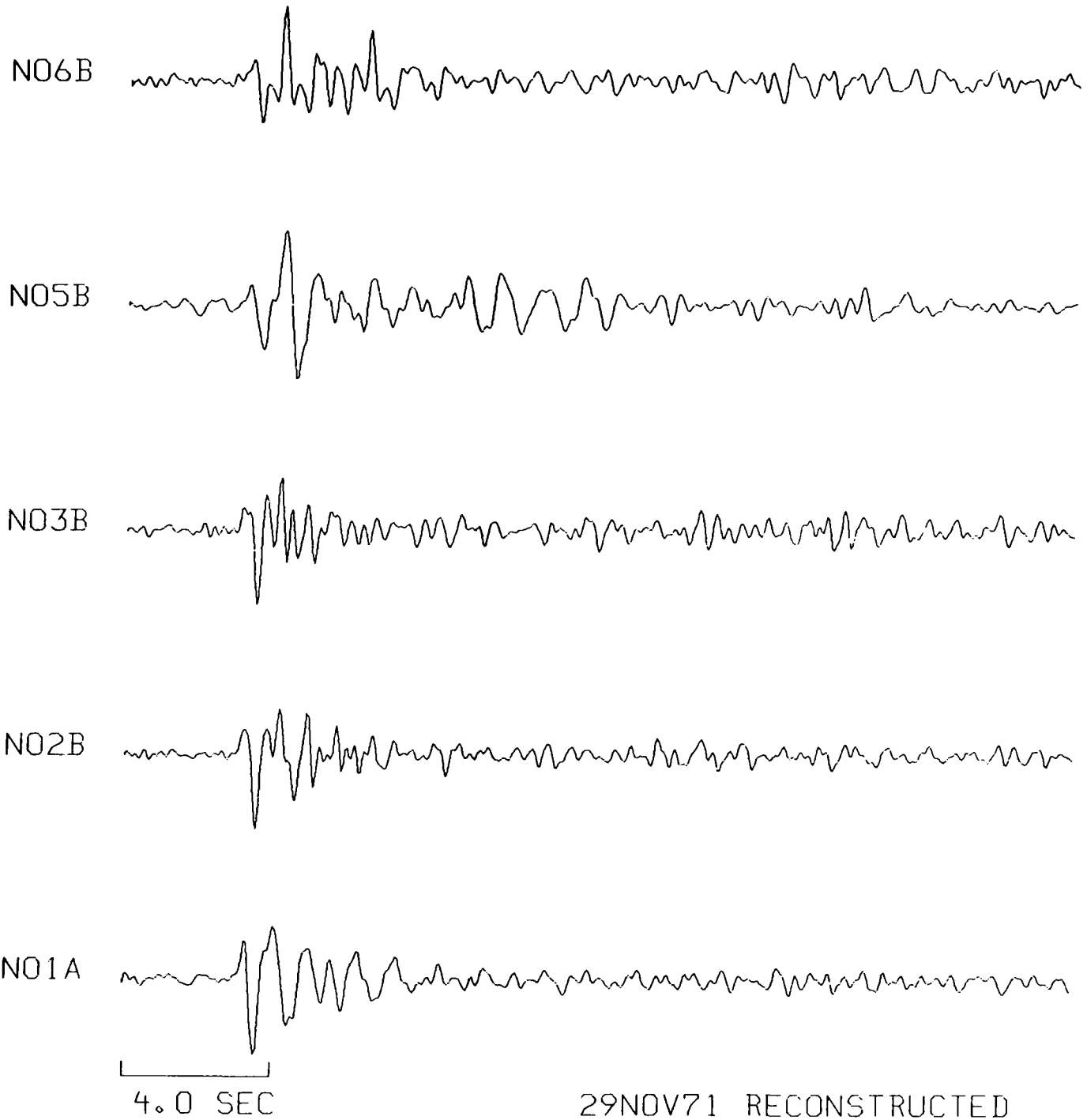
22MAR71 RECONSTRUCTED



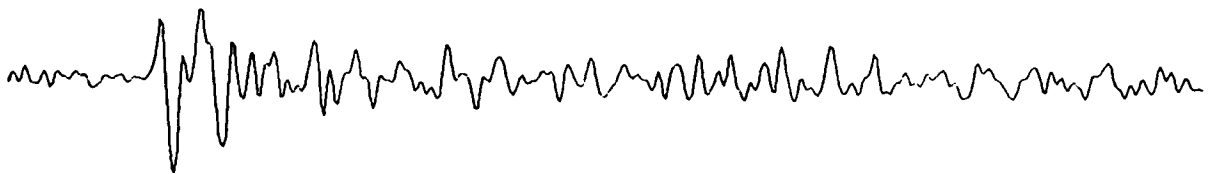


4.0 SEC

30JUN71 RECONSTRUCTED



N02C

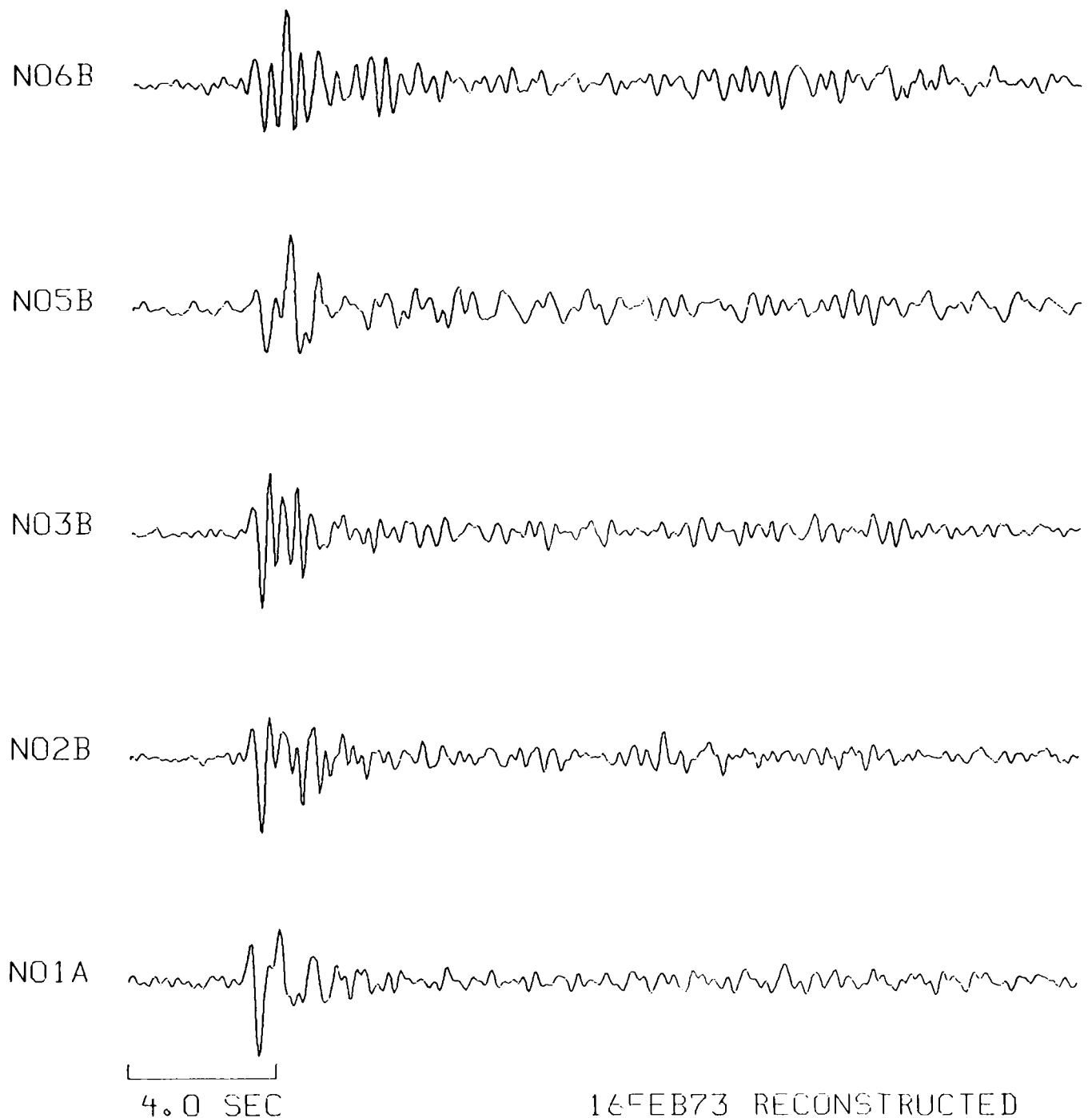


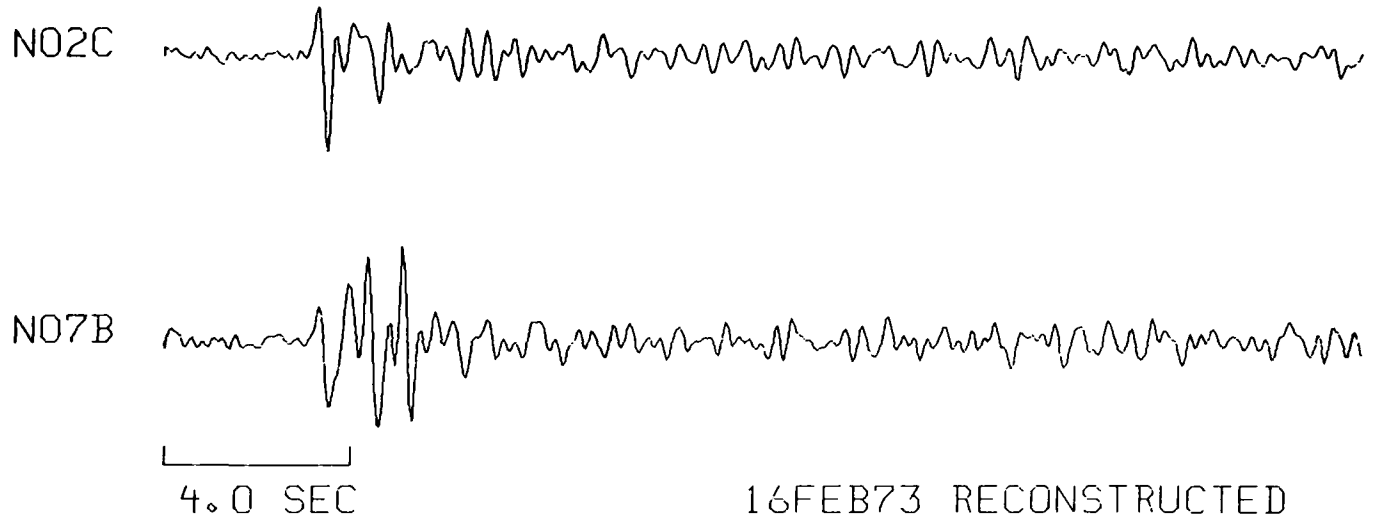
N07B



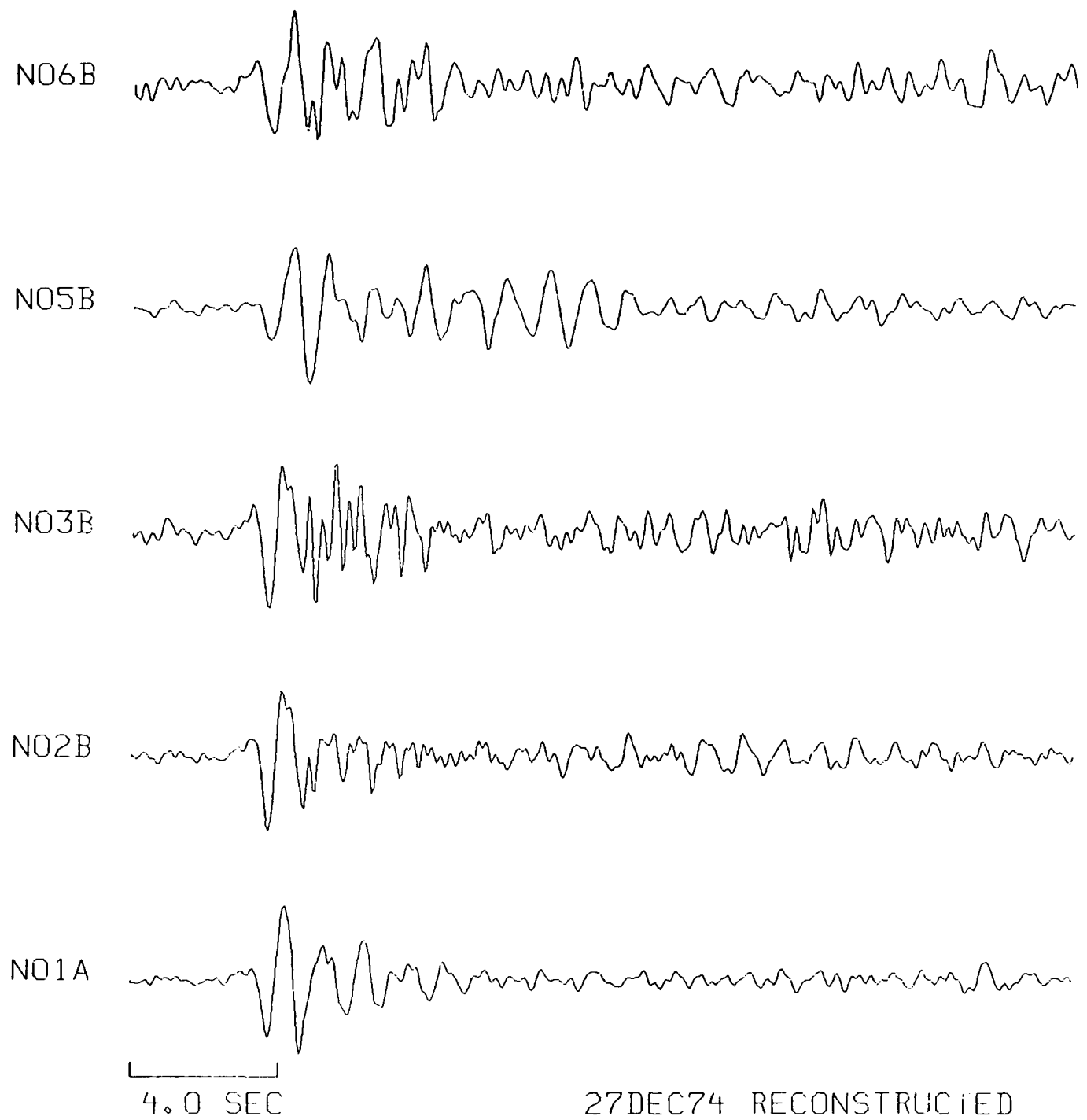
4.0 SEC

29NOV71 RECONSTRUCTED

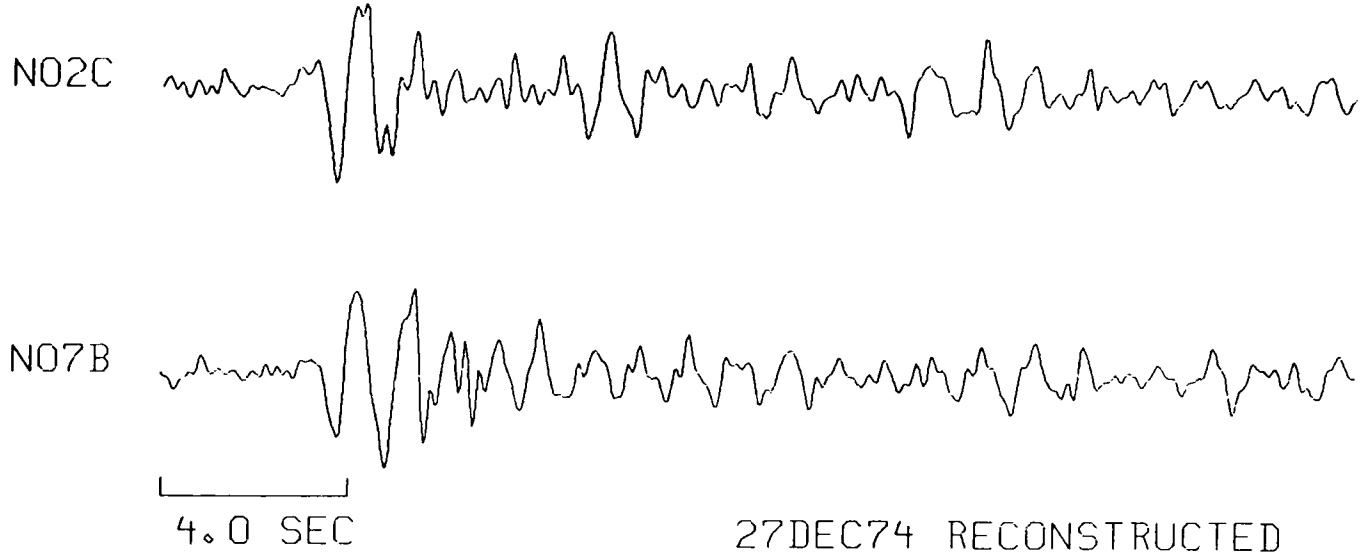




16FEB73 RECONSTRUCTED

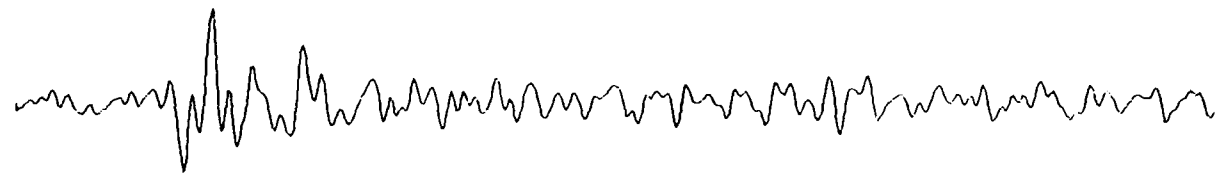


27DEC74 RECONSTRUCTED



27DEC74 RECONSTRUCTED

N06B



N05B



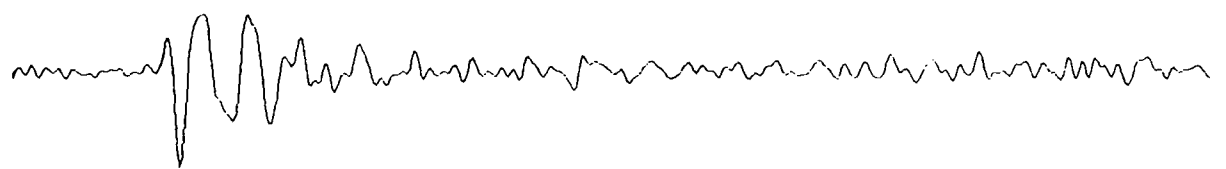
N03B



N02B



N01A



4.0 SEC

11MAR75 RECONSTRUCTED

N02C

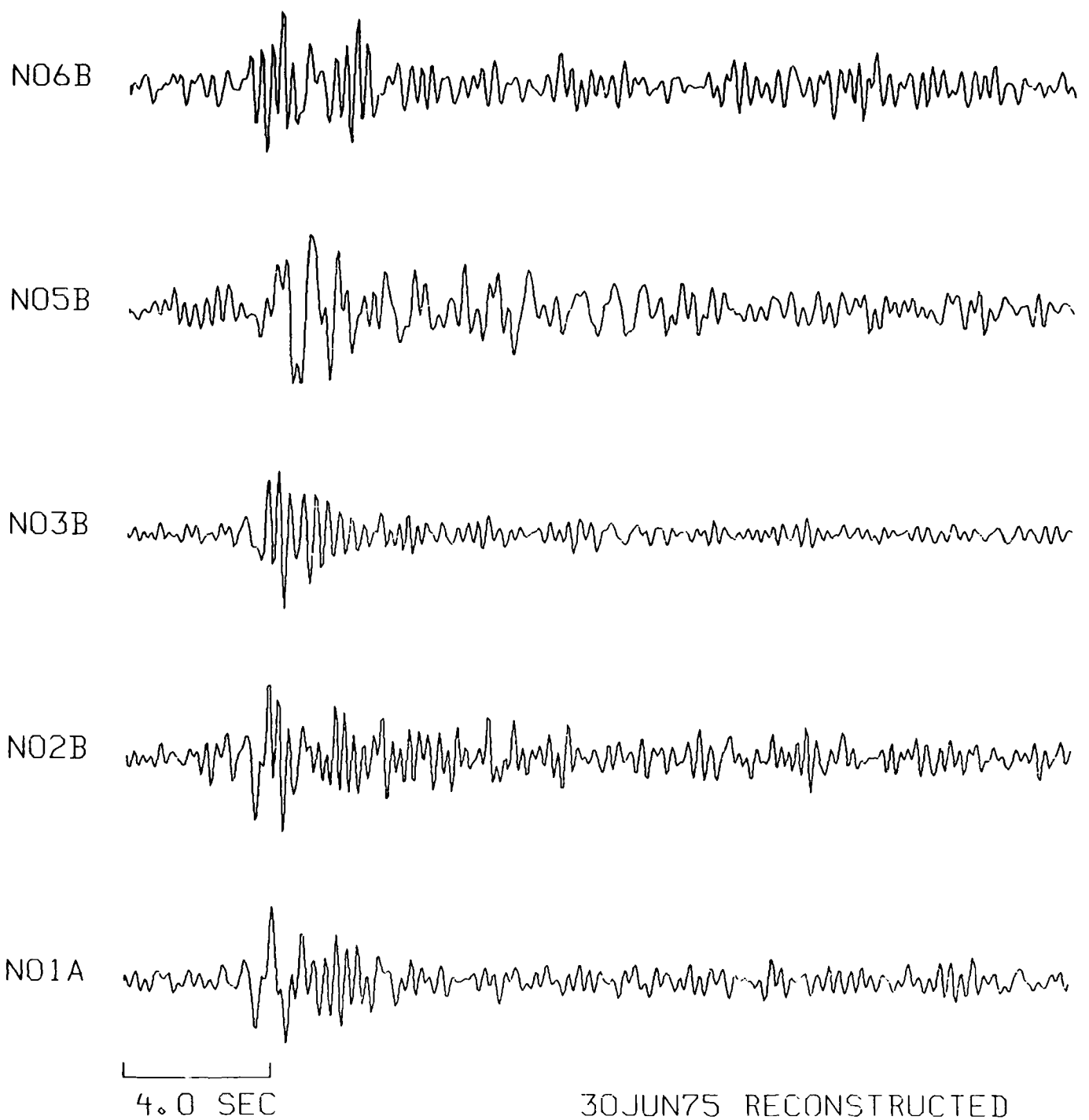


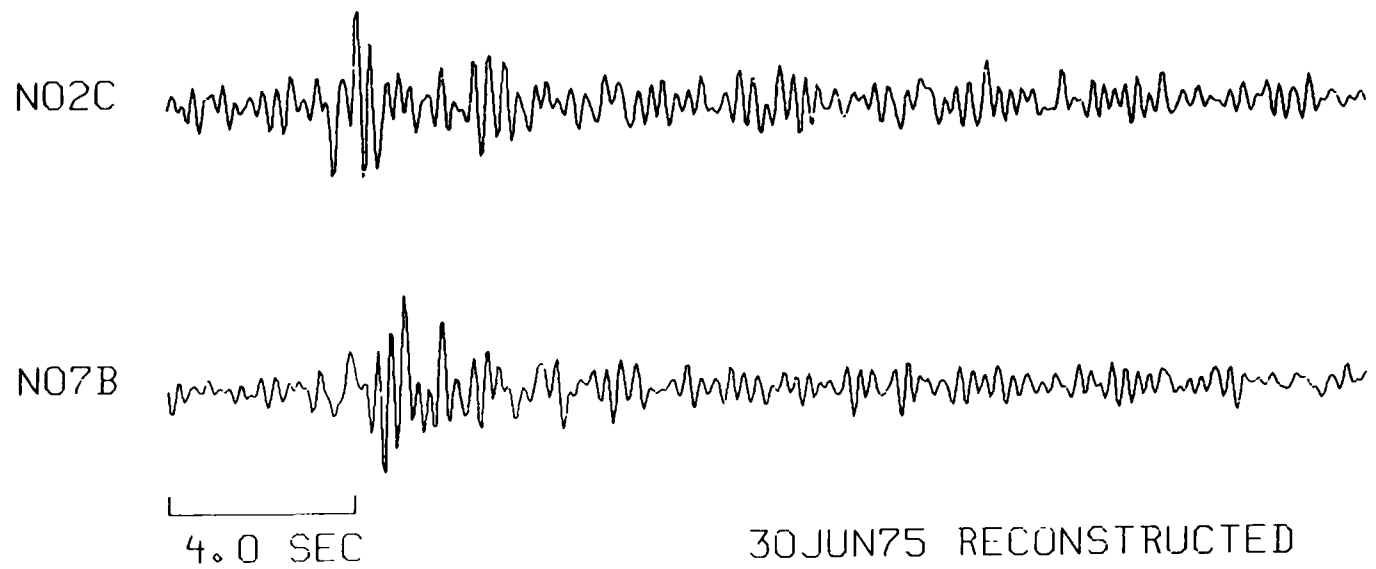
N07B



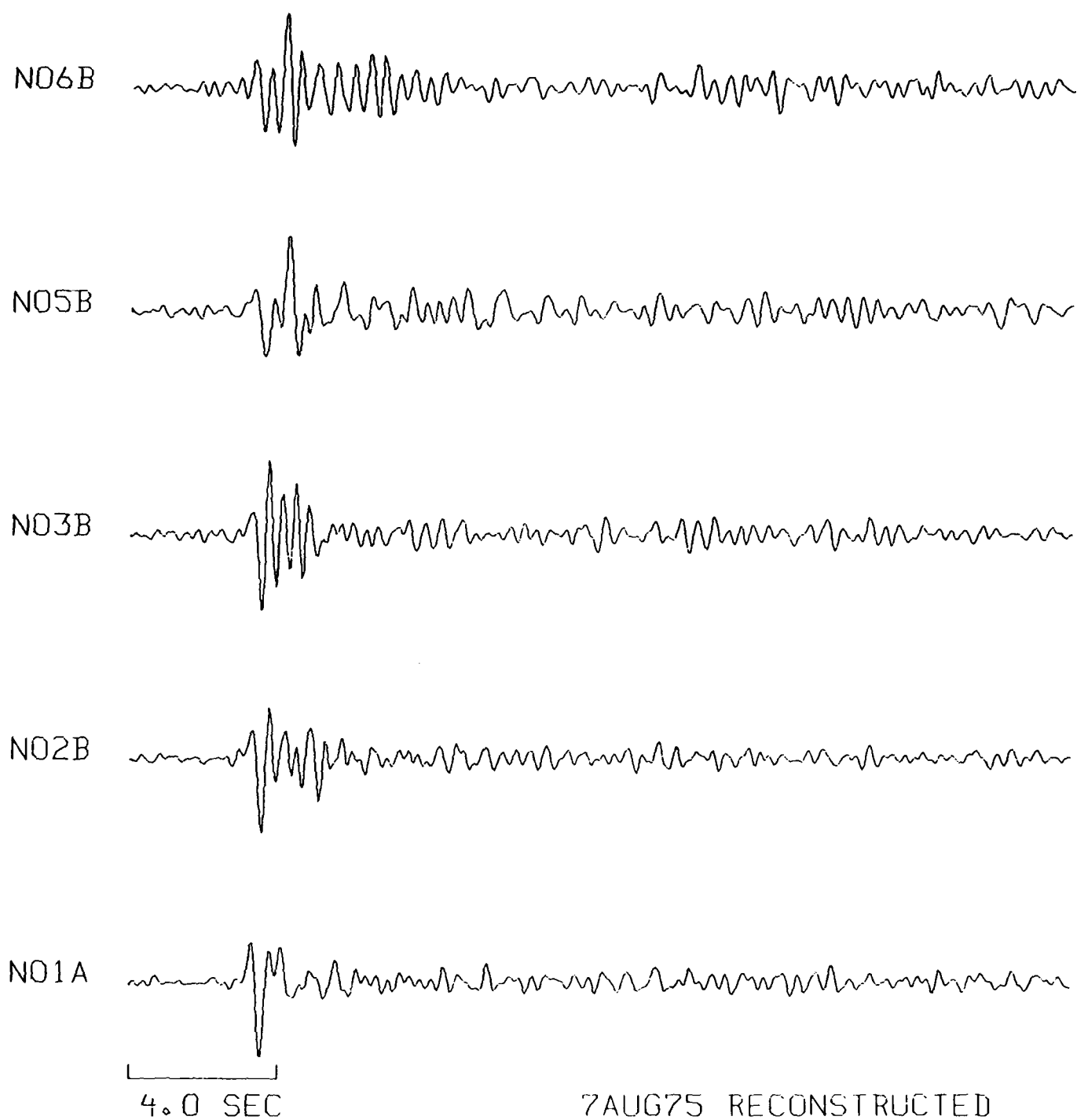
4.0 SEC

11MAR75 RECONSTRUCTED





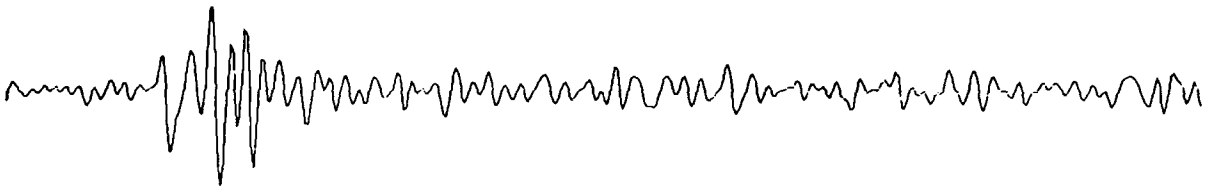
30JUN75 RECONSTRUCTED



N02C



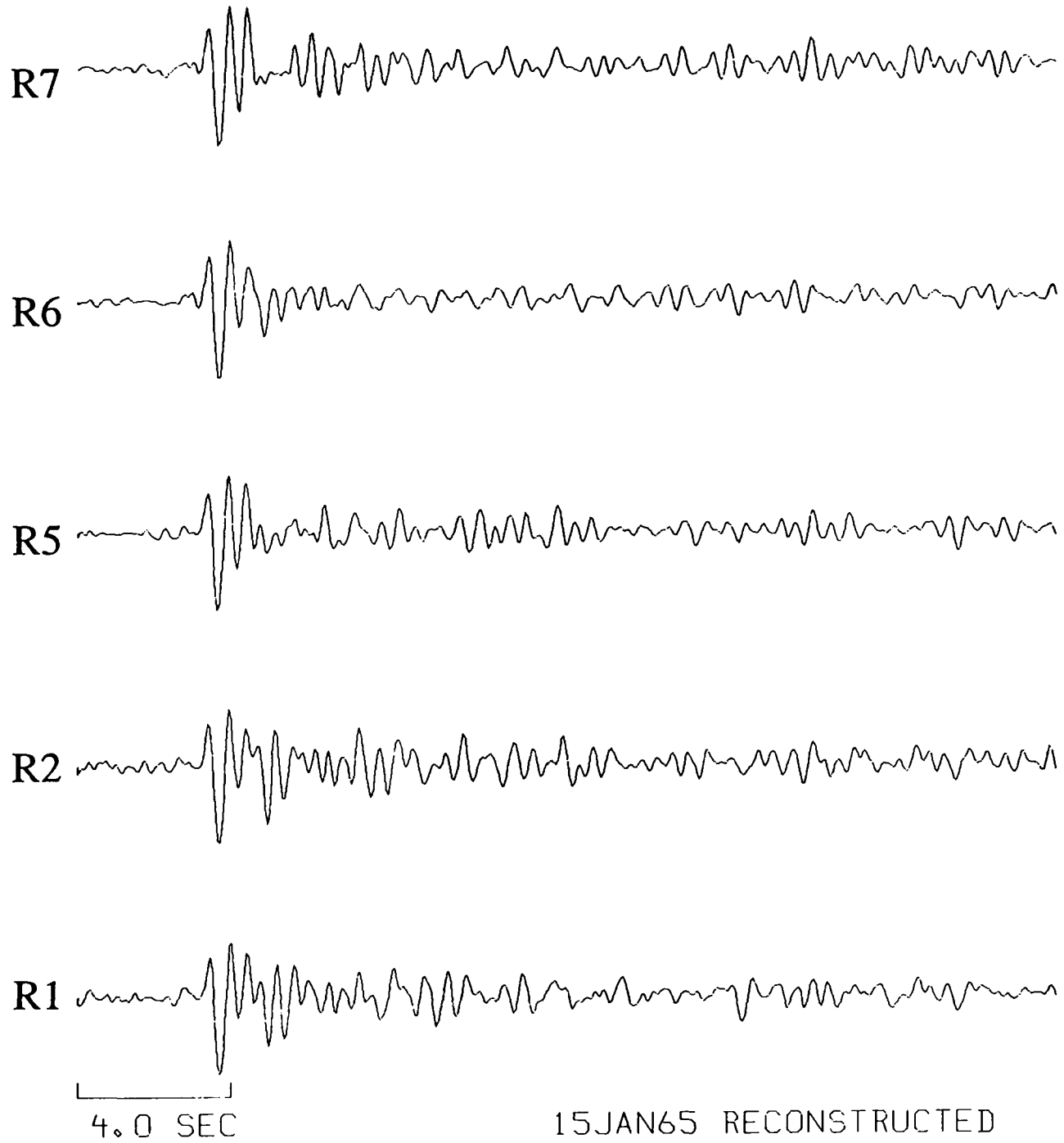
N07B

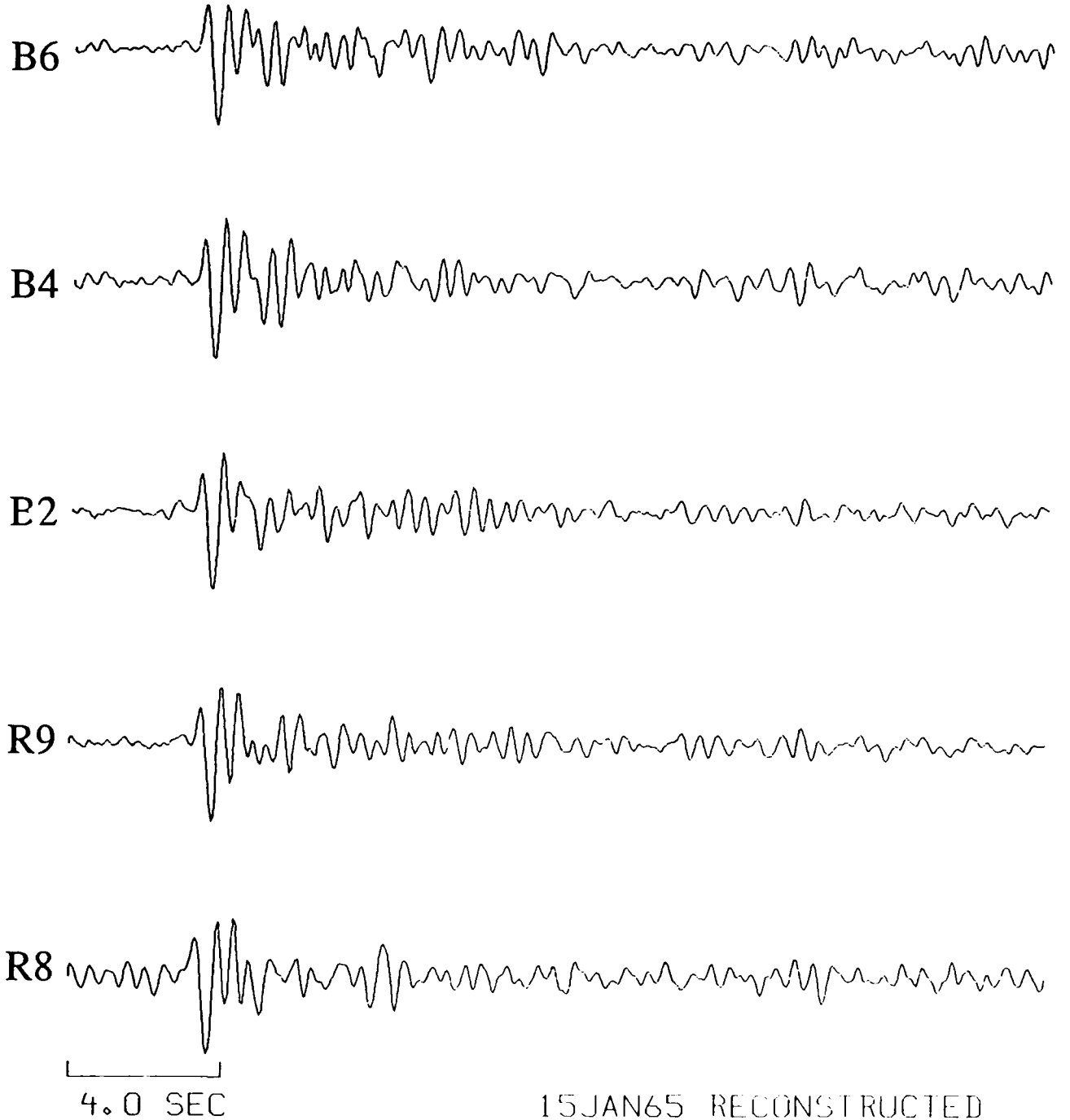


4.0 SEC

7AUG75 RECONSTRUCTED

**Kazakh data recorded at EKA.**

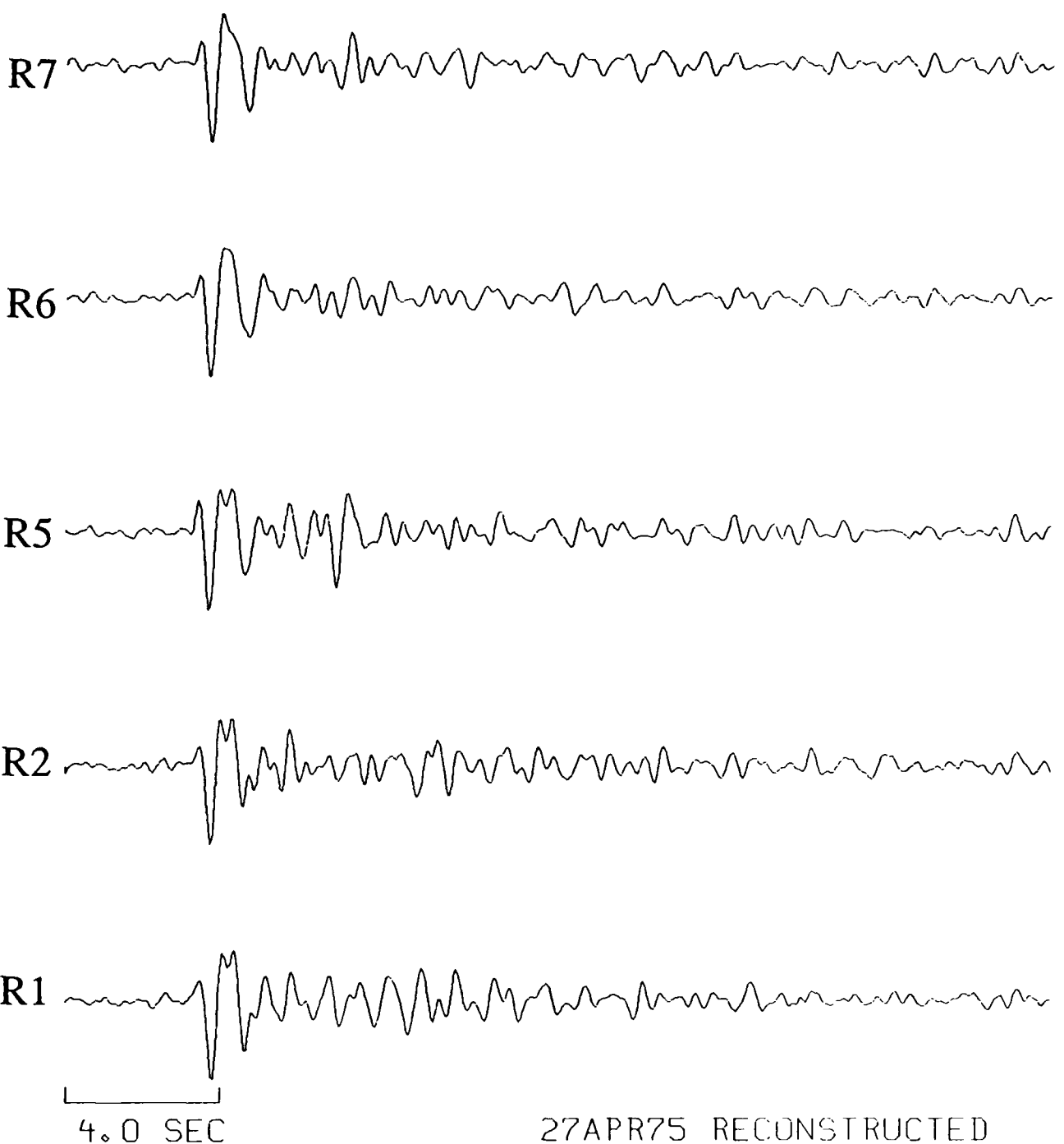




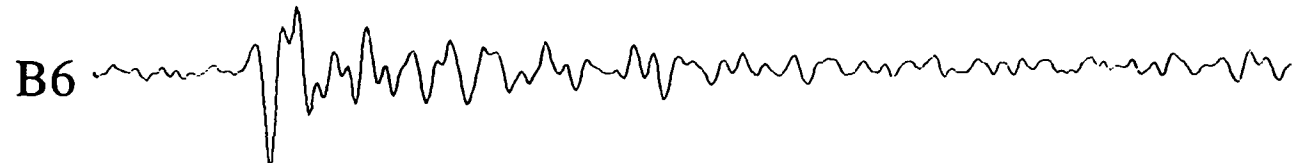


4.0 SEC

15JAN65 RECONSTRUCTED

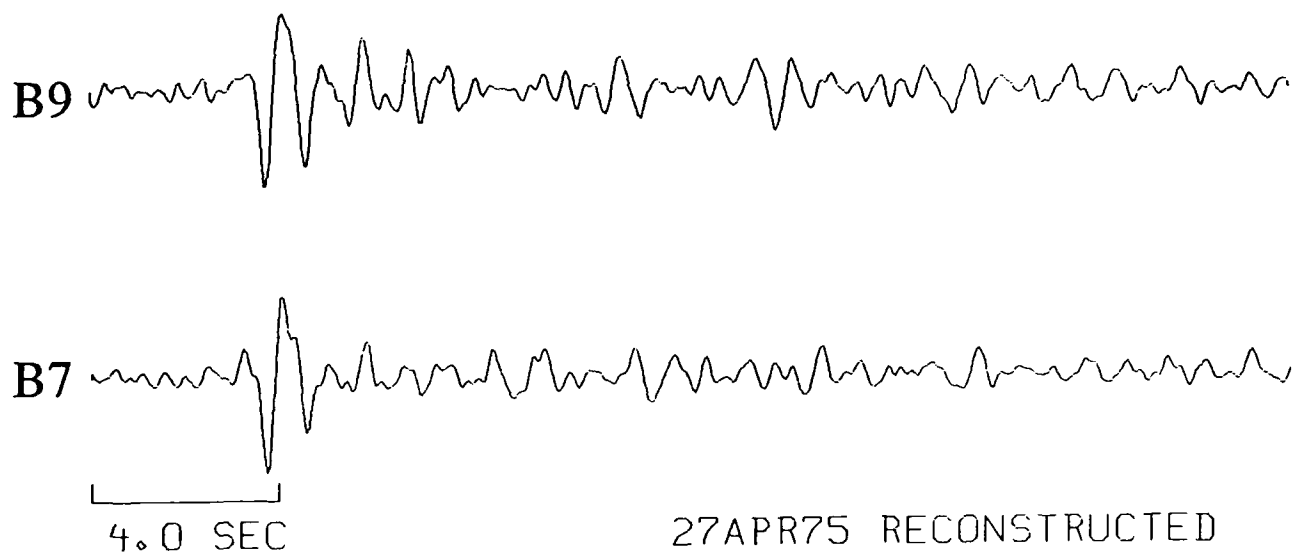


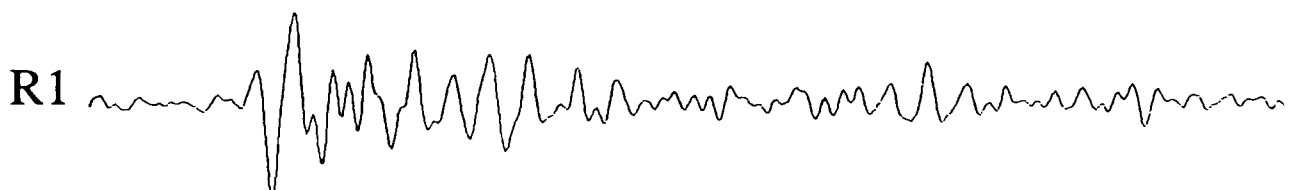
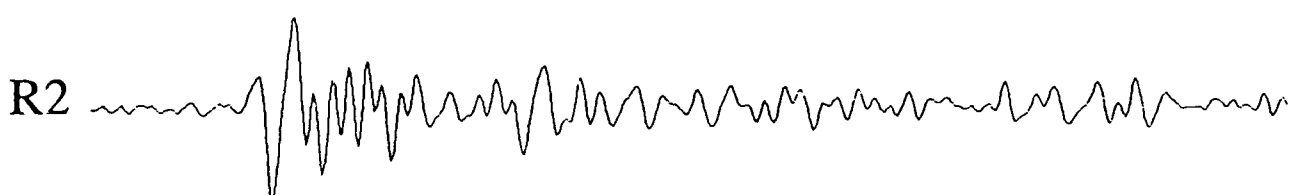
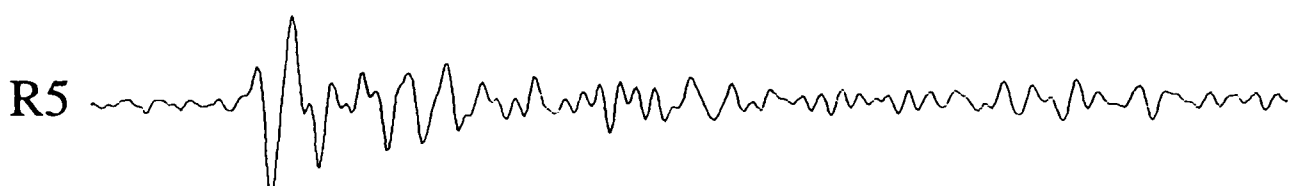
27APR75 RECONSTRUCTED



4.0 SEC

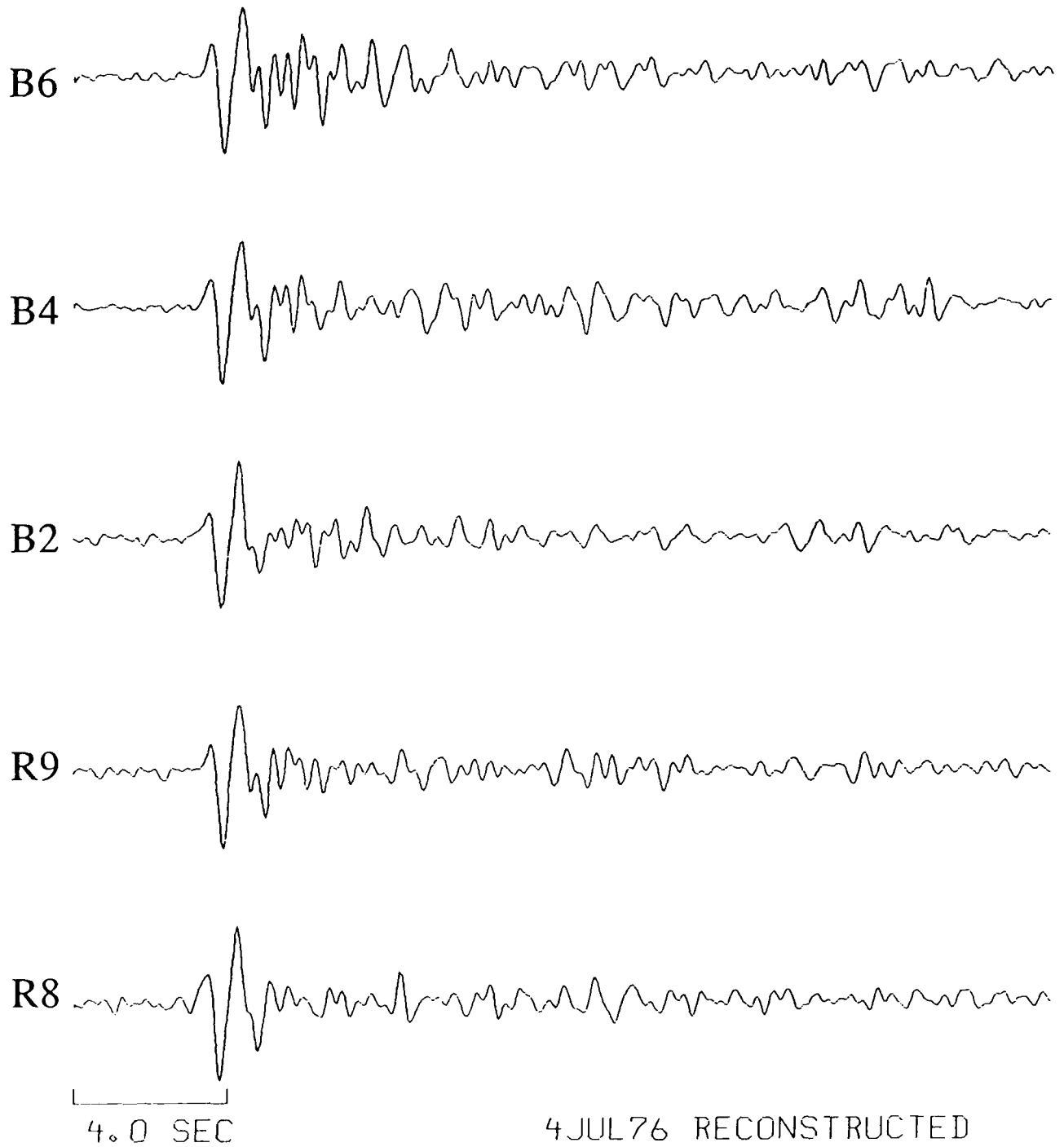
27APR75 RECONSTRUCTED



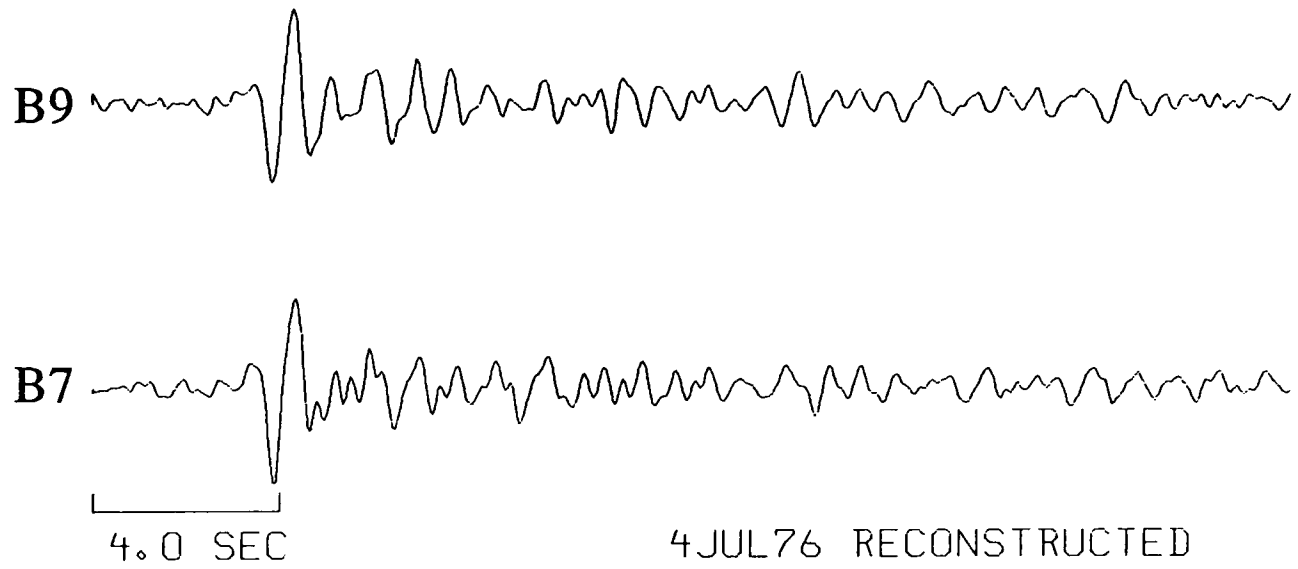


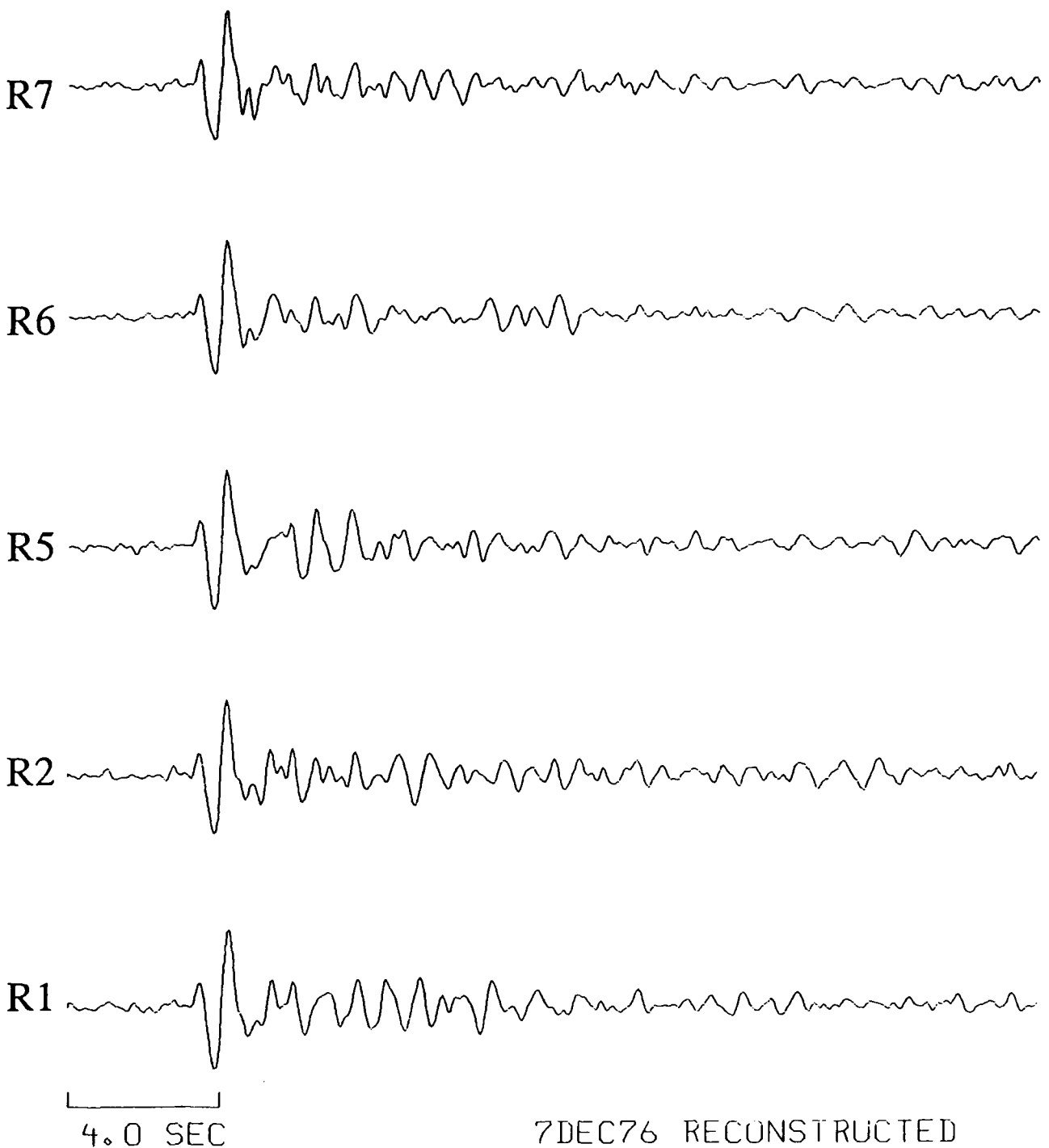
4.0 SEC

4JUL76 RECONSTRUCTED

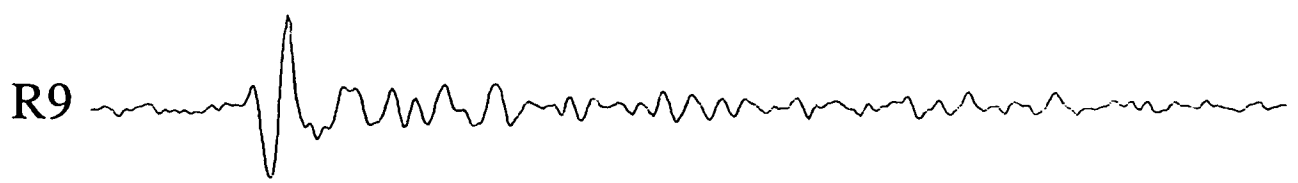
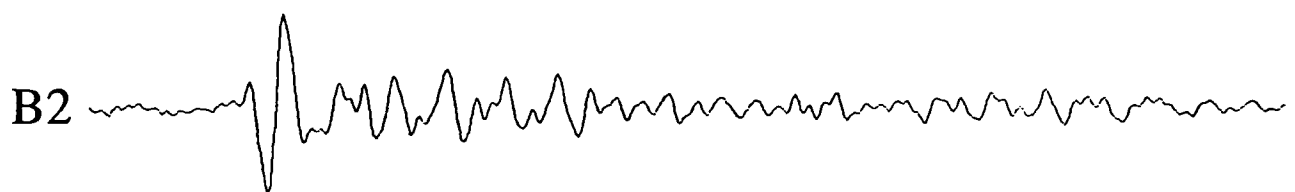
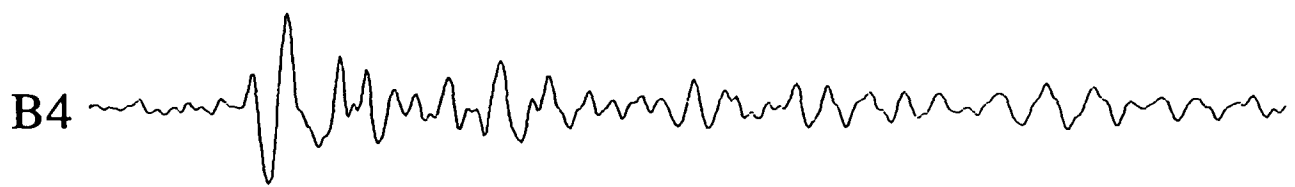


4JUL76 RECONSTRUCTED





7DEC76 RECONSTRUCTED



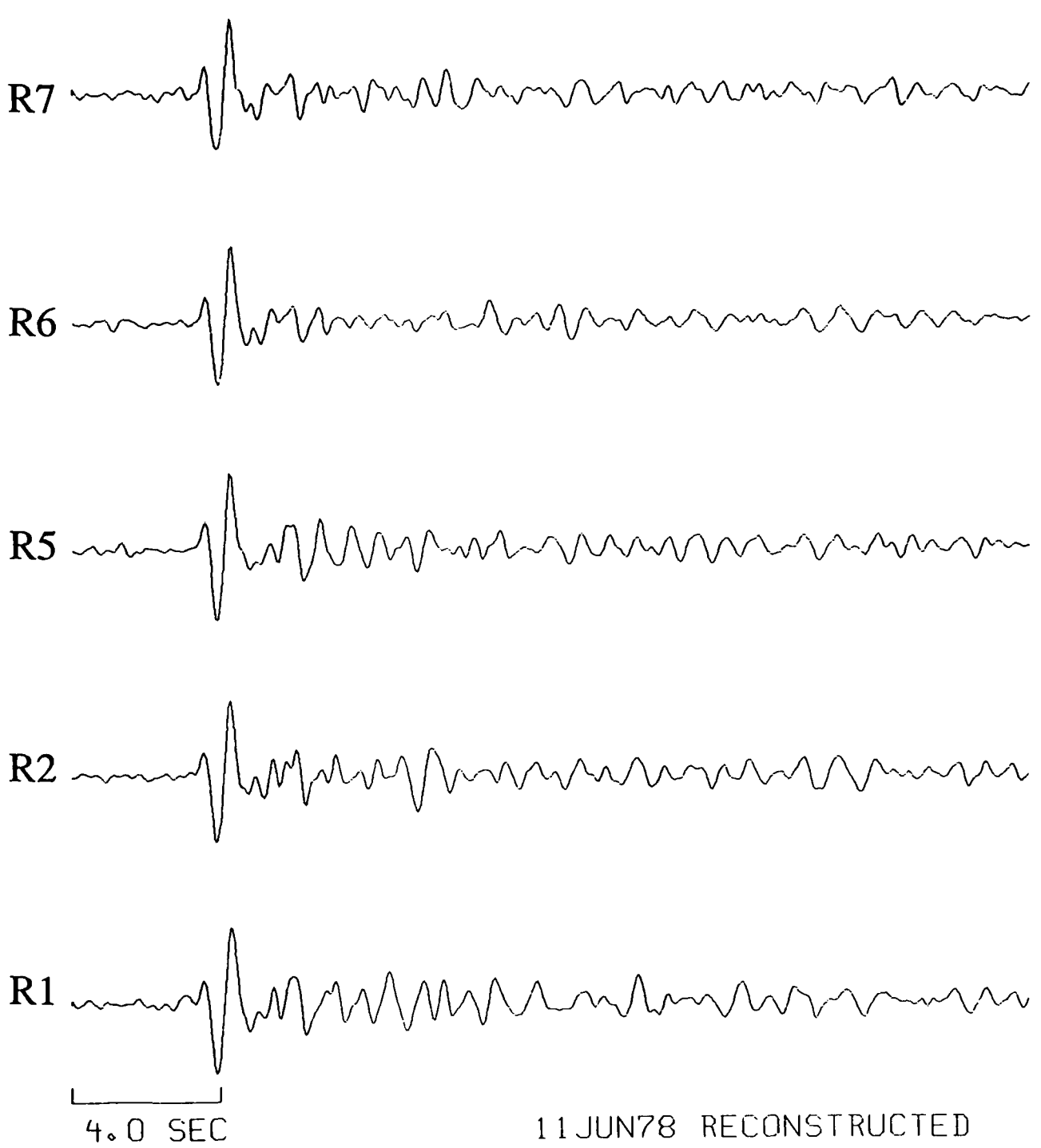
4.0 SEC

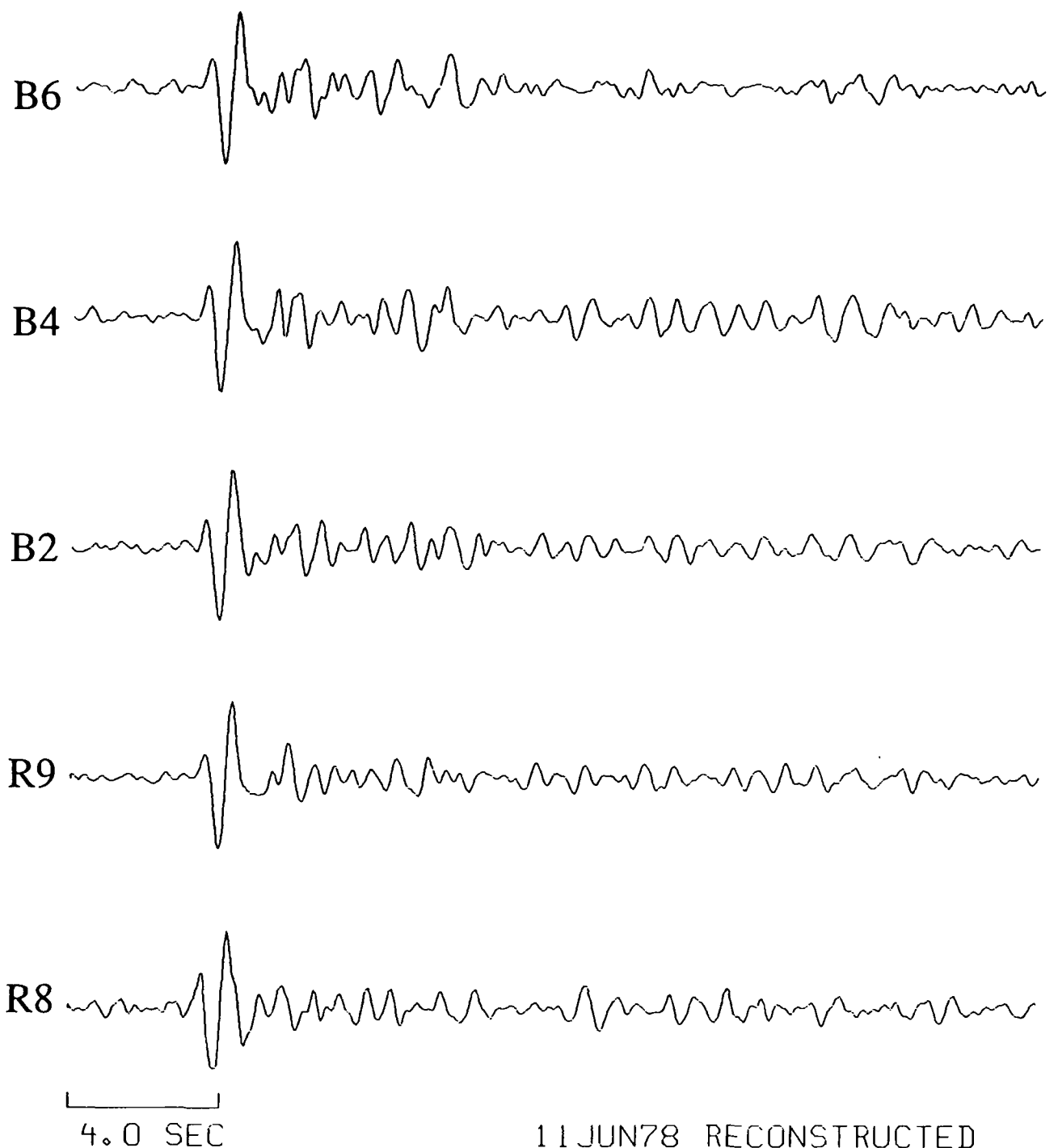
7DEC76 RECONSTRUCTED

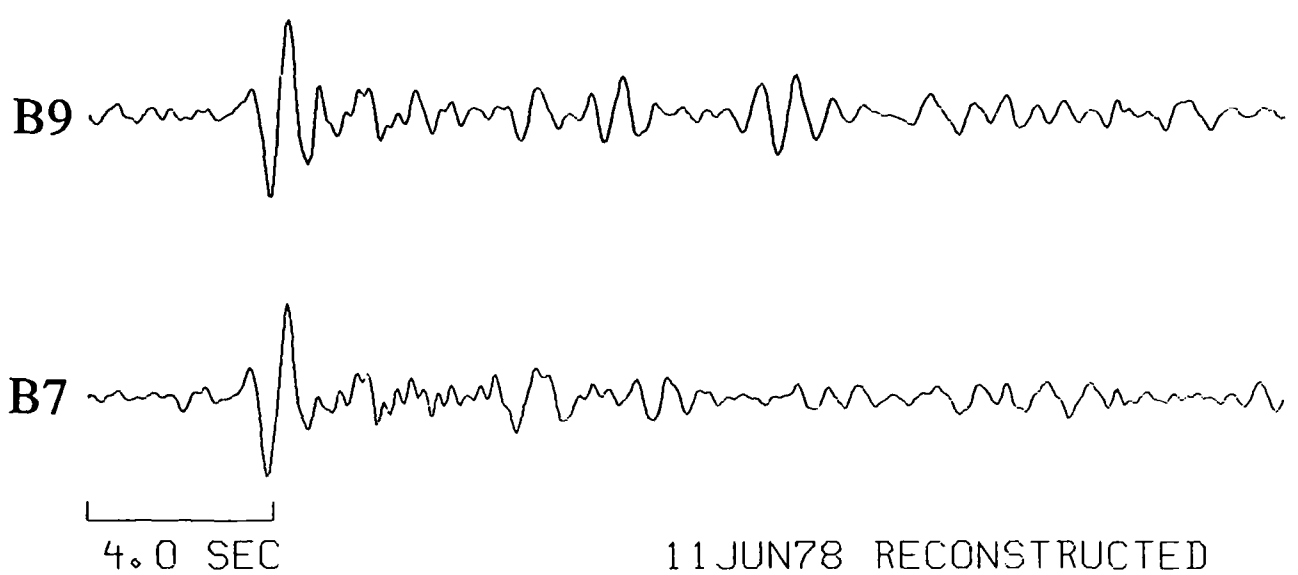


4.0 SEC

7DEC76 RECONSTRUCTED







11 JUN 78 RECONSTRUCTED

**Azgir data recorded at the RSTN.**

RSSD



RSON



RSNY



RSNT



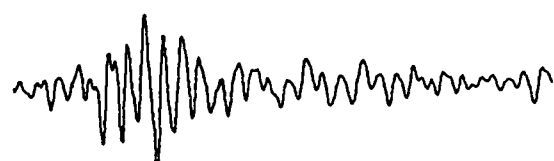
4.0 SEC

Event1 RECONST

RSSD



RSON



RSNY



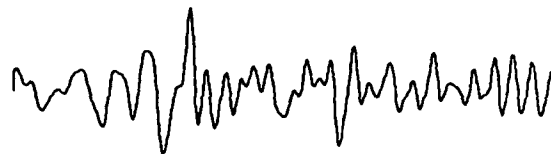
RSNT



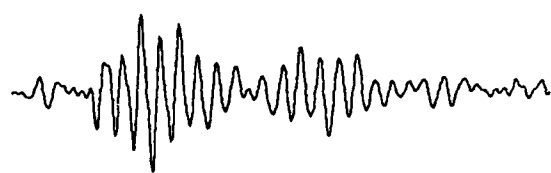
4.0 SEC

Event2RECONST

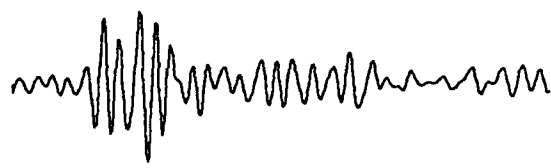
RSSD



RSON



RSNY



RSNT



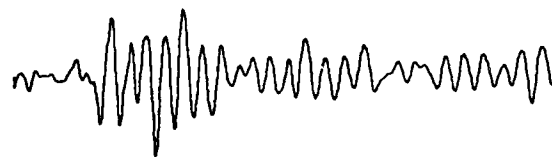
4.0 SEC

Event3RECONST

RSSD



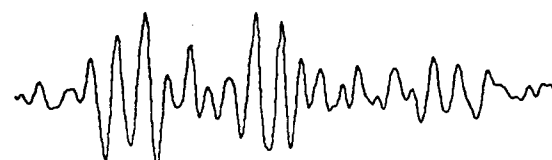
RSON



RSNY



RSNT



4.0 SEC

Event4 RECONST